IUTAM-SYMPOSIUM
ON
DYNAMICS OF SLENDER VORTICES

ABSTRACTS

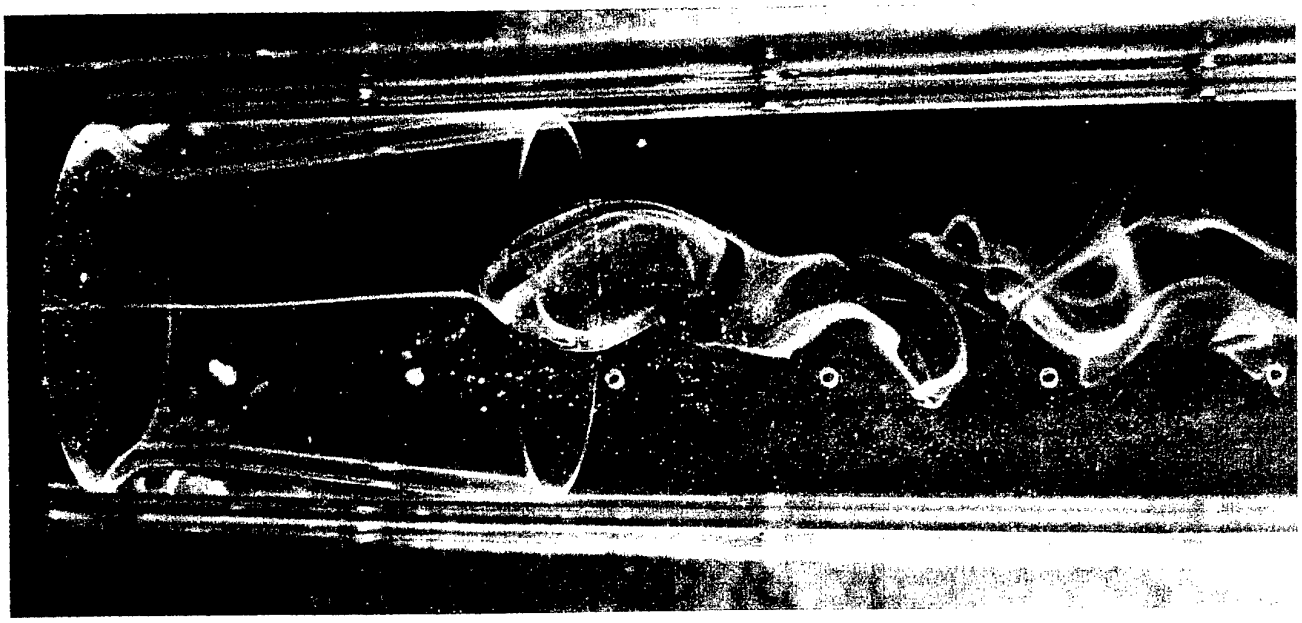

RWTH AACHEN
KARMAN-AUDITORIUM
AACHEN, GERMANY

August 31 - September 3, 1997

REPORT DOCUMENTATION PAGE

Form Approved OMB No. 0704-0188

1. AGENCY USE ONLY (Leave blank)	2. REPORT DATE	3. REPORT TYPE AND DATES COVERED
	4 September 1997	Conference Proceedings

4. TITLE AND SUBTITLE

IUTAM Symposium on Dynamics of Slender Vortices

5. FUNDING NUMBERS

F6170897W0034

6. AUTHOR(S)

Conference Committee

7. PERFORMING ORGANIZATION NAME(S) AND ADDRESS(ES)

Aerodynamisches Institut de RWTH-Aachen
RWTH Aachen
Aachen D-52062
Germany

8. PERFORMING ORGANIZATION REPORT NUMBER

N/A

9. SPONSORING/MONITORING AGENCY NAME(S) AND ADDRESS(ES)

EOARD
PSC 802 BOX 14
FPO 09499-0200

10. SPONSORING/MONITORING AGENCY REPORT NUMBER

CSP 97-1003

11. SUPPLEMENTARY NOTES

12a. DISTRIBUTION/AVAILABILITY STATEMENT

Approved for public release; distribution is unlimited.

12b. DISTRIBUTION CODE

A

13. ABSTRACT (Maximum 200 words)

The Final Proceedings for IUTAM Symposium on Dynamics of Slender Vortices, 31 August 1997 - 3 September 1997

14. SUBJECT TERMS

International Collaboration

15. NUMBER OF PAGES

103

16. PRICE CODE

N/A

17. SECURITY CLASSIFICATION OF REPORT	18. SECURITY CLASSIFICATION OF THIS PAGE	19. SECURITY CLASSIFICATION OF ABSTRACT	20. LIMITATION OF ABSTRACT
UNCLASSIFIED	UNCLASSIFIED	UNCLASSIFIED	UL

IUTAM-SYMPOSIUM
ON
DYNAMICS OF SLENDER VORTICES

RWTH Aachen, Kármán-Auditorium

Aachen, Germany

August 31 - September 3, 1997

ABSTRACTS

Scientific Committee

E. Krause, Chairman

K. Gersten, Co-Chairman

F. Hussain, USA

K. Kuwahara, Japan

M. Lesieur, France

C. H. Liu, USA

H. K. Moffatt, UK

L. Ting, USA

Sponsors of the Symposium

We wish to thank the following for their contribution to the success of this symposium

Deutsche Forschungsgemeinschaft

Ministerium für Wissenschaft und Forschung des Landes Nordrhein-Westfalen

Stadt Aachen

International Union of Theoretical and Applied Mechanics

Rheinisch - Westfälische Technische Hochschule Aachen

United States Air Force European Office of Aerospace Research and Development

Kluwer academic publishers

The Scientific Committee

CONTENTS

SESSION 1

ASYMPTOTIC THEORIES

Asymptotic theory of slender vortex filaments – old and new

Lu Ting, Courant Institute of Mathematical Sciences, New York University, New York, NY 10012, USA

Rupert Klein, Fachbereich Sicherheitstechnik, Bergische Universität, D-42097 Wuppertal, Germany

Omar M. Knio, Dep't Mech. Engrg, The Johns Hopkins University, Baltmore, MD 21218, USA

We give a brief historical account of the asymptotic theories of the motion of slender vortices and the evolution of the core structures. We emphasize the motivations, the choice of length and time scales for a given problem and explain the physical meaning of the asymptotic solutions and the consistency conditions for the core structures. We present some highlights of the extensions of the asymptotic theories in the past decade. They include the use of multiple length scales in the axial variation of the core structure and in the interaction of filaments. The study of the interaction of filaments with a solid body and sound generation, and the applications of asymptotic theory to numerical simulations and experimental investigation of slender vortex dynamics are also presented. We then describe a few vortical flow problems currently under investigation.

Extended Abstract

We consider an incompressible flow induced by an initial vorticity distribution concentrated in a slender tube-like region, representing a slender vortex filament. It is well known that the velocity of a filament depends on its core structure and is not defined in the limit of zero core size [1], a vortex line. The Biot-Savart formula is valid for the velocity field away from the vortex line. Near the vortex line, the formula yields three singular terms [2]: the first term has a factor r^{-1}, corresponding to the singular term of a two-dimensional point vortex, the second has $\log r$, and the third is not single valued as $r \to 0$, where r denotes the distance to the vortex line. This problem has two typical length scales, the core size δ and the length ℓ of the flow field with their ratio $\epsilon = \delta/\ell \ll 1$. With ϵ as the small parameter, matched asymptotic analyses were carried out in a sequence of papers from the two-dimensional cases by Ting and Tung [3] in 1965 to the three dimensional cases with both large circumferential and axial velocity components admitted in the core structure by Callegari and Ting [2] in 1978. To account for both the effect of viscous stresses and the inviscid effect via filament stretching on the temporal variation of the core structure, the analyses were carried out in the *distinguished limits*, i. e., by assuming $\epsilon = O(1\sqrt{R_e})$, with $R_e = \Gamma/\nu$, where R_e, Γ and ν denote the Reynolds number, the circulation around the filament and the kinematic viscosity. The effect of viscosity is important in the initial stage when the core size is small but is also needed to account for to the accumulation of the viscous effects over long time.

The asymptotic theory in the time scale of the flow field, $T = \ell^2/\Gamma$, defines the velocity of the filament center line, the evolution of the core structure and the restrictions on the initial data. Besides that on the initial velocity of the filament there are restrictions on the core structure. For example, if either the circumferential or the axial components does not vary along the filament, then the other component does not also.

In explaining the asymptotic theory for slender filaments, we assume that the background flow is a potential flow, to avoid the complication of the variation of the background flow induced by the filaments. It was shown, however, that the asymptotic theory for filaments remains valid when the background flow is rotational with $O(1)$ vorticity. In that case, the background flow is nonlinear and is coupled with motion of the filaments. A numerical scheme was presented, accounting for the fact that the the background flow varies in the length scale ℓ, not in the scale of the core size, δ. The dynamics of the filaments is given by the same asymptotic theory for a background potential flow while the background velocity on a filament centerline is the instantaneous local velocity of the rotational flow. The analysis and examples were presented by Liu and Ting [4] for two-dimensional flows and by Ishii and Liu [5] for axi-symmetric flows in 1987.

A comprehensive account of the asymptotic theories, the physical meanings of the *distinguished limits*, the solutions and their restrictions, and the applications of the theories were given by Ting and Klein [6] in 1991. In [6], it was also shown that the analysis of Callergari and Ting [2] for a filament forming a closed loop of length $O(\ell)$ can be generalized to a long filament with length scale $L \gg \ell$ by the method of two-length scales, ℓ and L.

Simplifications of the asymptotic theories have been achieved by Klein and Majda et al, [7, 8], for special cases where there is an intermediate length scale λ between δ and ℓ, i. e., $\delta \ll \lambda \ll \ell$, with λ identified respectively as a typical radius of curvature of the filament centerline [7] and as the typical distance between two nearly parallel filaments [8]. In both cases, the leading order velocity of the filament is independent of the evolution of the core structure and hence the contribution of the filament self-induction can be represented by a nonlocal pseudo-differential operator.

A generalization of the theory of Callegari and Ting [2] was made by Klein and Ting [9] in 1992 to allow for axial variation of the core structure. Two constraints on the initial core structure are derived and their physical meanings are identified. These constraints have to be observed even in the inviscid limit. This generalization is needed so as to simulate the vortex breakdown phenomenon. This simulation will be reported in detail in a contributed paper by Schmitz and Klein [10].

It was noted that to construct an asymptotic solution we need the initial data of the shape of the filament centerline and core structure. The latter is usually not available from experimental data. This difficulty is removed by Klein and Ting [11] in 1994. They showed how the asymptotic analysis and experimental investigation complement each other in the study of the dynamics of vortex filaments. Also they together with Knio [12], [13] showed how to use the asymptotic theory to render the vortex element method applicable to the numerical simulation of the dynamics of vortex filament. The scheme and its recent improvement to remove the temporal stiffness and numerical examples will be reported by Klein et al [14].

An extension of the solution for vortex filament in free space to that in the presence of a solid body, a sphere, was made by Knio and Ting [15]. It was found that the leading acoustic field induced by vortex filament(s) in free space is represented by quadrupoles. In the presence of the body, there are dipoles. Details will be presented by Knio et al [16].

Currently, we are studying the solutions for slender filaments with an intermediate length scale λ in between the core size δ and the length ℓ, e. g., the interaction of three rings with the distances between them $O(\lambda)$ much small than their radii $O(\ell)$. The dynamics of the three rings shall then be analyzed as small perturbations from corresponding equilibrium or period configurations of three vortices in two-dimensional space [17, 18]. We shall also study the dynamics of many coaxial rings with $\lambda \ll \ell$ of a nearly helical filament with slowly varying core size and with small pitch $O(\lambda)$ and the interaction of several co-axial helical filaments with the distance between two adjacent filaments to be $O(\lambda)$.

References

[1] Lamb, H., *Hydrodynamics*, 6th ed., Dover, New York, 1932.

[2] Callegari, A. and Ting, L., SIAM J. Appl. Math., **35**, 148-175, 1978.

[3] Ting, L. and Tung, C., Phys. Fluids, **8**, 1039-1051, 1965.

[4] Liu, C. H. and Ting, L., J. Computer and Fluids, **15**, 77-92, 1987.

[5] Ishii, K. and Liu, C. H., AIAA-87-1342, 19th Fluid and Plasma Dynamics and Lasers Conf., 1987.

[6] Ting, L. and Klein, R., *Viscous Vortical Flows*, Lecture Notes in Physics 374, Springer-Verlag, 1991.

[7] Klein R. and Majda, A., Physica D, **49**, 323-352, & **53**, 267-294, 1991.

[8] Klein, R., Majda, A. and Damodaran, K., J. Fluid Mech., **288**, 201-248, 1995.

[9] Klein, R. and Ting, L., Appl. Math. Letters, **5**, 99-103, 1992.

[10] Schmitz M. and Klein, R., "Recent Developments in the Asymptotic Theory of Vortex Breakdown", to be presented in this symposium.

[11] Klein, R. and Ting, L., Appl. Math. Letters, **8**, 45-50, 1995.

[12] Klein, R. and Knio, O., J. Fluid Mech., **284**, 275-321, 1995.

[13] Klein, L., Knio, O. and Ting, L., Phys. Fluids, **8**, 2415-2425, 1996.

[14] Klein, R. and Knio, O., "Optimized Vortex Element Schemes for Slender Vortex Simulation", to be presented in this symposium.

[15] Knio, O. M. and Ting, L., "Vortical Flow outside a Sphere and Sound Generation", to appear in SIAM J. Appl. Math. **57**, August 1997.

[16] Knio, O. and Ting, L., "Noise Emission due to Slender Vortex - Solid Body Interactions", to be presented in this symposium.

[17] Synge, J. L., Can. J. Math., **1**, 257-270 , 1949.

[18] Tavantzis, J. and Ting, L., Phys. Fluids, **31**, 1392-1409, 1988.

Motion of a thin vortex ring in a viscous fluid: higher-order asymptotics

Yasuhide Fukumoto *
Department of Applied Mathematics and Theoretical Physics,
University of Cambridge,
Silver Street, Cambridge CB3 9EW, UK

H. K. Moffatt
Isaac Newton Institute for Mathematical Sciences,
20 Clarkson Road, Cambridge CB3 0EH, UK

The motion of an axisymmetric vortex ring of small cross-section in a viscous incompressible fluid is investigated using a large-Reynolds-number asymptotic theory. Tung & Ting (1967) and Saffman (1970) considered the effect of decaying core-vorticity due to the action of viscosity. The vortex ring induces a local straining field on itself which deforms the core into an ellipse. The purpose of the present investigation is to elucidate the structure of strained core and its influence on the translation speed.

The method of matched asymptotic expansions has been developed to derive the velocity of a slender curved vortex tube in a fluid with and without viscosity (Tung & Ting 1967; Widnall *et al.* 1971; Callegari & Ting 1978; Klein & Majda 1991). However it is limited to the second-order curvature effect (Moore & Saffman 1972; Fukumoto & Miyazaki 1991). The self-induced straining field of a vortex ring makes its appearance at the second order in $\epsilon = (\nu/\Gamma)^{1/2}$, where ν is the kinematic viscosity of fluid and Γ is the circulation. In a different context, Moffatt *et al.* (1994, 1996) developed a large-Reynolds-number asymptotic theory to analyse the viscous core of a straight vortex tube subject to a weak strain. Combining these techniques, we

*Address after 1 January 1997: Graduate School of Mathematics, Kyushu University 33, Fukuoka 812–81, Japan

extend asymptotic expansions to a higher order and calculate the speed of a vortex ring up to $O(\epsilon^3)$. Our scheme is applicable also to the inviscid dynamics.

The outer solution is the potential flow induced by the ring. The inner solution of the Navier-Stokes equations is worked out in moving local cylindrical coordinates (r, θ), whose origin coincides with the centre of the core. The flow field was obtained up to $O(\epsilon)$ by Ting *et al.*, except for the axisymmetric part. This is shown to vanish on the basis of the solvability condition at $O(\epsilon^3)$. At $O(\epsilon^2)$, the streamfunction consists of the axisymmetric part and the part proportional to $\cos 2\theta$. The latter is found numerically. The solution for the former is available in a compact form once the axisymmetric vorticity distribution at $O(\epsilon^2)$ is determined by the solvability condition at $O(\epsilon^4)$. At $O(\epsilon^3)$, the streamfunction consists of the parts proportional to $\cos\theta$, $\sin\theta$ and $\cos 3\theta$. The $\cos\theta$ and $\sin\theta$ terms, along with the matching condition, determine the speed of the ring at $O(\epsilon^3)$.

In the absence of viscosity and assuming a uniform distribution of vorticity at leading order, we obtain Dyson's formula (1893) (see also Fraenkel 1972). The advantage of our procedure is that it is capable of capturing the global flow structure. Moreover, we have succeeded in calculating the expansion of the ring radius caused by the viscous drag.

References

Callegari, A. J. & Ting, L. *SIAM J. Appl. Math.* **35** (1978) 148–175.

Dyson, F. W. *Phil. Trans. Roy. Soc. Lond.* A**184** (1893) 1041–1106.

Fraenkel, L. E. *J. Fluid Mech.* **51** (1972) 119–135.

Fukumoto, Y. & Miyazaki, T. *J. Fluid Mech.* **222** (1991) 369–416.

Jiménez, J., Moffatt, H. K. & Vasco, C. *J. Fluid Mech.* **313** (1996) 209–222.

Klein, R. & Majda, A. J. *Physica* **49D** (1991) 323–352.

Moffatt, H. K., Kida, S. & Ohkitani, K. *J. Fluid Mech.* **259** (1994) 241–264.

Moore, D. W. & Saffman, P. G. *Phil. Trans. R. Soc. Lond.* A**272** (1972) 403–429.

Saffman, P. G. *Stud. Appl. Math.* **49** (1970) 371–380.

Tung, C. & Ting, L. *Phys. Fluids* **10** (1967) 901–910.

Widnall, S. E., Bliss, D. B. & Zalay, A. In *Aircraft Wake Turbulence and its Detection*, (ed. J. Olsen, A. Goldberg & N. Rogers, 1971), pp. 305–338. Plenum.

Recent development in the asymptotic theory of vortex breakdown

M. Schmitz
Institut für Technische Mechanik, RWTH Aachen
52056 Aachen, Germany

Rupert Klein
Fachbereich Sicherheitstechnik, Bergische Universität Wuppertal
D-42097 Wuppertal, Germany

Abstract

Slender vortex dynamics is dominated by two very different sources of nonlinearity. There is first the nonlinearity inherent in the motion of a vortex filament due to nonlocal self-induction and local curvature effects. Secondly, there is a highly nonlinear core flow, which produces local axisymmetric breakdown under suitable boundary and initial conditions. Both these aspects of slender vortex dynamics have been studied in the past using tools of matched asymptotic analysis. The well-known second non-axisymmetric mode of vortex breakdown appears to be due to an interaction of the core flow and the vortex centerline motion. Thus, it is a challenge to derive a unified formulation in the slender vortex limit which includes both the filament dynamics and nontrivial core structures.

One interesting issue in this context is the possibility of axial core structure variations. In this case, the sensitivity of the filament motion with respect to curvature varies along the vortex. Automatically, any large scale bending of the vortex centerline will lead to an additional deformation in the binormal direction. A concrete example would be a circular vortex ring, originally embedded in a plane: Axial core structure variations would amount to a bending of the filament in the third dimension out of the plane.

Klein & Ting [1], [2] have outlined the asymptotic theory for slender, three-dimensional vortex filaments with axial core structure variation, including vortex stretching and viscosity effects. While the equation of motion for the filament centerline is very similar to that for a vortex with axially homogeneous core, the core structure evolution equations reveal new insight. At the first order one recovers essentially the well-known slender vortex approximation for an inviscid, steady, axisymmetric and (locally) columnar vortex. It is also well known then, that the total head and circulation of the core flow are conserved along concentric surfaces of constant axial mass flow, Ψ. Unsteady terms, the diffusion of vorticity and vortex stretching appear at the next order as observed ealier in [3] for vortices with axially homogeneous cores. For axially varying cores these terms attain a non-standard form: The net effect of molecular transport is obtained as the axial average of the viscous terms along the stream surfaces. Thus, in the present one-time scale asymptotics, viscosity is nonlocal with respect to the axial coordinate.

In preparation of a comprehensive model that will include all the effects listed above, Schmitz [4] considered the special case of a straight vortex. He was able to reveal the detailed solution structure near Benjamin's critical point, which is widely believed to be closely related to vortex breakdown. The theory is based on the Bragg-Hawthorne or Squire-Long equation

$$\Psi_{yy} + \frac{1}{2}\Psi_{ss} = \frac{dH}{d\Psi} - \frac{1}{2y}\frac{dI}{d\Psi}$$

for the stream function $\Psi(s, y)$ of an axisymmetric columnar steady vortex. Here $y = r^2/2$ is proportional to the square of the radial coordinate, the axial coordinate s is scaled - like r - by a

typical core diameter and $H(\Psi)$ and $I(\Psi)$ are essentially the total head and circulation on stream surfaces $\Psi(s,y) = const.$.

For slender filaments, where variations along the s-coordinate are slow, a rescaling according to $\xi = \delta s$ is appropriate, with $\delta \ll 1$ a core size parameter. The second axial derivative then disappears from the leading order equation in δ and one is left with the slender vortex version

$$\Psi_{yy} = \frac{dH}{d\Psi} - \frac{1}{2\,y}\frac{dI}{d\Psi}$$

of the above equation up to leading and first order in δ. The solutions depend on the scaled axial coordinate ξ merely parametrically through suitable initial and/or boundary conditions in y. Depending on these conditions, a "critical point" may develop near some $\xi = \xi_{\text{crit}}$ where there is no continuation in ξ within the framework of the slender vortex theory (see e.g., [5]). When the inviscid core flow approaches the critical point, there is one particular coordinate rescaling which allows one to resolve the internal structure of the region adjacent to the critical point. This rescaling includes a perturbation ansatz about the critical flow state and a coordinate stretching of the axial coordinate by a non-integer power of δ. In this fashion the influence of the second axial derivative in the original Bragg-Hawthorne equation re-enters the picture, thereby resolving details of the breakdown of the leading order theory. The critical layer is characterized by an amplitude equation of the following type

$$\alpha_{\xi\xi} + a\,\alpha^2 = b\,\xi \ ,$$

with coefficients a, b that depend on the distributions $H(\Psi), I(\Psi)$. Under certain conditions it is possible to pass through criticality, whereas in other situations a strong singularity develops inside the critical layer at a finite location in terms of the rescaled inner coordinate ξ. In this case, the critical layer terminates with a flow region whose structure precludes the application of any slenderness approximation.

This lecture will summarize the generalized asymptotic theory involving axial core structure variations on a three-dimensional slender vortex filament. It will describe in some detail the critical layer theory. Results include a comparison with direct numerical simulations done at Aerodynamisches Institut, RWTH Aachen.

References

[1] Ting L., Klein R., "Viscous Vortical Flows", Lecture Notes in Physics, **374**, Springer-Verlag, (1991).

[2] Klein R., Ting L., "Vortex filaments with axial core structure variation", Appl. Math. Lett., **5**, 99–103, (1992).

[3] Callegari A., Ting L., "Motion of a curved vortex filament with adecaying vortical core and axial velocity", SIAM J. Appl. Math., **35**, 148–175, (1978).

[4] Schmitz M., "Axiale Entwicklung der Kernstruktur schlanker Wirbelfäden", Dissertation, RWTH-Aachen, (1995)

[5] Benjamin T.B., "Some developments in the theory of vortex breakdown", J. Fluid Mech., **28**, 65–84, (1967)

The complete first order expansion of a slender vortex ring

Margerit Daniel

Dynamic equations for the axisymmetric part of the velocity field and for the equation of motion of a slender vortex ring are given at first order. This is the correction to the known leading order given by Callegari & Ting [1].

Length scales of the vortex ring different from the thickness δ (that is to say : the curvature radius, the length of the ring,...) are of the same order L with $\delta/L = O(\varepsilon) << 1$. The central curve is described parametricaly with the use of a function $\mathbf{X} = \mathbf{X}(s,t)$. A local curvilinear co-ordinate system (r,φ,s), with a frame $(\mathbf{r},\theta,\tau)$, is introduced near this central curve [1]. Consequently there is an *outer problem* defined by the *outer limit* : $\varepsilon \to 0$ with r fixed, which describes the situation far from the central line and an *inner problem* defined by the *inner limit* : $\varepsilon \to 0$ with $\bar{r} = r/\varepsilon$ fixed, which describes the situation near the central line.

The velocity is decomposed as follows : $\mathbf{v}(r,\varphi,s,t,\varepsilon) = \overset{\circ}{\mathbf{X}}(s,t,\varepsilon) + \mathbf{V}(r,\varphi,s,t,\varepsilon)$ where $\mathbf{V} = u\mathbf{r} + v\theta + w\tau$ and $\overset{\circ}{\mathbf{X}} = \dfrac{\partial \mathbf{X}}{\partial t}$. The following forms are chosen for the inner expansions of the velocity field :

$$
\begin{aligned}
u^{inn} &= && u^{(1)}(t,\bar{r},\varphi,s)+... \\
v^{inn} &= \varepsilon^{-1}v^{(0)}(t,\bar{r},s) + && v^{(1)}(t,\bar{r},\varphi,s)+... \\
w^{inn} &= \varepsilon^{-1}w^{(0)}(t,\bar{r},s) + && w^{(1)}(t,\bar{r},\varphi,s)+...
\end{aligned}
$$

with an expression of the central curve of the form :

$$\mathbf{X} = \mathbf{X}^{(0)}(t,s) + \varepsilon\ \mathbf{X}^{(1)}(t,s)+...$$

Callegari & Ting [1] considered the case where $v^{(0)}, w^{(0)}$ are independent of s so that some compatibility conditions are satisfied. They deduced evolution equations for $v^{(0)}, w^{(0)}$ from Navier Stokes second order equations, and those for $\mathbf{X}^{(0)}(t,s)$ from the matching of Navier Stokes equation with the outer Biot & Savart equation.

In the same way that first order Navier Stokes equations give compatibility equations for $v^{(0)}, w^{(0)}$, second order Navier Stokes equations give compatibility equations for the axisymmetric part $v_c^{(1)}, w_c^{(1)}$ of $v^{(1)}, w^{(1)}$. These equations are automatically satisfied if $v_c^{(1)}, w_c^{(1)}$ are assumed to be independent of s. Then evolution equations for $v_c^{(1)}, w_c^{(1)}$ can be extracted from third order Navier Stokes equations. We did this with the use of symbolic calculus (on maple) in the following way : we obtained third order Navier Stokes equations, then we assumed that $v_c^{(1)}, w_c^{(1)}$ are independent of s, and finally we carried out the θ-

Daniel.Margerit@ensem.u-nancy.fr
http://www.ensem.u-nancy.fr/Ensem/laboratoires/lemta/daniel.html

average and s-average of the axial and circumferential components of the third order momentum equations using the third order continuity equation to eliminate $u_c^{(2)}$. Lots of terms vanished and we found equations for $v_c^{(1)}, w_c^{(1)}$. Note that Fukumoto & Miyazaki ([2] page 378) postulated $v_c^{(1)} = 0$, kept $w_c^{(1)}$ dependent of s, and did not have equation for $w_c^{(1)}$.

These equations for $v_c^{(1)}, w_c^{(1)}$ are linked to $\mathbf{X}^{(1)}(t,s)$, so we need an evolution equation for $\mathbf{X}^{(1)}$ to have a closed system of equations for the first order solutions $v_c^{(1)}, w_c^{(1)}$ and $\mathbf{X}^{(1)}$. The best attempt to find this equation is by Fukumoto & Miyazaki ([2] page 382), where contribution from Navier Stokes equations up to order ε^1 have been found in order to performed the matching. We may note that in their expression the term due to first order curvature $K^{(1)}$ is missing. Moreover, their expression for $\mathbf{X}^{(1)}$ is not complete, as local and non-local (named $\mathbf{Q}$ in [2]) contribution from Biot & Savart integral are given only up to order ε^0 in Fukumoto & Miyazaki ([2] page 373) and Callegari & Ting ([1] page 173), while we obviously need order ε^1 to obtain complete and correct equation for $\mathbf{X}^{(1)}$.

In order to find these lacking terms we performed the outer limit in Biot & Savart integral up to order ε^1 and obtained the expansion of this order ε^1 term when r vanished. In order to check this result, we performed the inner expansion of the Biot & Savart integral up to order ε^1 [3] and obtained its expansion when $\bar{r} = r/\varepsilon$ becomes infinite. This gives the same result as with the outer approach. We then did the matching and found lacking terms in equation of $\mathbf{X}^{(1)}$.

We therefore have a closed and complete system of dynamic equations for first order terms $v_c^{(1)}, w_c^{(1)}$ and $\mathbf{X}^{(1)}$ of a slender vortex ring. Note that equations to this order are able to describe the evolution of Helicity.

References :

[1] CALLEGARI,A.J. & TING,L. 1978 Motion of a curved vortex filament with decaying vortical core and axial velocity, *SIAM J. Appl. Math.***35** (1), 148-175

[2] FUKUMOTO,Y. & MIYAZAKI,T. 1991 Three dimensional distortions of a vortex filament with axial velocity, *J. Fluid Mech.* **222**, 369-416

[3] MARGERIT,D. & BRANCHER,J.P. On the velocity field and the motion of a non-circular slender vortex ring, (in submission)

Daniel.Margerit@ensem.u-nancy.fr
http://www.ensem.u-nancy.fr/Ensem/laboratoires/lemta/daniel.html

SELF-INDUCED MOTION OF HELICAL VORTICES

P.A. Kuibin, V.L. Okulov

Institute of Thermophysics
Lavrentiev Ave 1, 630090 Novosibirsk, RUSSIA
Tel. 7-383-2-357128, Fax. 7-383-2-357880
E-mail: aleks@otani.thermo.nsk.su.

Yet in 1867 Lord Kelvin had derived a formula for self-induced velocity for simplest canonical shape of curved vortex - vortex ring. The another canonical shape - the helical one - is more complex object of studying (it is characterized not only by the curvature but also by the torsion unlike the ring filament). For the helical geometry the result that may be considered as complete is the result obtained again by Kelvin in 1880 for one particular case of weakly curved column-like vortex. The further investigations were limited as a rule by consideration of thin vortex filaments. Their self-induced velocity was being determined through the velocity of vortex ring with equivalent curvature (Widnall, 1972; Moore & Saffman, 1972). The additional terms arising due to different geometry were evaluated numerically. The problem is to determine a constant that remains after separation of singularities in the formula of asymptotic expansion of binormal velocity component in the neighbourhood of helical vortex filament.

The most complete analysis of the constant behaviour was made numerically by Ricca (JFM, 1994) by means of velocity calculation at finite distance from filament for three limited intervals of helix's pitch variations.

The present work is devoted to analytic derivation of the constant dependencies on torsion that determines a full expansion of the velocity field induced by helical vortex filament as in unbounded space as well as in cylindrical tube.

It is shown in Batchelor's "Introduction to Fluid Dynamics" that velocity field near the curved vortex filament may be written as sum of pole, logarithmic singularity and constant independent of distance from filament. The first of these terms does not influence on self-induced motion of vortex. The second term depends on circulation, curvature and core size and the dependence on torsion is hidden in the last term. The formula for self-induced velocity look out analogously but without the first term and with distance replaced by core radius. Of course the constants may be different. To find the concrete expansion of the velocity field near the helical vortex filament let us use an exact solution forthe velocity field induced by infinitely thin helical vortex filament in tube (Borissov, Kuibin, Okulov, Acta Mechanica, 1994). This solution was represented as infinite seria of modified Bessel's functions and coincided with Hardin's solution (Physics of fluids, 1982) for unbounded case. To separate the singularities we use the asymptotic representation of modified Bessel's functions with high value of indices. As a result the constant is written as infinite seria. Nevertheless for the cases of small and large pitches of helix asymptotic formulas are derived. Moreover a simple expression written through elementary functions is suggested for the whole range of the torsion variations.

The problem on determination of self-induced velocity is shown to be connected with the problem described above by very simple interrelation: for the case of thin helical vortex with uniform vorticity distribution in the core the constant differs from constant of velocity expansion by addend 1/4. This correlation is true for the case of weakly curved column-like-vortex too and approximately valid for any intermediate relations of vortex sizes. Thus the self-induced velocity for any uniform helical vortex is found.

The obtained solution allowed to define the frequency of vortex precession in cylindrical tube. The last was found to be proportional to binormal self-induced velocity. Derived formula was tested with measurements results known from literature. The comparisons show that the coincidence is good and all the terms of the formula: corresponding to logarithmic singularity, walls influence, contribution due to nonzero velocity on tube axis and contribution of constant itself may be of the same order and all they should be accounted.

This work was partially supported by Russian Foundation of Basic Research (grant N 94-02-05812) and by joint foundation INTAS-RFBR (grant N 95-IN-RU-1149).

SESSION 2

NUMERICAL SIMULATION

This Page Intentionally
Left Blank

Simulation of Vortex-dominated Flow

Kunio Kuwahara

Institute of Space and Astronautical Science

Vortex structure behind a bluff body looks very complicated because of the separated vortices. Many experimental investigations have been done. But nobody yet can tell definitely the dominant structure even for a simple sphere. On the other hand, in two dimensions, Karman vortex street is known to be most dominant.

To find the essential three-dimensional structures, we computed these flows extensively and visualized them. From these computations, in this paper, we suggest the most important structure behind a bluff body is the U-shape vortex attached partially to the body and two tail flows down. Computation is now easier and more effective to see those phenomena than experiments.

Computational method

The governing equations are the unsteady incompressible Navier-Stokes equations . For high-Reynolds-number flows, time-dependent computations are required owing to the strong unsteadiness.
These equations are solved by a finite-difference method. The numerical procedure is based on the MAC method. The pressure field is obtained by solving the Poisson equation.

Two types of grid generation system are employed. The one is body-fitted coordinates system, and the other is Cartesian coordinate system with equal distance mesh.

All the spatial derivative terms are represented by the central difference approximation except for the convection terms. For the convection terms, the third-order upwind difference is used. This is the most important point for high-Reynolds-number computations.

There is another important problem in high-order upwind schemes. That is, the accuracy decreases when the flow direction is not well parallel to one of the coordinate lines.

To overcome this problem we introduced the multi-directional upwind method. A non-staggered mesh system is employed where the defined positions of velocity and pressure are coincident.

For the temporal integration of the Navier-Stokes equations, the Crank-Nicolson purely implicit scheme is utilized. This scheme has second-order accuracy in time. These equations and the Poisson equation are iteratively solved at each time step by the successive overrelaxation (SOR) method.

Results

Figure 1 shows the flow past a circular cylinder with slanted base set parallel to the flow. Instantaneous streamlines are visualized. Typical U shape vortex is clearly seen. This strong vortex makes the drag coefficient very high. If the angle of the slanted base increases, the vortex breaks and the force acting on the base decreases sharply.

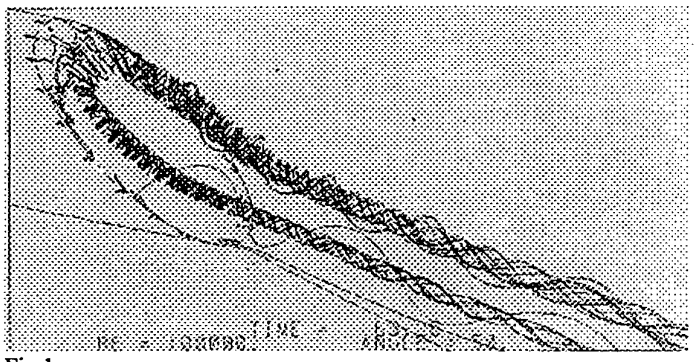

Fig.1

Figure 2 shows the U shape vortex on the lee side of the ellipsoid. Imaginary particle traces on a sectional planes are visualized.

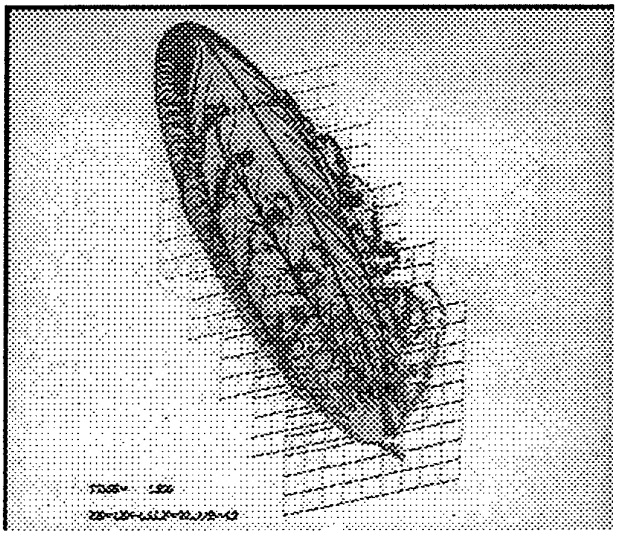

Fig.2

Figure 3 shows the vortex on a delta wing at angle of attack 30 degrees. The U shape vortex is the main cause of the lift of the wing.

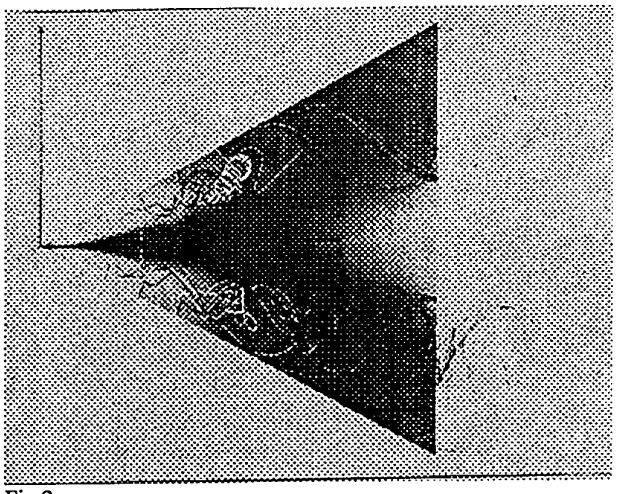

Fig.3

Figure 4 shows the U shape vortex behind a car.

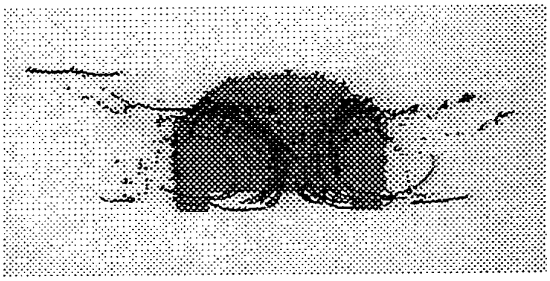

Fig.4

Fig.5 is the flow past a sphere. It looks complicated but detailed consideration after well-visualizing the flow, the essential structure is also U shape vortex. The symmetry is too good and the beginning point of the U shape vortex is always changing, therefore it looks complicated.

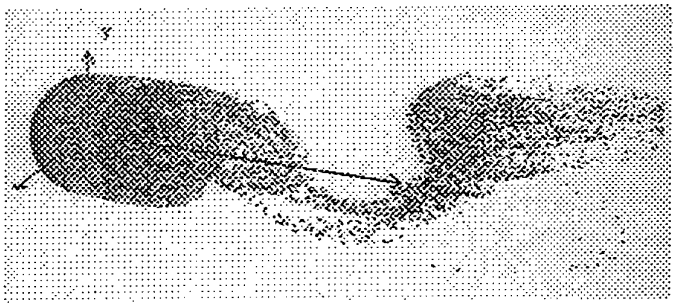

Fig.5

The final example is U-shape vortex formation behind a square cylinder with a slanted base.

Conclusions

From those examples it is becoming clear that behind a bluff body the U-shape vortex plays the most important role in the flow.

It is very difficult to see those structures by experiments. Computational approach is the most appropriate means of investigation.

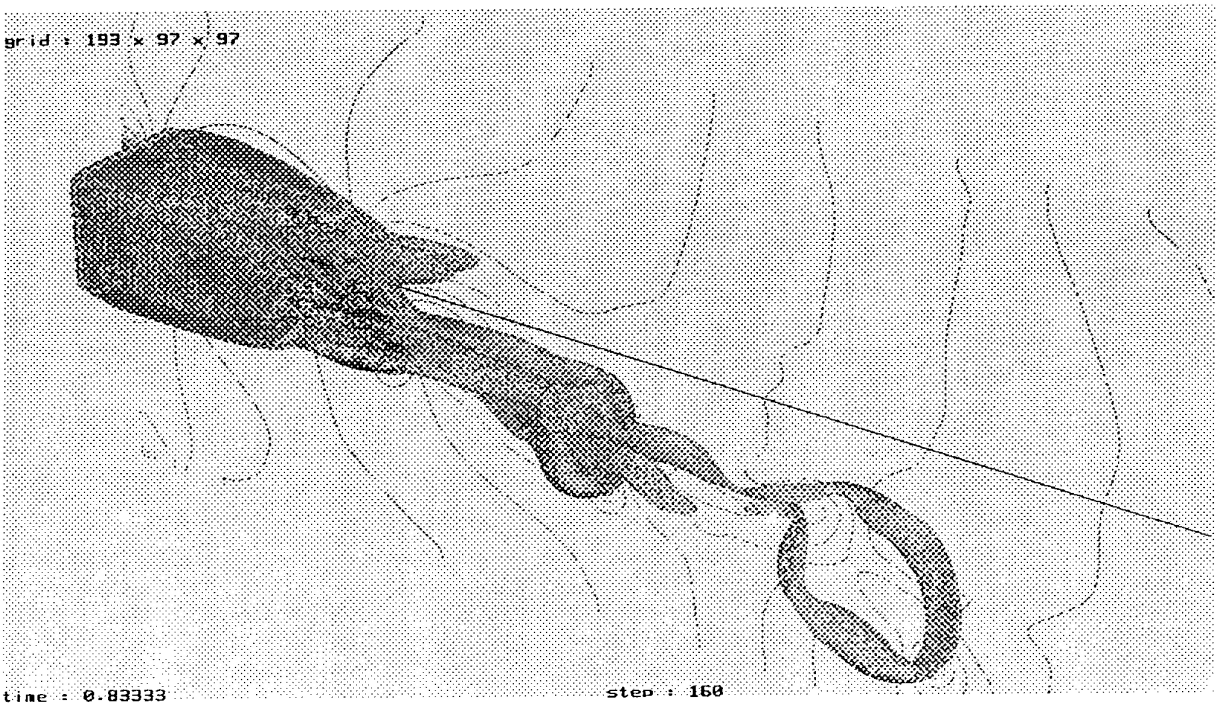

Optimized vortex element schemes for slender vortex simulations

Rupert Klein
Fachbereich Sicherheitstechnik, Bergische Universität Wuppertal
D-42097 Wuppertal, Germany

Omar M. Knio
Department of Mechanical Engineering, The Johns Hopkins University
Baltimore, MD 21218, USA

Abstract

Vortex element numerical schemes are designed for application to flows with highly concentrated vorticity. These schemes are based on discretization of the vorticity field into spherically smoothed Lagrangian elements of overlapping cores, and transport of these elements along particle trajectories. The advantages of this approach stem from the Lagrangian discretization which naturally concentrates computational elements into regions of high vorticity, and from the Lagrangian transport procedure which minimizes numerical diffusion.

Application of vortex element schemes to the simulation of slender vortex filaments is generally faced with two diffculties. The first is due to the extreme concentration of vorticity around the vortex filament centerline, which generally requires a very narrow spacing between vortex elements. As a result, very small time steps must be used that are by an order of magnitude smaller than normally required by the geometrical evolution of the filament centerlines. The second problem is due to the resolution of the time dependent vortex core structure, which would lead to a prohibitively expensive computation in terms of storage and computation time.

One ad hoc ansatz for the latter problem is to use a single chain of vortex elements and to let the numerical vortex element smoothing funtion represent the vortex core [1]. Klein & Knio [2] show that in the resulting thin-tube model $O(1)$ errors in the prediction of the vortex filament centerline motion occur. A detailed asymptotic analysis of both the numerical and the physical vorticity structures in the vortex core reveal the origin of the discrepancy and naturally lead to a correction of the scheme. These ideas are extended by Klein, Knio & Ting [3] to include nontrivial vortex stretching as well as the effects of viscosity.

While the problem of the core structure representation is thus resolved, the issue of temporal stiffness remains at this stage. This lecture will summarize recent efforts by the authors aiming at overcoming the time step restriction. Various approaches will be presented and evaluated. The authors propose, in particular, two techniques both of which have the following desirable features:

1. Rather than evaluating explicitly the leading curvature-binormal term in the filament equation of motion,

$$\dot{\mathbf{X}} = \frac{\Gamma}{4\pi}\kappa(\ln(\frac{1}{\delta}) + C)\,\mathbf{b} + \mathbf{Q}^f \ , \tag{1}$$

the proposed scheme includes these curvature effects automatically and accurately through a judicious choice of the numerical vortex element core size parameter. In (1) Γ is the vortex filament total circulation, κ its local curvature, $\mathbf{b}$ the local binormal unit vector, C a parameter depending on the detailed core vorticity distribution, $\delta \ll 1$ the core size parameter, and $\mathbf{Q}^f$ the so-called finite part of the line Biot-Savart integral.

2. The temporal stiffness is overcome. Thus, the time step may be chosen to resolve the dynamics of the filament centerline motion. The extremely large circumferential velocities in the vortex

core, which do not contribute directly to the overall filament evolution, do not influence the numerical stability and/or the numerical time step.

In our first ansatz, element velocities are evaluated twice, based on two different and relatively large values of the numerical core size parameter. The results are then (logarithmically) extrapolated obtain to the velocity associated with the physically correct value of the core size and core structure parameter. The storage and time step requirements for this scheme are expected to scale with those associated with the two larger values of the core size used, rather than with the smaller physical one.

The second ansatz first introduces a discrete representation of the filament centerline that has no higher resolution than required to satisfy numerical accuracy requirements regarding the filament geometry representation. Most of the discrete integration of the Biot-Savart integral uses this coarse mesh of elements. Only in the immediate vicinity of an element whose velocity is being computed it is necessary to employ a more refined representation of the vorticity field. Here we reconstruct the vorticity distribution that would be available in a high resolution computation by placing virtual overlapping vortex elements along a limited curve segment embracing the element considered. For this purpose, the centerline is reconstructed using a suitable high-order interpolation scheme (see e.g. [2]). The scheme has storage and computation time requirements scaling with the desired numerical resolution of the centerline geometry, rather than with the (often times) much smaller vortex core size.

The presentation will contrast the two methods outlined above with existing alternatives in the literature. Comparison with high-resolution computations as in [2], [3] will allow us to quantify the performance of the proposed schemes. Applications will include stretched vortex filaments with and without the influence of viscosity.

References

[1] O.M. Knio, A.F. Ghoniem, "Numerical study of a three-dimensional vortex method", J. Comput. Phys. **86**, 75, (1990).

[2] R. Klein & O.M. Knio, "Asymptotic vorticity structure and numerical simulation of slender vortex filaments," *J. Fluid Mech.* **284**, 275, (1995).

[3] R. Klein, O.M. Knio & L. Ting, "Representation of Core Dynamics in Slender Vortex Filament Simulations," *Phys. Fluids* **8**, 2415, (1996).

A new approach to the modeling viscous diffusion in vortex element methods

B.Yu. Scobelev and O.A. Shmagunov
Institute of Theoretical and Applied Mechanics of the Russian Academy of Sciences, Novosibirsk, 630090, Russia

Vortex element methods become more and more widely applied to modeling various flows. Ideal vortex elements describe sufficiently well integral characteristics of separated flows around various aircraft and large-scale turbulent structures [1,2]. To describe fine-scale turbulence, a viscosity needs to be taken into account. At present time there are various approaches to this problem [1,3,4], which use the equation of vortex viscous diffusion, in one form or another. In the present paper the totally different approach is suggested.

The main idea of the suggested method is as follows. As known, in transition from a circular vortex to a point one the vortex area tends to zero, and the vorticity tends to infinity in such a way that in the limit the vortex circulation remains finite. Let us take a circular vortex in a viscous fluid and perform the passage to the limit of point vortex. To keep the contribution of the viscous term into the motion equations finite, let us turn the initial viscosity to zero in such a way that integral contribution of the viscosity term corresponded to a specified viscosity. As a result, we will have an opportunity to describe a viscous fluid flow by the motion of ideal point vortices. This opportunity is realized by correcting the integral characteristics of the point vortices system, such as energy and vorticity dispersion.

The ideas described above are realized in a numerical algorithm for two-dimensional flows. This algorithm is based on the following two hypotheses.

Hypothesis I

The motion of a system of ideal point vortices simulates the viscous flow if the regular part of the vortex energy E satisfies the following equation

$$\frac{dE}{dt} = -\mu\sum_{i=1}^{N}\Gamma_i^2; \qquad E = \rho\left[\frac{5}{32\pi}\sum_{i=1}^{N}\Gamma_i^2 - \frac{1}{4\pi}\sum_{i\neq j}^{N}\Gamma_i\Gamma_j \ln|r_i - r_j|\right] \qquad (1)$$

Γ_i, $r_i = (x_i, y_i)$ *are circulations and coordinates of N point vortices.*

Hypothesis II

Both the vorticity discretization (passage from continuous distribution to point vortices) and discretization of the motion equations are equivalent to the passage to certain non-inertial coordinate systems. Therefore, obtaining the results in the initial, physical coordinate system needs the performing of inverse transformation of the coordinates and time after each step of numerical integration of the motion equations. These transformations are determined by conditions.

$$\Delta E = -\nu\Delta t\sum_{i=1}^{N}\Gamma_i^2; \qquad \Delta L^2 = 0; \qquad L^2 = \sum_{i=1}^{N}\Gamma_i(x_i^2 + y_i^2) \qquad (2)$$

While obtaining equations (1), (2), the expressions for invariants of nonviscous vortex flow [5] and equations describing the invariants variation under the viscosity [6,7] were used.

The calculation of the dependence of the Strouhal number for the von Karman vortex street on the Reynolds number for a transverse flow around a plate was carried out by the method [1]. Example of the von Karman vortex streets at the dimensionless time $t = 70$ is shown in Fig. 1 for $Re = 100$. Comparison of the Strouhal number Sh values with experimental data [8] is shown in Fig. 2. The circles denote the results of the numerical simulation.

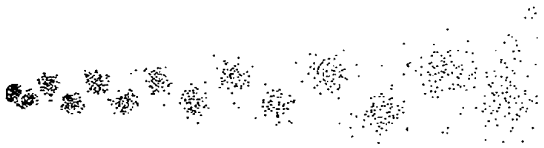

Fig. 1

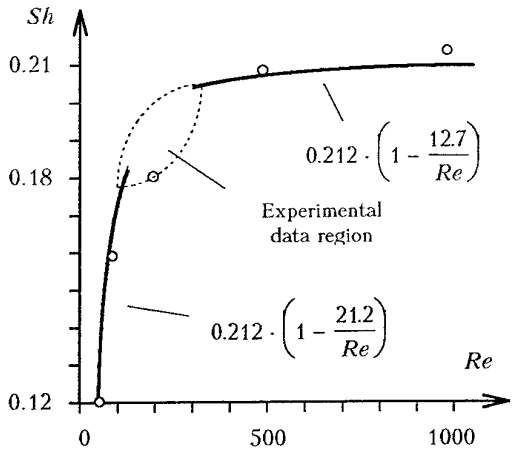

Fig. 2

Further, numerical calculation of motion of point vortices system modeling a circular vortex (see Fig. 3) was carried out.

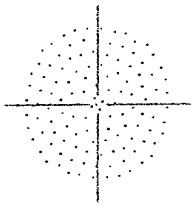

Fig. 3

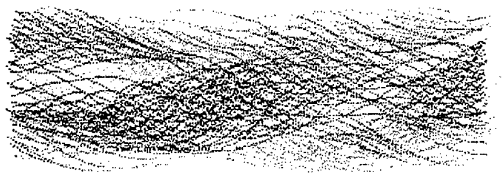

Fig. 4

The vorticity diffused due to the viscosity from region of point vortices was taken into account with the help of a virtual point vortex. Circulation of this vortex was equal to total loss in point vortices circulation under the influence of viscosity and had an opposite sign. Coordinates of the virtual vortex were obtained from the condition of conservation of vorticity center coordinates.

Fig. 4 shows a quasi-three-dimensional picture, which illustrates the result of the simulation at Re=100 and a time period $0 < t_1 < t < t_2$ (Reynolds number Re was gained from radius of circular vortex and circulation velocity). The Fig. 4 was obtained under assumption that for each moment t there is a correspondent coordinate $z=Vt$, where V is a some velocity.

In the future, we plan to extend our concept of viscosity to three-dimensional flows.

References

[1] Belotserkovsky S. M., Lifanov I. Method of Discrete Vortices. CRC Press, USA, 1994.
[2] A. Leonard, *Annu. Rev. Fluid Mech.* **17**, 523 (1985).
[3] Chorin A. J. *J. Fluid Mech.*, **57**, 785 (1973).
[4] Winckelmans G. S., Leonard A. *J. Comp. Phys.*, **109**, 247 (1993).
[5] Batchelor G. K. An Introduction to Fluid Dynamics. Cambridge at the University Press, 1970.
[6] Moffat H. K. *J. Fluid Mech.*, **35**, 117 (1969).
[7] Shavaliev M. Sh. In: Mechanics of Inhomogeneous and turbulent flows. Moscow, Nauka, 1989, p.63-69. [Russian]
[8] Roshko A. NACA TN, N2913, 1953.

Simulation of Vortex Ring Interaction

M. Meinke, J. Hofhaus, A. Abdellfattah
Aerodynamisches Institut, Wüllnerstraße zw. 5 und 7, 52062 Aachen, Germany
+49-241-805410, meinke@aia.rwth-aachen.de

First, a numerical solution of the Navier-Stokes equations for incompressible flows is used to study the interaction of isolated vortex rings in unbounded domains. The algorithm is based on a pressure correction scheme, in which the Poisson equation for the pressure is solved with a preconditioned conjugate gradient method. The preconditioning method applied is an incomplete lower-upper decomposition. The integration in time is carried out with an explicit Adams-Bashforth scheme. The algorithm is efficiently implemented for a non-staggered moving mesh with a momentum interpolation on vector-parallel computers. Hill's solution of the Euler equations for vortex rings is used as an initial condition of the velocity field. The time development of two vortex rings approaching each other under an angle of 40-90 degrees is simulated on a grid, moving with the propagation velocity of the vortex rings. It is known that the vortex rings connect to a single ring and then reseparate provided the interaction angle is large enough. For a Reynolds number of 500 this angle is determined to be $\approx$70 degrees. The results for an interaction angle of 90 degrees is depicted in Fig. 1: shown is a surface of constant pressure for different time levels, which demonstrate the connection and reseparation of the vortex rings. A more detailed analysis of the flow field will be presented at the symposium.

Secondly, a solution of the Navier-Stokes equations for compressible flows is used to simulate the generation and connection of vortex rings in a bounded domain, a cylinder of a piston engine. In this case an explicit time-stepping scheme with a centrally discretized convective and viscous terms is applied on general curvilinear coordinates in block-structured grids. An additional equation for the cell volume is integrated to account for the time varying grid coordinates. Two vortex rings are generated by the flow through the open intake valves. During the intake stroke the vortex rings grow in size and strength. At a crank angle of about 100 degrees, the vortex rings connect to a single vortex, which is deformed by the surrounding velocity field. Different visualization techniques were applied in order to extract the flow topology from the time dependent solution. In Fig. 2 the flow during the early intake stroke with two ring vortices below the intake valves is shown. Detailed results, including vortex lines and other characteristics will be presented at the symposium.

References

[1] Hill. On a Spherical Vortex. *Phil. Trans. A*, 1894.

[2] J. Hofhaus, M. Meinke, and E. Krause. Parallelization of Solution Schemes for the Navier-Stokes Equations. In E.H. Hirschel, editor, *Flow Simulation with High-Performance Computers II*, volume 52 of *Notes on Numerical Fluid Mechanics*, pages 102–116. Vieweg Verlag, Braunschweig, 1996.

[3] Jörn Hofhaus. *Numerische Simulation reibungsbehafteter instationärer inkompressibler Strömungen – Vergleich zweier Lösungsansätze.* Dissertation, Aerodynamisches Institut der RWTH-Aachen, Dezember 1996.

[4] T. T. Lim. An Experimental Study of a Vortex Ring Interacting with an Inclined Wall. *Experiments in Fluids*, 7:453–463, 1989.

[5] M. Meinke, A. Abdelfattah, and E. Krause. Simulation of Piston Engine Flows in Realistic Geometries. In *15th ICNMFD, June 24-28, Monterey, California*, 1996.

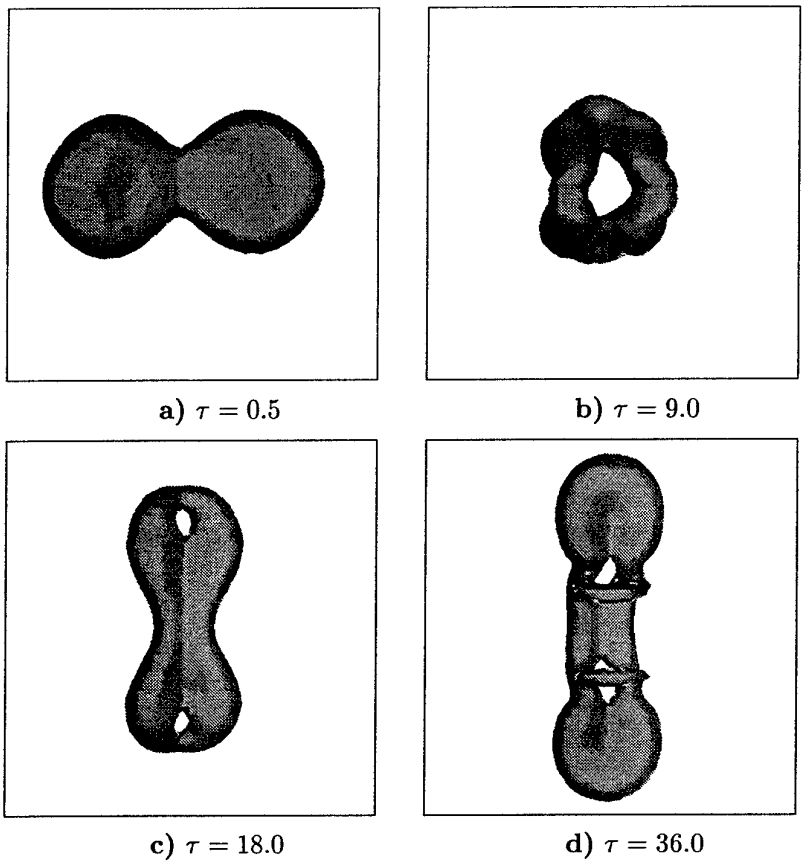

Figure 1: Numerical simulation of the collision of two vortex rings. Surface of constant pressure, the Reynolds number is 500.

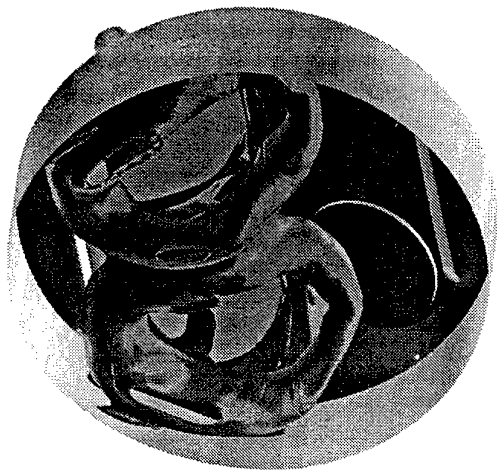

Figure 2: Ring vortices below the intake valves of a piston engine. Surface of constant pressure at a crank angle of 60 degrees.

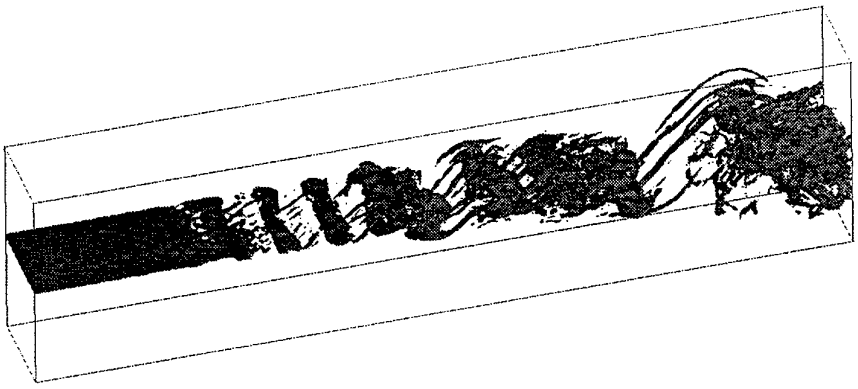

Figure 1: LES of a mixing layer forced upstream quasi two-dimensionally; the vorticity modulus is shown.

LARGE-EDDY SIMULATIONS OF LONGITUDINAL VORTICES IN SHEAR FLOWS

By Pierre COMTE and Marcel LESIEUR[1]

LEGI/IMG, BP 53, 38041 Grenoble-Cedex 09, France.

Presented at the IUTAM Symposium on Dynamics of Slender Vortices, Aachen, August 31st September 3rd, 1997.

We first recall the philosophy of large-eddy simulations followed in Grenoble, with the spectral eddy viscosity and conductivity in Fourier space, and the family of structure-function models (filtered or selective) in physical space (see Lesieur and Métais, 1996, Ann. Rev. Fluid Mech., **28**, and Lesieur, 1997, *Turbulence in fluids*, third updated and revised edition). These models are used in the present work to study various shear flows.

In the incompressible temporal mixing layer case, we start initially from a hyperbolic tangent velocity profile, to which a small random perturbation is superposed. The molecular Reynolds number is infinite. If the perturbation is quasi two-dimensional, intense longitudinal hairpins stretched between the Kelvin-Helmholtz spiral vortices are found. Their magnitude is several times the maximum initial spanwise vorticity. We explain the formation of these hairpins by the exponential amplification, in the first principal axis of deformation direction, of the vorticity existing in the stagnation zones. If the initial perturbation is three-dimensional, on the other hand, one shows the formation of dislocated Kelvin-Helmholtz vortices. In the latter case, the statistics of the turbulent flow are in very good agreement with the experiments. We consider now a spatially-growing mixing layer, initiated upstream by a thin vortex sheet of vorticity ω_i, with a random forcing regenerated at each time step. When the upstream forcing is quasi two-dimensional, one recovers the same structure of intense thin hairpins stretched by quasi 2D Kelvin-Helmholtz vortices, as in the

[1]also *Institut Universitaire de France*

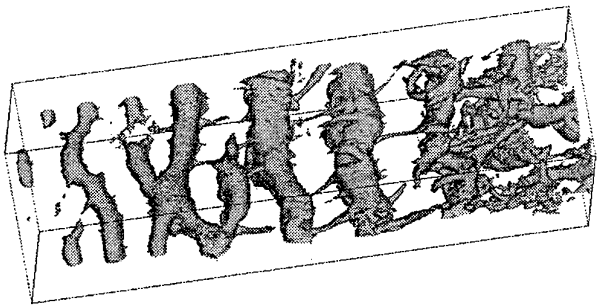

Figure 2: Same as Figure 1, but with a three-dimensional upstream white-noise forcing, low-pressure field.

above temporal simulations, and the spatial mixing-layer experiments of Bernal and Roshko (1986, J. Fluid Mech., **170**). This is shown on Figure 1, presenting the vorticity-modulus field at a threshold $(2/3)\omega_i$. Colour animations indicate also that longitudinal vortices of same sign are subject to pairing. More specifically, these vortices turn around each other by mutual induction and merge, exactly as the primary Kelvin-Helmholtz vortices. It is by this pairing mechanism of spanwise and longitudinal vortices that self-similarity is preserved in the spatial mixing layer. When the forcing is a three-dimensional random white noise, helical pairing occurs upstream, as indicated by the low-pressure maps of Figure 2. Further downstream, it seems that quasi two-dimensionality is restaured, with stretching of longitudinal vortices. Calculations in longer domains are necessary, in order in particular to know if the flow is chaotically attracted between quasi 2D and helical-pairing states.

Longitudinal vortices stretched between Karman vortices of opposite sign are also found in LES of a plane wake. In a round jet with an upstream velocity close to a top hat and forced by a 3D white noise, we find in the developed region a double-helix structure, due to an out-of-phase reconnexion of vortex rings. Such a phenomenon is the axisymmetric equivalent of the helical pairing observed in the mixing layer. This double helix is intermittently replaced by a simple helix or even by quasi 2D vortex rings stretching longitudinal hairpins, as in the quasi 2D mixing layer (Urbin and Métais, 1996, submitted to Phys. Fluids).

We study finally a boundary layer at Mach 0.5, spatially developing upon an adiabatic flat plate. The upstream flow corresponds to a TS wave, to which is superposed a 3D white-noise perturbation of same amplitude. The simulation shows first the formation at a critical level of big quasi two-dimensional billows of relatively low pressure and high vorticity, travelling with the wave velocity. Transition occurs through the growth of a staggered mode developing on the "TS billows", accompanied with weak low- and high-speed streaks for the longitudinal velocity at the wall. After transition, local Kelvin-Helmholtz instabilities arise above the low-speed regions, resulting into extremely assymmetric longitudinal hairpins ejected away from the wall (see Ducros et al., 1996,

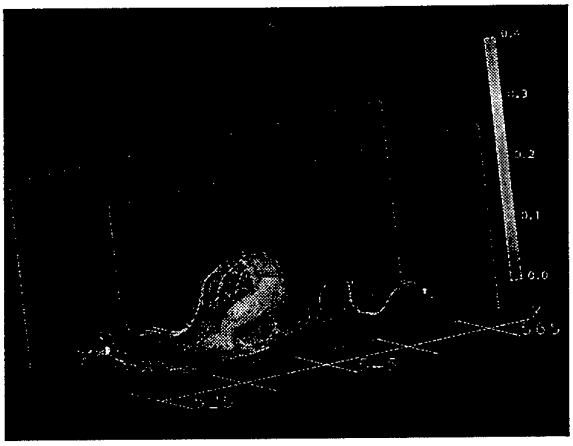

Figure 3: LES of a spatially-developing weakly-compressible boundary layer. Hairpin vortex ejected above the wall.

J. Fluid Mech., **326**). Such a hairpin is shown on Figure 3. We have checked that the vorticity thus produced in these hairpins is very weak (≈ 0.1 in wall units for the modulus), so that they cannot correspond to intense longitudinal vortices, contrary to what many authors claim. In the wall region, the highest vorticity fluctuations (of order 2) are spanwise and at the wall, under the high-speed regions.

Aknowledgements: this work was sponsored by Institut Universitaire de France, CEA, CNRS, INPG and UJF.

This Page Intentionally
Left Blank

Numerical simulation of nonlinear interactions in subsonic and supersonic free shear layers.

A.N. Kudryavtsev, D.V. Khotyanovsky

Institute of Theoretical and Applied Mechanics, Novosibirsk 630090, Russia

Instabilities and nonlinear wave phenomena in high-speed shear layers are important in various fluid dynamics problems, such as noise generation, supersonic combustion, gasdynamic lasers, astrophysical jets and many others. It is known from investigations of linear stability of compressible shear layer that increasing the relative Mach number $M_r = \frac{U_1 - U_2}{(a_1+a_2)/2}$ of mixing streams causes essential changes in the instability mechanism. Here U_1 and U_2 are velocities of the streams, a_1 and a_2 are sound speeds in them. The 2D Kelvin-Helmholtz instability dominates at the moderate M_r. With increasing M_r higher than a critical value the subsonic Kelvin-Helmholtz waves become stable and the flow dynamics is governed by the development of supersonic unstable modes.

In the present study the direct numerical solution of two-dimensional Euler and Navier-Stokes equations at M_r up to 3.0 is carried out to research nonlinear development of both instability modes. We simulate a temporal as well as a spatial evolution of the shear layer. In the former case streamwise periodicity of the flow is assumed and at the initial moment it forced by the disturbances that is a superposition of the most unstable linear eigenfunction with its subharmonics. In simulations of the spatially developing shear layer the disturbances are introduced at the inflow boundary of the computational domain. This approach seems to be more relevant and physically consistent though it demands much more computer resources.

An inherent feauture of supersonic shear layers dynamics is the formation of shocks. Consequently, numerical method used should provide robust shock capturing in addition to high resolution when wavelike processes are simulated. We used the essentially non-oscillatory (ENO) scheme of the third order [1] or the weighted ENO scheme of the fifth order [2] to approximate the convective terms, and respectively the second or the fourth order central differences for the diffusive terms.

The typical flow patterns at various relative Mach numbers resulted from simulations of the temporal evolution are shown in Fig. 1. Pattern at $M_r = 1.0$ closely resembles its incompressible counterpart. However, at $M_r = 1.5$ closed regions where the velocity of fluid is supersonic with respect to large-scale structures arise and weak shock waves adjacent to vortices are formed. The computations of nonlinear development of the supersonic mode at $M_r = 3.0$ demonstrate formation of the secondary flow that is very unlike Kelvin-Helmholtz vortices. The inclined shock waves appear in outer region. In all cases the pairing of large scale structures occurs but for supersonic disturbances this process is very slow.

Flowfields of spatially developing shear layer are presented in Fig.2 at two different values of the relative Mach number. It is evident that there are certain common features with the temporal simulations. The comparison between results of temporal and spatial computations have been carried out in the energy of harmonics and the vorticity thickness.

Simulations of shear layer dynamics in a number of more complex situations have been also performed. They include the Kelvin-Helmholtz instability of the contact surface emanating from the triple point in the case of Mach reflection of an oblique shock wave, the generation of vorticity by the shock wave impinging on the shear layer and the interaction of two closely-spaced parallel shear layers.

[1] C.-W.Shu, S.Osher. J. Comput. Phys., vol. 83, pp. 32-78 (1989).
[2] G.-S.Jiang, C.-W.Shu. J. Comput. Phys., vol. 126, pp. 202-228 (1996).

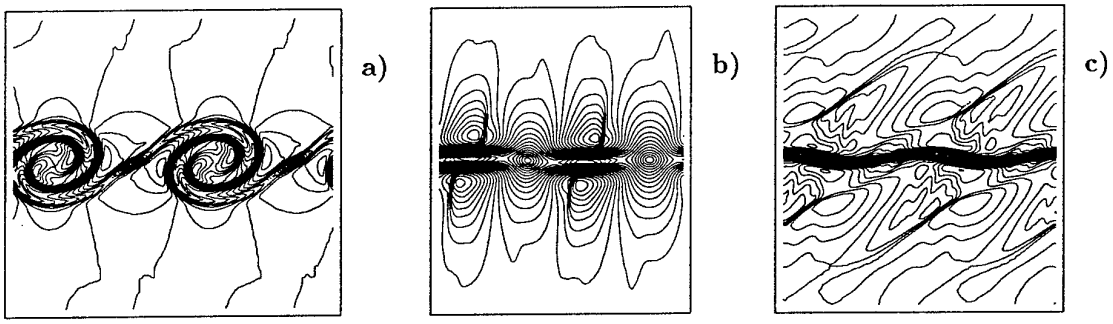

Fig.1. Typical flow patterns of temporal shear layer at a) $M_r = 1.0$ (vorticity contours), b) $M_r = 1.5$ and c) $M_r = 3.0$ (Mach number contours).

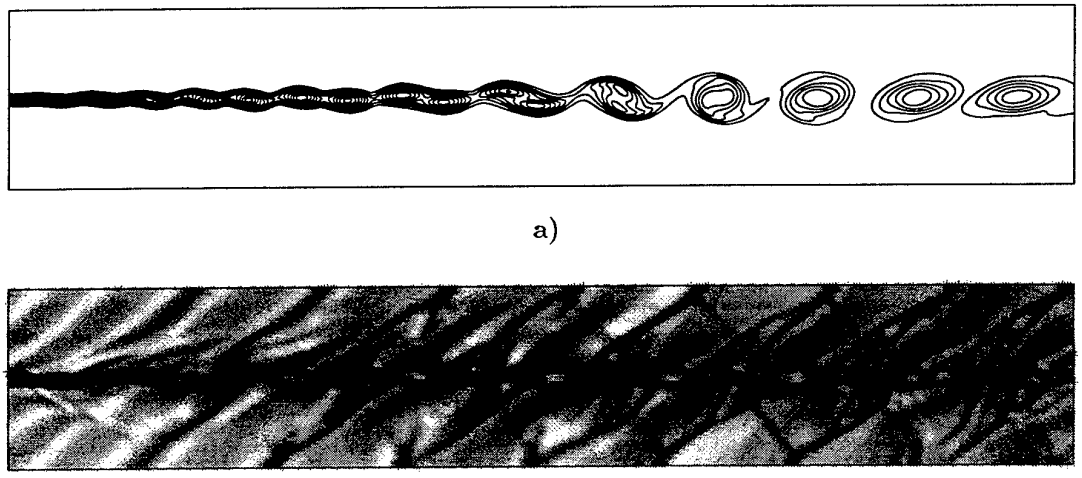

Fig.2. Spatial evolution of a) Kelvin-Helmholtz instability at $M_r = 0.8$ (vorticity contours) and b) supersonic instability at $M_r = 2.5$ (density gradient).

Core Dynamics of Vortex Pairs and Rings

Monika Nitsche

Department of Mathematics, Ohio State University, OH 43202

ABSTRACT

This paper considers the vortex pair and the vortex ring formed via Klein's "Kaffeelöffel Experiment." A flat rectangular plate is immersed in an inviscid fluid and given an impulse in direction normal to itself. If the plate is dissolved, a planar vortex sheet remains in the fluid in place of the plate. Analogously, the impulsive motion and subsequent dissolution of a flat circular disk results in an axisymmetric vortex sheet in place of the disk. Klein (1910) predicted that if these vortex sheets are allowed to evolve freely, they roll up into a vortex pair and a vortex ring respectively. Nitsche & Krasny (1996) studied the vortex

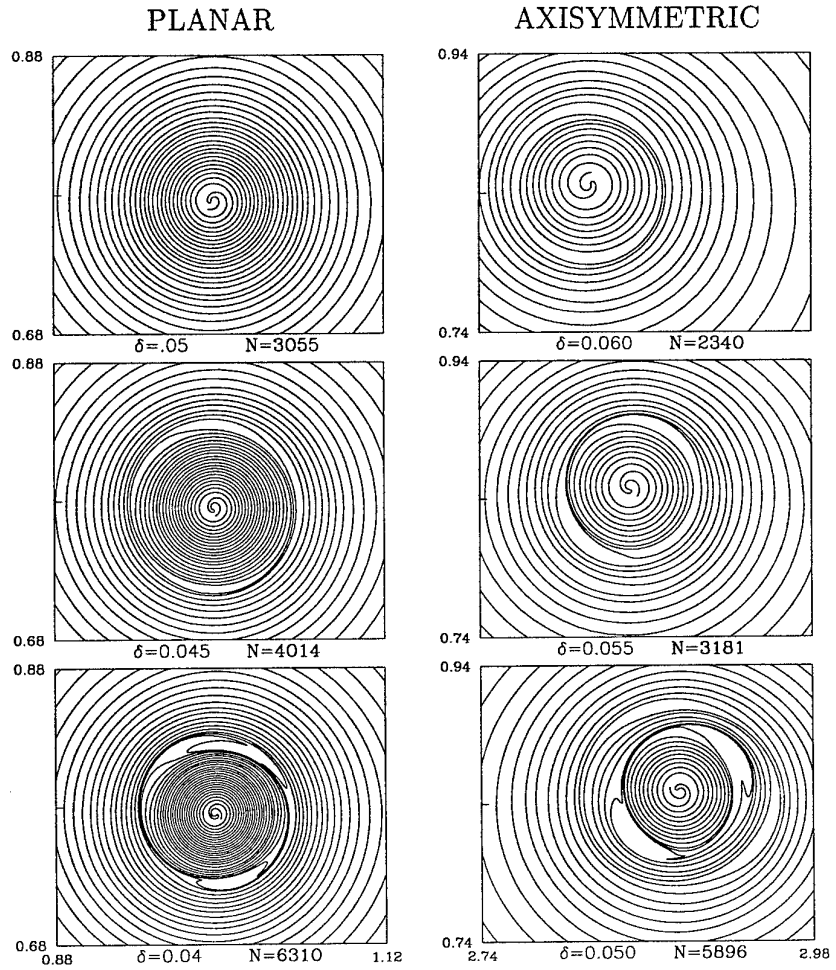

FIG. 1: Core of the vortex pair (left column) and the vortex ring (right column) formed from the rollup of an initially flat vortex sheet. Results at a fixed time $t = 10$ computed with the indicated values of δ are shown.

sheet evolution numerically using the vortex blob method. That work led to a closer study of the core dynamics which is presented here.

The vortex blob method consists of regularizing the governing equations by convolution with a smoothing parameter δ. The computations are performed with $\delta > 0$ and information about the vortex sheet is inferred from the limit $\delta \to 0$. Under the regularized equations, $\delta > 0$, the initially flat vortex sheets roll up into a spiral at the edge. The vorticity is concentrated in the spiral core and the roll-up represents a vortex pair and vortex ring respectively. At a fixed time $t > 0$, the outer turns of the spiral appear to converge as $\delta \to 0$, while the number of spiral turns increases. The spiral core for a sequence of decreasing δ is shown in Fig. 1. One observes annular regions about the core within which the particle motion becomes irregular and the spiral roll-up appears to develop gaps. The results shown in Fig. 1 are numerically resolved and represent the exact solution to the regularized equations. We are interested in studying this behaviour since it may represent one of the mechanisms by which the flows become turbulent.

The following questions arise. What is the reason for the irregular behaviour near the core? As δ decreases, do the gaps remain confined to an annular region? An alternative regularization of the original equation is provided by fluid viscosity ν. Does similar behaviour occur in the limit $\nu \to 0$? That is, is this behaviour present in a real viscous flow? In this talk we attempt to answer some of these questions.

Rom-Kedar, Leonard & Wiggins (1990) studied the onset of chaos in a periodic unsteady flow induced by two point vortices. Parallels between that flow and the flows presented here can be drawn to explain the present observations. We will give further evidence that the flow becomes chaotic by analysing a return map of the flow. Furthermore, we will present numerical studies of the viscous flow in the limit $\nu \to 0$ and investigate whether the gaps occur in a real flow.

REFERENCES

Klein, F. 1910 Über die Bildung von Wirbeln in reibungslosen Flüssigkeiten, *Z. Math. Phys.* **59**, 259.

Nitsche, M. & Krasny, R. 1996 Comparison of planar and axisymmetric vortex sheet roll-up, *in preparation.*

Rom-Kedar, V., Leonard, A. & Wiggins, S. 1990 An analytical study of transport, mixing and chaos in an unsteady vortical flow, *J. Fluid Mech.* **214**, 347.

SESSION 3

VORTICES IN SHEAR LAYERS

This Page Intentionally
Left Blank

DYNAMICS OF SLENDER VORTICES NEAR THE WALL IN A TURBULENT BOUNDARY LAYER

Fazle Hussain
University of Houston

ABSTRACT

It is now well-established that the enhanced drag and heat transfer of turbulent boundary layers is dominated by slender longitudinal vortices immediately near the wall. Despite their immense practical significance, the geometry and dynamics of near-wall vortices are not well understood and often controversial. To gain new insight into the near-wall dynamics, we educe coherent structures (CS) near the wall from a numerically simulated turbulent channel flow using a conditional sampling scheme which extracts the entire extent of locally dominant vortical structures. Such structures are detected from the instantaneous flow field using our newly developed vortex definition - a region of negative lamda[2], the second largest eigenvalue of the tensor S[ik]S[kj] + Omega[ik]Omega[kj] - which accurately captures the structure details, unlike velocity, vorticity or pressure-based eduction schemes. Extensive testing shows that lamda[2] correctly captures vortical structures, even in the presence of strong shear occurring near the wall of a boundary layer. Our conceptual model of the CS array reproduces nearly all experimentally observed events reported in the literature, such as VITA, gradient and counter-gradient Reynolds stress distributions (Q1,Q2,Q3 and Q4 and their relative contributions), wall pressure variation, elongated low-speed streaks, spanwise shear, etc. Notably, the often heralded hairpin vortices, not to be confused with hairpin-shaped vortex line bundles, are absent both in the instantaneous and ensemble-averaged fields. We have also discovered a new instability mechanism for generation of these dominant longitudinal vortices from a basic flow initially containing no streamwise vorticity. The structure evolution agrees quite well with that observed in DNS of minimal channel flow.

* [.] denotes subscript

This Page Intentionally
Left Blank

Vorticity Dynamics around a Straight Vortex Tube in a Simple Shear Flow

Shigeo KIDA[a)], Genta KAWAHARA[b)], Mitsuru TANAKA[c)], Shinichiro YANASE[d)]

a) Theory and Simulation Center, National Institute for Fusion Science, Nagoya 464–01, Japan
b) Depart. of Mechanical Engineering, Ehime Univ., Matsuyama 790–77, Japan
c) Depart. of Mechanical and System Engineering, Kyoto Institute of Tech., Kyoto 606, Japan
d) Depart. of Engineering Science, Okayama Univ., Okayam 700, Japan

ABSTRACT

The mechanism of wrapping, tilting and stretching of vorticity lines around a strong straight tubular vortex in a simple shear flow ($\boldsymbol{U} = SX_2\widehat{\boldsymbol{X}}_1$, S being a shear rate) is investigated analytically.

A straight vortex filament of circulation Γ is put at an initial instant with being inclined from the streamwise (X_1) direction both to the vertical (X_2) and the spanwise (X_3). An asymptotic solution to the Navier–Stokes equation at large Reynolds numbers $\Gamma/\nu \gg 1$, ν being the kinematic viscosity of fluid, is obtained by extending Moore's method (Moore 1985 *Proc. R. Soc. Lond.* A **399**, 367). A full expression of the vorticity field is given at short times $St \ll (\Gamma/\nu)^{\frac{1}{2}}$. We find the following interesting analytical results.

(1) Spirals of vorticity lines: The vorticity lines of the simple shear is wrapped around the vortex tube to form two spiral layers of high normal (to the vortex) vorticity (see Fig. 1).

(2) Generation of opposite-signed vorticity: These spirals induce axial flows of the same spiral shape with alternate sign in adjacent spirals which in turn tilt the simple shear vorticity toward the axial direction so that the simple shear vorticity is converted to the axial direction. The resulting axial vorticity has the opposite sign to that of the vortex tube at the outermost spirals where the magnitude is strongest (see Fig. 2).

(3) Disappearance of normal vorticity: In the central region, the viscous cancellation is effective in tightly wrapped vorticity of alternate sign, which leads to the disappearance of the normal vorticity (see Fig. 1).

(4) Dominance of cyclonic vortices: Only the axial component of the simple shear vorticity is left in the central region which is stretched by the simple shear flow itself. As a result, a cyclonic vortex (whose spanwise component of vorticity is the same as that of the simple shear vorticity) is intensified, while an anti-cyclonic vortex is weakened (see Fig. 2).

The above findings are actually observed in real turbulent flows (She, Jackson & Orszag 1990 *Nature* **344**, 226; Sendstad & Moin 1992 TF-57, Thermoscience Divison, Department

of Mechanical Engineering, Stanford University; Bernard, Thomas & Handler 1993 *J. Fluid Mech.* **253**, 385; Miyake & Tsujimoto 1996 Submitted to *Phys. Fluids*).

Figures 1 and 2 respectively show, on a cross-section of the vortex tube, the spatial distributions of the magnitude of normal vorticity and of axial vorticity for (a) cyclonic, (b) neutral and (c) anti-cyclonic cases. Vorticity lines projected on this plane is drawn by solid curves. The vortex tube is viewed from the upstream and the vortex rotates clockwise. The magnitude of vorticity components are represented by colour; red denotes the highest value and blue the lowest. Vorticity (which is positive) of the vortex tube itself is not shown.

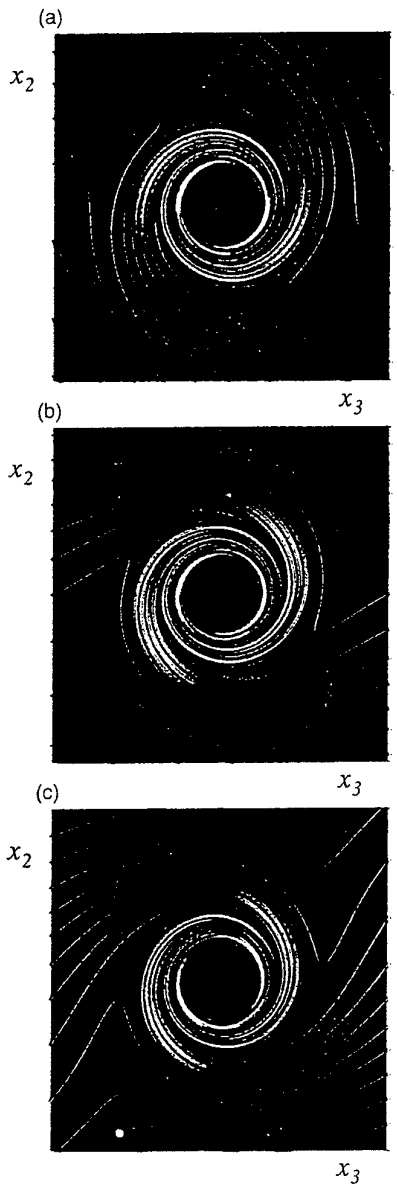

Figure 1

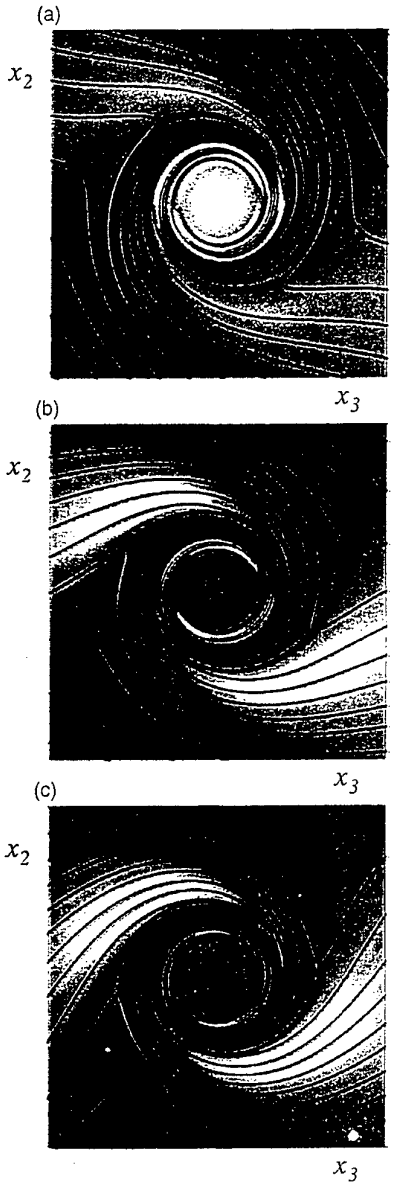

Figure 2

GENESIS OF LONGITUDINAL VORTICES IN NEAR-WALL TURBULENCE

Wade Schoppa

University of Houston

ABSTRACT

Using direct numerical simulations of turbulence near one wall of a channel flow, we present a new linear instability mechanism for generation of near-wall longitudinal vortices in turbulent boundary layers.

We formulate a two-dimensional base flow, containing no x-dependence or streamwise vorticity, to represent the streaks of low-speed fluid known to be prevalent near the wall. Linear instability is indicated by sustained exponential growth of low-amplitude perturbations; evidence suggests that this streak instability is inviscid in nature, despite the proximity of a no-slip wall. We demonstrate that the instability mechanism is inherently 3D, driven by sinuous streak displacement (along the span) induced by elliptical streamwise vorticity layers and quite analogous to oblique instability in free shear flow.

Varicose modes corresponding to possible hairpin vortices are found to be stable.In the nonlinear regime, sinuous instability directly creates an array of new longitudinal vortices, a regeneration process dominated by the stretching of perturbation streamwise vorticity, caused by streak waviness. The dynamics of vorticity production, along with the wrapping, tilting, and accumulation of vortex lines comprising the initial vorticity sheet, are outlined and correspond well to observations of near-wall turbulence in minimal computational domains.

The 3D features of the generated vortices,including counterrotation,tilting in the (x,z) plane and staggering in x, also agree well with the educed (dominant) coherent structures, suggesting that this mechanism is a dominant agent of longitudinal vortex regeneration near the wall.These results suggest strategies for realistic, large-scale (in contrast to fragile MEMS) control of drag and heat transfer over bodies.

This Page Intentionally
Left Blank

Theory of non-axisymmetric Burgers vortex with arbitrary Reynolds number

K. BAJER[1] & H. K. MOFFATT
Department of Applied Mathematics and Theoretical Physics,
University of Cambridge, Silver Street, Cambridge, CB3 9EW, UK
http://www.damtp.cam.ac.uk/user/tfd

G. I. Taylor (1938) recognised the fact that the competition between stretching and viscous diffusion of vorticity must be the mechanism controlling the dissipation of energy in turbulence. A decade later Burgers (1948) obtained exact solutions describing steady vortex tubes and layers in locally uniform straining flow where the two effects are in balance. The discovery of the exact solutions stimulated the development of the models of the dissipative scales of turbulence as random collections of vortex tubes and/or sheets.

The intermittent nature of the vorticity field was observed in experiments by taking statistical measurements which indicated the existence of the small-scale localised structures (Townsend 1951). Only recently have these structures been directly observed, first in the numerical simulations (see, for example Vincent & Meneguzzi 1991) and then in the laboratory experiments where a new visualisation technique was employed (Douady, Couder & Brachet 1991).

The Burgers vortex has axial symmetry unlikely to be found in real flows, hence the need to find solutions describing non-axisymmetric stretched vortices. Let us consider incompressible fluid with viscosity ν. We look for a steady state of a vortex having stream-function $\Psi(x,y)$, vorticity $\boldsymbol{\omega} = -(\nabla^2\Psi)\hat{\mathbf{z}}$ and total circulation Γ subjected to the ambient irrotational straining flow

$$\boldsymbol{U} = (\alpha x, \beta y, \gamma z) \quad , \qquad \alpha+\beta+\gamma = 0 \quad , \qquad \alpha < 0, \quad \gamma > 0 \tag{1}$$

characterised by the parameter

$$0 \le \lambda = \frac{\alpha-\beta}{\alpha+\beta} \tag{2}$$

which measures the departure from axisymmetry. Taking $\sqrt{\nu/\gamma}$ and γ^{-1} to be units of length and time respectively we obtain the steady state equation in polar coordinates (r,θ),

$$\frac{1}{r}\frac{\partial(\Psi,\omega)}{\partial(r,\theta)} = -R_\Gamma\left(L_0\omega + \lambda L_1\omega\right), \tag{3}$$

where $R_\Gamma = \Gamma/\nu$ is the Reynolds number of the vortex and L_0, L_1 are linear operators.

Robinson and Saffman (1984) solved this equation numerically for $0 < R_\Gamma < 100$ and found that the vortex has a quasi-elliptical shape with the minor axis inclined at an angle $\phi(R_\Gamma,\lambda)$ to the principal axis of strain. They found numerically that $\phi(R_\Gamma,\lambda) \to 0$ as $R_\Gamma \to 0$. They developed a theory for $R_\Gamma \ll 1$ involving *double* expansion in powers of both λ and R_Γ. Their computations showed that as R_Γ increases $\phi(R_\Gamma,\lambda)$ settles to a constant value $\phi_c \approx 45°$. The value of ϕ_c was theoretically derived by Moffatt, Kida & Ohkitani (1994) who developed an asymptotic theory for $R_\Gamma \gg 1$ later adapted to diffusing vortices in two-dimensional strain for which much more numerical data, including details of the vortex structure, are available (Jiménez, Moffatt & Vasco 1996).

Here we develop a new theory based on the expansion in powers of λ,

$$\omega = \omega_0 + \lambda\omega_1 + \lambda^2\omega_2 + \dots \quad , \tag{4}$$

$$\Psi = \Psi_0 + \lambda\Psi_1 + \lambda^2\Psi_2 + \dots \quad . \tag{5}$$

[1]Present address: University of Warsaw, Institute of Geophysics, ul. Pasteura 7, 02-093 Warsaw, Poland

We find that ω_0 is the Burgers solution, while the order $O(\lambda)$ consists of a single Fourier mode:

$$\Psi_1 = \mathrm{Re}\left(S(r)\mathrm{e}^{\mathrm{i}2\theta}\right) \quad , \qquad \omega_1 = \mathrm{Re}\left(H(r)\mathrm{e}^{\mathrm{i}2\theta}\right) \quad . \tag{6}$$

The radial profiles $S(r)$, $H(r)$ satisfy two coupled ordinary differential equations

$$wH'' + (w+1)H' + \left[\mathrm{i}R_\Gamma w^{-1}(\mathrm{e}^{-w}-1) + 1 - w^{-1}\right] H + \mathrm{i}R_\Gamma \mathrm{e}^{-w} S = w\mathrm{e}^{-w} \quad , \tag{7}$$

$$wS'' + S' - w^{-1}S + H = 0 \quad , \tag{8}$$

where $w = \frac{1}{4}r^2$ is a new variable. The angle of inclination of the vortex is given by

$$\tan 2\phi(R_\Gamma, \lambda) = -\frac{\int_0^\infty dr\, r^3 \mathrm{Im}H(r)}{\int_0^\infty dr\, r^3 \mathrm{Re}H(r)} \quad . \tag{9}$$

Plotting $\phi(R_\Gamma, \lambda)$ as a function of R_Γ we find excellent agreement with the numerical results of Robinson & Saffman for *all* values of R_Γ, provided $\lambda < 0.25$.

Calculating higher orders in (4-5) is straightforward, but tedious. Therefore the λ-expansion provides a scheme for solving (3) for *all* values of the Reynolds number and thus bridges the gap between the low-R_Γ of Robinson & Saffman and the high-R_Γ assymptotic expansion of Moffatt, Kida & Ohkitani.

The nonlinearity of (3) makes it difficult to assess whether the λ-expansion (4-5) is an asymptotic or a convergent series and what its radius of convergence may be. In a closely related *linear* problem of stretched magnetic flux-tube with thin central vortex we argued that λ-expansion is convergent for *all* values of λ (Bajer & Moffatt 1997). The same is likely to be true in the present non-linear case.

References

BAJER, K. & MOFFATT, H. K. 1997 On the effect of a central vortex on a stretched magnetic flux tube. *J. Fluid Mech.* **339**, 121–142.

BURGERS, J. M. 1948 A mathematical model illustrating the theory of turbulence. *Adv. Appl. Mech.* **1**, 171–199.

DOUADY, S., COUDER, Y. & BRACHET, M. E. 1991 Direct observation of the intermittency of intense vorticity filaments in turbulence. *Phys. Rev. Lett.* **67**, 983–986.

JIMÉNEZ, J., MOFFATT, H. K., VASCO, C. 1996 The structure of the vortices in freely decaying two-dimensional turbulence. *J. Fluid Mech.* **313**, 209–222.

MOFFATT, H. K., KIDA, S. & OHKITANI, K. 1994 (MKO94) Stretched vortices – the sinews of turbulence; large-Reynolds-number asymptotics. *J. Fluid Mech.* **259**, 241–264.

ROBINSON, A. C. & SAFFMAN, P. G. 1984 Stability and structure of stretched vortices. *Stud. Appl. Maths.* **70**, 163–181.

TAYLOR, G. I. 1938 Production and dissipation of vorticity in a turbulent fluid. *Proc. Roy. Soc.* A **164**, 15–23.

TOWNSEND, A. A. 1951 On the fine-scale structure of turbulence. *Proc. Roy. Soc.* A **208**, 534–542.

VINCENT, A. & MENEGUZZI, M. 1991 The spatial structure and statistical properties of homogeneous turbulence. *J. Fluid Mech.* **225**, 1–25.

SESSION 4

INTERACTION OF VORTICES

This Page Intentionally
Left Blank

Interaction of two vortex tubes and the singularity formation

Akio FUKUYU

Department of mathematical Sciences,
Tokyo Denki University,
Hatoyama-machi, Hiki-gun, Saitama-ken 350-03 Japan

The goal of the present investigation is to find a possible dynamical mechanism which may lead to finite time singularity formation in inviscid ideal flow. As a candidate for this mechanism, we examine the interaction of two vortex tubes having different strength. Suppose that a weak curved vortex tube of intensity Γ_1 approaches to a strong vortex tube of intensity Γ_2 ($\Gamma_1<\Gamma_2$). If two tubes are locally anti-parallel near the closest points of approach, the former continues to approach and at the same time it winds round to the latter, and due to the induced velocity of the weak wound tube, the strong tube is notably stretched at some portion of the tube (we represent this portion by O and call the center of stretching) which means a notable amplification of the vorticity at O. In the previous paper (J. Phys.Soc. Jap. **64** (1995) 2000, hereafter, cited as I), two vortex tubes are replaced by two thin vortex filaments (single filament model). The numerical simulations done in I were based on Biot-Savart's law for vortex interaction. Each filament is replaced by a set of small vortex segments. The end effect of filament was ignored. Let the ratio of the strength be $G=\Gamma_1/\Gamma_2$. Fig.1 show the evolution in time of the core length σ at O of the strong filament and the distance d between two filaments for G=0.2. This figure shows that there exists a finite time T such that the inter vortex distance d and the vortex core σ shrinks as $(T-t)^{-q}$ as time t approaches to T. Similar results can be

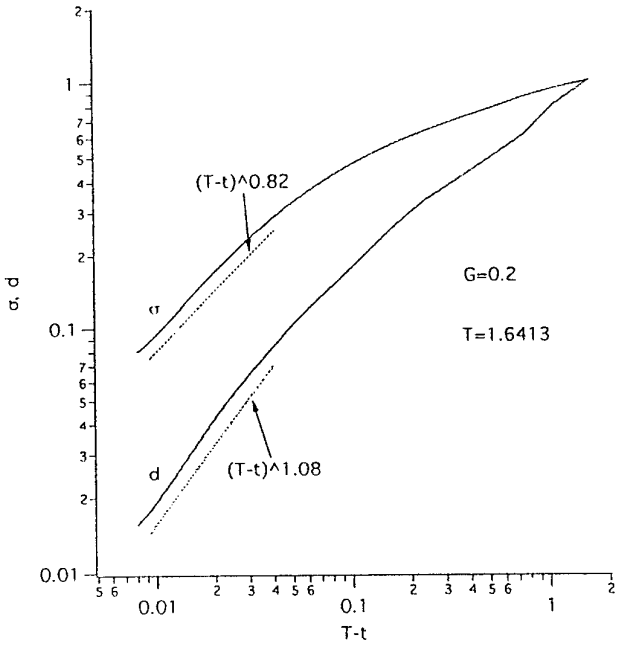

Fig.1

obtained for other values of G<1. But the power q for d is larger than that for σ, i.e. $q_d > q_\sigma$. This means that even if we have thin vortex tube in the initial instant, overlap of vortex core may occur later in this model, so that at the final stage of singularity formation , the effect of finite vortex core must be taken into account. The numerical results in I also show that, the overlap of core is delayed more for smaller value of G.

If a vortex core shrinks at some portion of the tube, the adverse pressure gradient appears which may have the effect to flatten the core, that is, the contraction of the tube. Thus, the mechanism we examine in this paper is the competition of two effects, one is the stretching due to the induced velocity of wound tube and the second is the contraction due to adverse pressure gradient.

To see the effect of finite vortex core, in this paper, we replace the initial strong straight vortex tube by a set of M straight vortex filaments and for the sake of simplicity, weak curved tube is represented by a single filament as the single filament model above. If a vortex tube is represented as a set of vortex filaments, the end effect of finite filament can not be ignored, thus in the simulations in this paper, we add, to the velocity at each nodal point on the vortex segments, the induced velocity due to the half-infinite straight line vortex placed at the end points of each finite filament. Among M filaments one is placed at the center of the tube (axial filament) and the rest on the circumference of the tube. Long time calculation like I is difficult because of numerical instability of interaction among component filaments of the tube. Fig.2 show the evolution in time of Δ and 1/ω for M=9 where Δ is area of polygon composed of M-1 points on M-1 circumferential filaments at the center and 1/ω is the inverse of vorticity at the center of axial filament. Δ and 1/ω are normalized to 1 at initial instant. Dotted line corresponds to M=1, that is, single filament model. This figure shows that at least at the initial stage of stretching processes, strong tube is stretched in a similar manner as the single filament model which has $(T-t)^q$ dependence for core length.

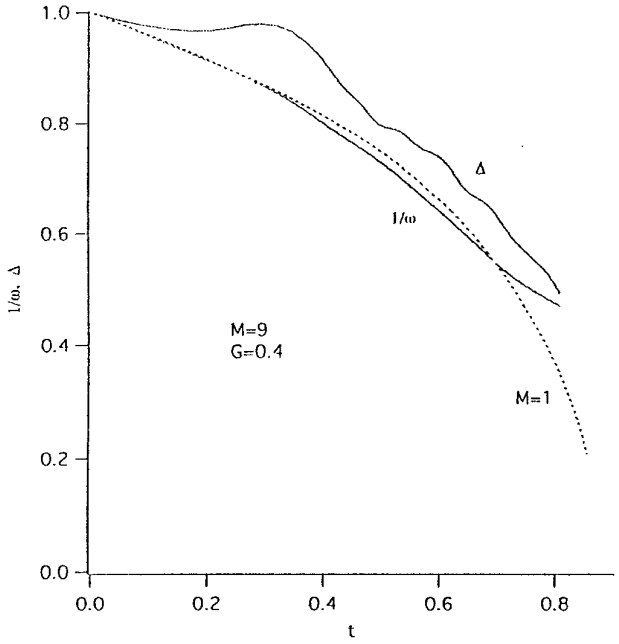

Fig.2

Non-uniqueness and instabilities of two-dimensional vortex flows in two-sided lid-driven cavities

H. C. Kuhlmann, M. Wanschura, M. Kamp and H. J. Rath
ZARM — University of Bremen, Am Fallturm, 28359 Bremen, Germany

Abstract

The three-dimensional vortex flow in a long rectangular box is investigated experimentally and numerically. A sketch of the geometry is shown in figure 1. In the experiment, the aspect ratio of the cross section is $\Gamma = 1.96$ and the length aspect ratio is $\Lambda = 6.55$. The flow is driven by moving the two facing walls at $x = \pm\Gamma/2$ at constant velocities V_i $(i = 1, 2)$ in y-direction. This setup is a generalization of the well-known (one-sided) lid-driven cavity flow problem [1]. Depending on the aspect ratios and the Reynolds numbers $Re_i = V_i h/\nu$ (h: heigth in y-direction, ν: kinematic viscosity) a variety of different vortex flows can be realized. These flows give rise to new types of instabilities not previously observed in one-sided lid-driven cavities.

In particular, we consider the case when both walls move in opposite directions. For small and equal Reynolds numbers the flow in the present geometry consists of two co-rotating nearly two-dimensional straight parallel vortices, slightly perturbed by finite size effects near the stationary end walls at $z = \pm\Lambda/2$. On a quasi static increase of both Reynolds numbers this flow undergoes a jump transition to another quasi two-dimensional flow, in which the previously well separated vortices partly merge. This merging can occur when the two opposing wall jets that originate from the down-stream corners of both moving walls remain confined to a sufficiently small boundary layer on the stationary walls. In that case each jet gets entrained by the boundary layer of the moving wall on the other side of the cavity thus forming a large convection loop. The transition is experimentally found to be hysteretic. The non-uniqueness of the quasi-two-dimensional flow has also been confirmed by two-dimensional numerical calculations. If the both side wall Reynolds numbers are of equal magnitude the flow is found to be non-unique, if the conditions $\Gamma \gtrsim 2$ and $Re \gtrsim 310 \times (\Gamma - 1.2)$ are satisfied. The non-uniqueness can be described by a cusp catastrophe of the solution manifold. The region of non-uniqueness for $Re_1 = Re_2$ is given by the triangular shaped area shown in figure 2.

The merged state is found to be unstable with respect to a stationary three-dimensional cellular flow. It developes supercritically out of the merged state. This instability has been verified by a numerical linear stability analysis using periodic boundary conditions in direction of the axis of the basis state vorticity. For $\Gamma = 1.96$ we find a critical Reynolds number $Re^{(1)} = 257.2$ with a wave number $k^{(1)} = 2.25$. The calculated stability boundaries and the experimentally determined transition Reynolds numbers show a good agreement even for moderately different Reynolds numbers.

By use of energy transport equations it can be shown that the instability is due to the elliptic instability process [2]. The critical three-dimensional mode receives its energy from the strong straining motion in the center of the merged vortex state. One advantage of the present geometry is the possibility to study the nonlinear supercritical flow patterns that result from the elliptic instability in the form of stationary convection cells. Previous investigations were limited to transient processes (see, e. g. [3]). Further results can be found in [4].

References

[1]KOSEFF, R. J. & STREET, R. L. 1984 The lid-driven cavity: a synthesis of qualitative and quantitative observations. *J. Fluids Eng.* **106**, 390.

[2]WALEFFE, F. 1990 On the three-dimensional instability of strained vortices. *Phys. Fluids* A **2**, 76.

[3]GLEDZER, E. B. & PONOMAREV, V. M. 1992 Instability of bounded flows with elliptical streamlines. *J. Fluid Mech.* **240**, 1.

[4]KUHLMANN, H. C., WANSCHURA, M., & RATH, H. J. Flow in two-sided lid-driven cavities: Non-uniqueness, instabilities, and cellular structures. *J. Fluid Mech.* (to appear).

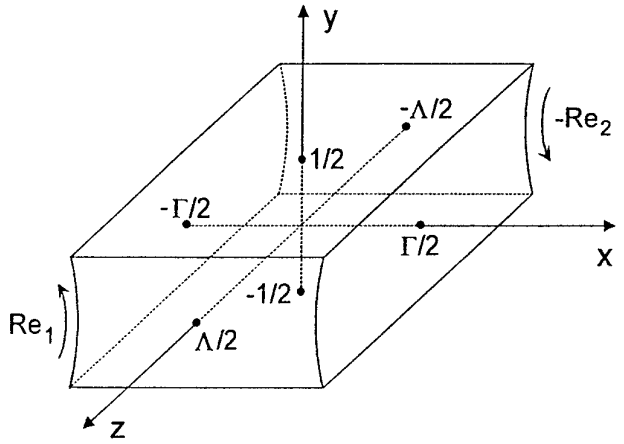

Figure 1: Sketch of the cavity and coordinate system.

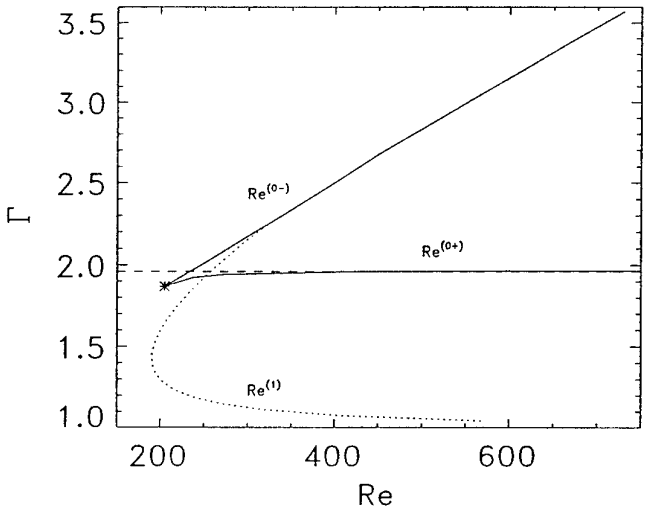

Figure 2: Region of non-uniqueness of the basic two-dimensional flow (full lines) bounded by $Re^{(0+)}$ (upper existence Reynolds number for the two-vortex state) and $Re^{(0-)}$ (lower existence Reynolds number for the merged flow state) for symmetrical driving ($Re_1 = Re_2$). The asterisk indicates the bifurcation point. The dotted line is the linear stability boundary $Re^{(1)}$ of the merged flow. It intersects with $Re^{(0-)}$ at $\Gamma^* = 2.283$, $Re^* = 334$. The experimental aspect ratio $\Gamma = 1.96$ is shown as a dashed line.

Long-Wavelength Instability and Reconnection of a Vortex Pair

THOMAS LEWEKE* and CHARLES H. K. WILLIAMSON
Sibley School of Mechanical and Aerospace Engineering
Cornell University, Ithaca, NY 14853, USA

We present new experimental results concerning the dynamics of a pair of parallel counterrotating vortices. This flow provides a prototype system for the study of elementary interactions of slender vortices. In addition, a strong link to engineering applications exists, since similar flow structures are found in the far wake of aircraft and play an important role in flight safety at airports. In this presentation we will concentrate on one of several different features we observed in this flow: a long-wavelength instability and the associated phenomenon of vortex reconnection occurring in the long-time development of this instability. Although analytical studies of vortex pairs have considered such an instability (e.g. Crow 1970), it is surprising that neither detailed quantitative measurements nor even a clear demonstration of such structure in laboratory experiments can be found in the literature. The same applies to the study of vortex reconnection or cross-linking, which has mainly been investigated via numerical simulations (e.g. Melander & Hussain 1990).

Despite the fact that experiments on vortex pairs are often conceptually simple, they are remarkably difficult to carry out effectively. Our own approach has been to pay extreme care to the experimental set-up, including the mechanical arrangement, vibrations, convection currents, visualization technique, end conditions, etc. The vortex pair is generated in a water tank at the sharpened parallel edges of two flat plates, hinged to a common base and moved in a prescribed symmetric way by a computer-controlled stepper motor. The vortices are typically separated by a distance of 2 cm, and their length is approximately 170 cm. This high aspect ratio of the vortex pair is necessary to limit the influence of end effects that spread rapidly into the central part of the flow. Visualization is achieved using fluorescent dye, illuminated by laser light. Quantitative characteristis of the vortex pair, i.e. circulation, core size, velocity profile, and spacing, are found from flow field measurements using digital particle image velocimetry (DPIV). Other measurements concerning the spatial structure and the growth rate of the instability were obtained from image analysis of flow visualizations recorded on video. The Reynolds number based on the initial vortex circulation ($Re=\Gamma/\nu$) is of the order of 2000 in this study.

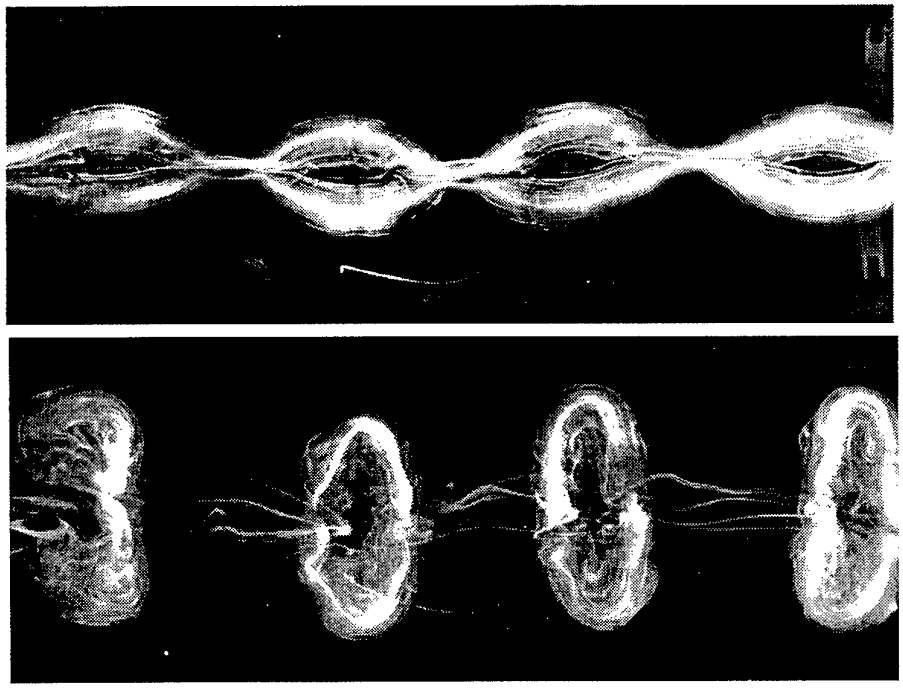

(a)

(b)

Figure 1. Visualization of the long-wavelength instability of a vortex pair. The pair is moving towards the observer. (a) Initial waviness of the vortices. (b) Late-time evolution: periodic vortex rings.

* *present affiliation:* Institut de Recherche sur les Phénomènes Hors Équilibre (IRPHÉ), Marseille, France.

Figure 1 shows the overall features of the long-wavelength vortex pair instability. The initially straight and parallel vortices develop a waviness whose axial wavelength is about 5 times the vortex separation. Photographs taken simultaneously from two perpendicular directions show that the plane of the waves is inclined about 45° with respect to the plane containing the pair (see also Fig. 2a). This waviness is amplified in time until the vortex cores touch, break up, and reconnect to form periodic vortex rings, linked by thin strands of dyed fluid. At later times, the rings elongate in the transverse direction into oval vortices (Fig. 2b), which subsequently exhibit a well-known oscillatory behaviour. The self-induced average propagation speed of the large-scale vortex structures as a function of time was determined from recordings of side and axial (end) views of the flow, and was found to be almost unchanged after reconnection.

The linear growth rate of the initial waviness was measured for different axial wavelengths, which could be imposed on the flow using a small-amplitude modulation of the vortex-generating plate edges. For a meaningful comparison with theoretical growth rate curves, deduced from the work of Crow (1970) and Widnall *et al.* (1971), knowledge of the entire initial flow field is necessary. In our case it was obtained from DPIV measurements. The results show good agrement between experiment and theory.

The process by which the wavy vortices "break" and reconnect to form vortex rings was also studied in detail. The visualization in Fig. 2a of the flow in the reconnection plane shows that a tail of dyed fluid is left behind by the descending pair when the vortex cores approach each other. The DPIV measurement of the vorticity in the same plane (Fig. 2b), made approximately at the same time, reveal that this structure corresponds indeed to a tail of vorticity. Similar measurements at later times show that the remaining, highly stretched vorticity links between the vortex rings in Fig. 1b still contain about 10% of the initial vortex circulation. The characteristic reconnection time was obtained from the evolution of the circulation in the reconnection plane.

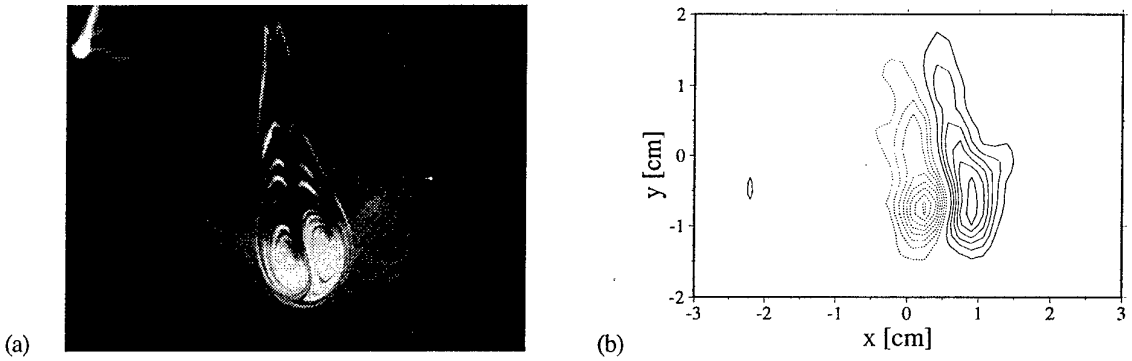

Figure 2. Flow in the plane perpendicular to the vortex axes where the perturbed vortices come closest to each other. In this view the vortices move down. (a) Dye visualization using a laser sheet; the planes of the wavy perturbations are visible on the remaining parts of the pair in the backgound. (b) Contours of axial vorticity.

In conclusion, our study provides one of the first clear demonstrations of a long-wavelength vortex pair instability in a controlled experiment. Extensive flow visualization and quantitative velocity measurements using digital particle image velocimetry have given detailed information about this flow. Concerning the initial growth of the instability, a complete quantitative comparison between experimental measurements and theoretical predictions was achieved for the first time, showing good agreement between the two. Furthermore, observation and analysis of the non-linear evolution of the flow has provided new experimental results concerning the fundmental process of vortex reconnection, as well as the motion of the remaining large-scale vortex structures, which is important for the study of aircraft wakes.

This work was supported by the US Office of Naval Research under Contract No. N00014-95-1-0332, and by NATO under Grant No. CRG 970259. TL acknowledges the financial support from the Deutsche Forschungsgemeinschaft, Grant No. Le 972/1-1.

Crow, S.C. 1970, AIAA J. **8** (12), 2172-2179.

Melander, M.V., Hussain, F. 1990, in "Topological Fluid Dynamics" (eds. H.K. Moffatt & A. Tsinober), Cambridge University Press, 485-499.

Widnall, S.E., Bliss, D., Zalay, A. 1971, in "Aircraft Wake Turbulence and its Detection" (eds. J.H. Olsen, A. Golgberg & M. Rogers), Plenum Press, 339-354.

Stability of stretched and unstretched vortices subjected to a planar strain

Christophe Eloy & Stéphane Le Dizès

Institut de Recherche sur les Phénomènes Hors Equilibre,
12, avenue Général Leclerc, F-13003 Marseille, France.

Recent laboratory experiments [1] and numerical simulations of turbulent flows have demonstrated that vorticity tends to concentrate in localized structures such as filaments. These structures have been generally associated with axisymmetric vortices for which the vorticity is simultaneously concentrated by axial stretching and diffused by viscosity. In a uniform stretching field, the equilibrium vortex configuration is the famous Burgers vortex which is characterized by its circulation Γ and its radius $\delta = \sqrt{\nu/\gamma}$ where γ is the stretching rate and ν the viscosity. Without stretching, such a vortex diffuses according to the Lamb vortex : its radius increases as $\delta = \sqrt{\nu(t+t_0)}$ with a constant circulation. By adding a global strain field $\mathbf{U} = (\varepsilon y, \varepsilon x, 0)$ perpendicular to the vortex axis, Moffatt *et al* [2] and Ting & Tung [3] have obtained non-axisymmetric analogues for Burgers and Lamb vortices in the limit of large Reynolds numbers $Re = \Gamma/\nu$. The goal of this talk is to show that these two non-axisymmetric vortices are subjected to the 3D Widnall instability.

In the limit of large Reynolds numbers, small strain and small stretching, both vortices are, in first approximation, axisymmetric, stationary, with a Gaussian vorticity profile. They admit neutral Kelvin modes of the form $\mathbf{u} = \mathbf{v}(r)\exp(ikz - i\omega t + im\theta)$. The non-dimensionalized quantities $\tilde{k} = k\delta$, $\tilde{\omega} = \omega\delta^2/\Gamma$ and m are related through a dispersion relation $D(\tilde{\omega}, \tilde{k}, m) = 0$ which satisfies an important symmetry property: the transformation $(\tilde{\omega}, \tilde{k}, m) \to (-\tilde{\omega}, \tilde{k}, -m)$ leaves invariant the dispersion relation. This property guarantees that the stationary helicoidal modes $m = 1$ and $m = -1$ resonate for certain values $\tilde{k}_c$ of the wavenumber [see table below]. This resonance is triggered by the strain field, and gives rise to the so-called Widnall instability [4,5] when viscous and stretching effects are not considered. The growth rate of the instability is $O(\varepsilon)$ and the amplified wavenumbers are in an interval $\Delta\tilde{k} = O(\varepsilon\delta^2/\Gamma)$ around the most unstable values $\tilde{k}_c$ [5].

For both vortices, viscosity damps the perturbations with a $O(k^2\nu)$ rate. It cuts off large wavenumbers but has a negligible effects on small wavenumbers.

For the non-axisymmetric Lamb vortex, viscous diffusion also limits the period of resonance. Indeed, since the radius δ varies, the non-dimensionalized wavenumber $k\delta$ is in the interval $[\tilde{k}_c - \Delta\tilde{k}, \tilde{k}_c + \Delta\tilde{k}]$ only during a finite time. The growth of the helicoidal waves is then transient. The gain of amplitude across the region of resonance can be estimated in first approximation by $\exp(K_L\varepsilon^2 Re\delta^4/\Gamma^2)$. An asymptotic analysis for the critical scaling $\varepsilon \sim \Gamma/(\delta^2\sqrt{Re})$ permits to fully describe the transient growth and gives, for each region of resonance, the values of K_L displayed on the table below.

For the non-axisymmetric Burgers vortex, stretching plays a similar role by modifying the axial wavenumber according to $k = k_0 e^{-\gamma t}$. The Widnall instability is then also transient in that case. The gain of amplitude across the region of resonance is also of the form $\exp(K_B\varepsilon^2 Re\delta^4/\Gamma^2)$ where the values of K_B are given below.

These results show that both Burgers and Lamb vortices are destabilized by a sufficiently strong strain perpendicular to their axis. They provide an explanation for the disappearance of the filaments observed in turbulence experiments [1].

$\tilde{k}_c$	K_L	K_B
1.13	468.50	235.23
1.97	446.97	225.79
2.80	441.35	222.77

References

[1] O. Cadot, S. Douady and Y. Couder, "Characterization of the low pressure filaments in three-dimensional turbulent shear flow," Phys. Fluids **7**, (3), 630-646 (1995).

[2] H. K. Moffatt, S. Kida and K. Ohkitani, "Stretched vortices—the sinews of turbulence; large-Reynolds-number asymptotics," J. Fluid Mech. **259**, 241 (1994).

[3] L. Ting and C. Tung, "Motion and decay of a vortex in a non-uniform stream," Phys. Fluids **8**, 1039-51 (1965).

[4] C.-Y. Tsai and S. E. Widnall, "The stability of short waves on a straight vortex filament in a weak externally strain field," J. Fluid Mech. **73**, 721-33 (1976).

[5] D. W. Moore and P. G. Saffman, "The instability of a straight vortex filament in a strain field," Proc. Roy. Soc. **A346**, 413-25 (1975).

Axisymmetric and three-dimensional vorticity dynamics in a swirling jet model

J.E. MARTIN
Department of Mathematics, Christopher Newport University, Newport News, VA 23606-2998

E. MEIBURG
Department of Aerospace Engineering, University of Southern California, Los Angeles, CA 90089-1191, Phone: (213) 740-5376, Fax: (213) 740-7774, Email: eckart@spock.usc.edu

Submitted to the "IUTAM Symposium on Dynamics of Slender Vortices," Aachen, Germany, November 4, 1996.

Abstract

Swirling jets represent one of a handful of paradigm flows that, while of great practical significance, allow for the fundamental study of complex but generic dynamical processes and their interactions. They feature prominently in a variety of applications in such fields as propulsion, combustion, and mixing. At the same time, atmospheric conditions can give rise to swirling flows in nature, with both wake and jet-like axial velocity profiles. Examples concern tornados, dust devils and water spouts. All of the above situations are characterized by a complex interplay of a variety of competing dynamical mechanisms. The axial velocity profiles typically allow for shear induced instabilities similar to those encountered in nonswirling flows. However, the additional presence of swirl can result in an unstable radial stratification, thereby leading to centrifugal instabilities as well. Furthermore, the swirl can give rise to standing or propagating nonlinear inertial waves, similar to the internal waves observed in flows with density stratification. Finally, under certain conditions swirling jets are known to produce vortex breakdown events, an important generic phenomenon for which a universally accepted explanation is still elusive. An improved understanding of these mechanisms and their mutual coupling is a prerequisite for the successful development of active and passive control strategies, with the goal of tayloring the flow such as to generate the desired operating conditions.

For the purpose of studying the nonlinear dynamical interaction of shear and centrifugal instabilities in swirling jets, we recently introduced a simplified model (Martin and Meiburg 1994a) that is an extension to earlier ones proposed by Batchelor and Gill, Rotunno, and Caflisch, Li and Shelley. It lends itself well to analytical linear stability calculations, as well as to nonlinear Lagrangian vortex dynamics simulations. The model consists of an axial centerline vortex, which is surrounded by a nominally axisymmetric vortex sheet containing both streamwise and circumferential vorticity. While this model has obvious limitations when it comes to reproducing the detailed features of experimentally generated, and often geometry dependent velocity profiles, its simplicity offers several advantages. First of all, it allows for some analytical progress (Martin and Meiburg 1994a) in terms of a straightforward linear stability analysis, which illuminates the competition of centrifugal and Kelvin-Helmholtz instability waves. In order to gain insight into the nonlinear mechanisms of interaction and competition between

the various potential instabilities, we furthermore performed nonlinear, inviscid, three-dimensional vortex dynamics simulations for the above simplified model of swirling jets. By tracking the nonlinear evolution of vortex lines, they enable us to investigate the effects of the centrifugal instability, as well as of the Kelvin-Helmholtz instabilities feeding on both the azimuthal and the streamwise vorticity, onto processes of concentration, reorientation, and stretching of vorticity. A main goal lies in the investigation of the mechanisms by which the introduction of swirl affects the dynamics observed earlier for nonswirling jets (Martin and Meiburg 1991, 1992). Conversely, the question arises as to how the purely swirling flow examined by Caflisch, Li, and Shelley is modified by the addition of an axial velocity component. We find that the main effect of the added streamwise velocity lies in the breaking of the symmetry of the pure swirling flow. As a result, the counterrotating rings observed in the purely swirling flow are no longer of equal strength, as one of them is amplified, and the other one weakened, by the Kelvin-Helmholtz instability of the axial flow. On the other hand, the introduction of swirl drastically alters the dynamics of nonswirling jets, as it results in the formation of counterrotating vortex rings, whose circulations, in the absence of viscous effects, can grow in time without bounds. These rings promote a pinch-off mechanism leading to a dramatic decrease in the local jet diameter.

While the above mechanisms can be observed in axisymmetric swirling jets, an additional azimuthal perturbation leads to the formation of concentrated streamwise vortices as a result of a Kelvin-Helmholtz instability feeding on the streamwise jet shear layer vorticity. In contrast to nonswirling jets, the streamwise vortices in swirling jets are all of the same sign. The nature of the large scale vortical structures dominating the long term dynamics of the jet depends strongly on the ratio of the initial perturbation amplitudes in the azimuthal and streamwise directions. If this ratio is small, the centrifugal instability has enough time to form counterrotating vortex rings, before concentrated streamwise vortices can emerge in the braid regions between them. For a somewhat larger perturbation amplitude ratio, streamwise vortices grow more rapidly in the braid region between the like-signed primary vortex rings. In this way, they suppress the growth of the counterrotating rings. However, the centrifugal effects lead to a partial reorientation of the braid vortices in the azimuthal direction. Finally, for even larger initial azimuthal perturbation amplitudes, the streamwise vortices grow fast enough to suppress the growth of even the primary corotating vortex rings. In this case, the long term dynamics of the swirling jet is dominated by wavy like-signed axial vortical structures.

References

Martin, J.E. and Meiburg, E. Numerical investigation of three-dimensionally evolving jets subject to axisymmetric and azimuthal perturbations, J. Fluid Mech. 230, 271 (1991).

Martin, J.E. and Meiburg, E. Numerical investigation of three-dimensionally evolving jets under helical perturbations, J. Fluid Mech. 243, 457 (1992).

Martin, J.E. and Meiburg, E. On the stability of the swirling jet shear l ayer, Phys. Fluids 6, 424 (1994a).

Martin, J.E. and Meiburg, E. The nonlinear evolution of swirling jets, Meccanica 29, 331 (1994b).

Martin, J.E. and Meiburg, E. Nonlinear axisymmetric and three-dimensional vorticity dynamics in a swirling jet model, Phys. Fluids 8, 1917 (1996).

THEORY OF HELICAL VORTICES

S.V. Alekseenko, P.A. Kuibin, V.L. Okulov, S.I. Shtork

Institute of Thermophysics
Lavrentiev Ave 1, 630090 Novosibirsk, RUSSIA
Tel. 7-383-2-357128, Fax. 7-383-2-357880
E-mail: aleks@otani.thermo.nsk.su.

Results of both experimental and theoretical investigations of the large-scale helical-like vortices in swirl flows are presented. This work should give answers on the following questions:

1) Why do the commonly accepted characteristics of swirl flow (swirl parameter and flow rate or Reynolds number) not always uniquely identify arising helical vortex structures (Faler & Leibovich, 1977;
Alekseenko et al, 1994)?

2) Why the helical-like vortex may be screwed to the direction opposite to the fluid motion direction?

3) What the helical structures may arise in swirl flow?

4) What is the reason of arising counter flow in swirl flows and what sufficiently simple theoretical model may be applied to its description?

5) Can the vortex models by Rankine, Lamb etc. be generalized for successful description of the radial distribution of axial velocity in an actual columnar vortex?

6) What is the relation between the self-induced velocity of helical vortex rotation and frequency of vortex core precession and what is a reason of existence immobile curved vortices (of helical type)?

The experimental studies were carried out in a water vortex chamber of square cross section. A choice of such a set-up was due to the following reasons:

1) additional investigations showed a week influence of chamber cross section shape on the generation of large-scale vortex structures;

2) it is easy to perform the visual observations of flow in the rectangular chamber; 3) it is easy to control the flow regimes by changing of a channel geometry in the rectangular chamber.

The theoretical study was based on an exact analytical solution for velocity field induced by an infinitely thin vortex filament. A separation of the main singular part from this solutional-lows to describe analytically the basic spiral vortex structures with continuous distribution of vorticity in a core which are observed in experiment. The obtained solutions provide a

possibility of numerical visualization of the main kinds of flows with large-scale vortex structures.

It was found in our experiments that five different vortex structures may exist at the same swirl parameter and Reynolds number.

To account the structure of the flow new parameters are suggested: the pitch of the helical symmetry and velocity at flow axis. These characteristics are linked with fundamental feature of swirl flows: the axial velocity is linearly dependent on product of transversal velocity and current radius.

The stationary helical vortices were first observed visually in our set-up. We have found that boundary conditions at the camera bottom and at its outlet play the main role in generation of various stationary vortices.

As follows from theoretical analysis a left-hand helical vortex filament gives a delay of the flow on the chamber axis and a right-hand one - on the periphery. We have obtained a rectilinear stationary vortex as initial object of our investigation. Shifting
the outlet orifice from the chamber axis we have transformed therectilinear vortex into stationary left-hand helical vortex with a core screwed opposite to the flow rotation. To obtain right-hand helical vortex screwed along the flow rotation we incline vortex axis near the chamber bottom by mounting an inclined flat plate there. Some modification of this case made by installation of two slopes at the bottom gave stationary double helical vortex. Finally, new vortex structure was theoretically predicted and experimentally discovered. At combination of two contrary conditions at the top and bottom of a camera the stationary vortex with change of helical symmetry from right-hand screw to left-hand one was generated.

To generalize the wideknown models of Rankine's vortex, Lamb's vortex, etc., the governing hydrodynamic equations are written first in helical coordinates, and then the transfer to axi-symmetrical statement is made. This approach allowed to obtain new analytical solutions with nonuniform radial distributions of both tangential and axial components of the velocity vector unlike the models mentioned above that give the profile of the tangential component only.

While solving the problem on the frequency of vortex precession in cylindrical tube it was found to be proportional to binormal component of self-induced velocity of the vortex. The last was derived from expansion of velocity field near the helical vortex filament. The obtained formula was tested with measurements results known from literature and our own one. In particular, the formula clearly showed the possible reasons of existence of immobile vortices.

The obtained results are the basis for developing new approach to describing and controlling aerodynamics of vortex chamber and various installations with application of swirl flows.

This work was partially supported by Russian Foundation of Basic Research (grant N 94-02-05812) and by joint foundation INTAS-RFBR (grant N 95-IN-RU-1149).

SESSION 5

VORTEX BREAKDOWN

This Page Intentionally
Left Blank

IUTAM Symposium on Dynamics of Slender Vortices
RWTH Aachen, August 31st – September 3rd, 1997

Instabilities and vortex breakdown in swirling jets and wakes

P. Billant, J.M. Chomaz, I. Delbende, T. Loiseleux, **P. Huerre**,
C. Olendraru, A. Sellier

Laboratoire d'Hydrodynamique
Ecole Polytechnique
F-91128 Palaiseau Cedex
FRANCE

The objective of the presentation is two-fold : First, we report on recent results in the theoretical and numerical study of instabilities in swirling jets and wakes, particular attention being given to the determination of the absolute/convective nature of the instability. Secondly, we present a detailed experimental investigation of the onset of vortex breakdown in swirling jets.

1. Absolute/convective instabilities in the Batchelor vortex (Delbende et al., 1997 ; Olendraru et al., 1996).

The Batchelor vortex is frequently used as a convenient basic flow representation for trailing line vortices past airplanes. It is a typical example of a fully developed axial flow velocity profile. The absolute/convective instability properties of the Batchelor vortex are determined by direct numerical simulation of the linear impulse response. A novel decomposition procedure is applied to the computed wavepacket in order to retrieve the complex wavenumber and frequency prevailing along each spatio-temporal ray. In particular, the absolute wavenumber and frequency observed in the laboratory frame are determined as a function of swirl parameter and external flow. The introduction of a moderate amount of swirl is found to strongly promote absolute instability. In the case of wakes, the transitional helical mode that first undergoes a switch-over to absolute instability, is found to be m = -1 without requiring any external counterflow. In the case of jets, the transitional helical mode is very sensitive to swirl and varies in the range $-5 \leq m \leq -1$. Only a slight amount of external counterflow (1.5 % of centerline velocity) is then necessary to trigger absolute instability. The results of this numerical procedure are in good qualitative and quantitative agreement with those obtained by direct application of the Briggs-Bers criterion to the inviscid dispersion relation (Olendraru et al., 1996). Implications for the dynamics of swirling jets and wakes are discussed.

2. Absolute/convective instabilities in the Rankine vortex with axial flow. (Loiseleux et al., 1997)

In contrast with the previous case, the Rankine vortex with superimposed plug-like axial velocity profile provides an idealized representation of the flow conditions prevailing in the very near field of swirling jet flows. The Briggs-Bers criterion has been applied directly to the analytically derived dispersion relation, for different values of the swirl parameter and co-flow parameter. For wakes as for jets, transition to absolute instability may be triggered without necessitating the presence of an axial counterflow, provided that the swirl parameter is sufficiently large. The transitional helical mode is $m = -1$ for wakes and may take the values $m = -1$, $m = -2$, $m = -3$, etc. for jets. This simple model is found to yield a relatively good estimate of the critical Rossby number for vortex breakdown.

3. Experimental study of vortex breakdown in swirling jets (Billant et al. 1997).

A pressure driven water jet discharges into a large tank, swirl being imparted by means of a motor which sets into rotation a honeycomb within a settling chamber. The experiments are conducted by varying the swirl ratio S while maintaining the Reynolds number Re fixed in the range $300 < Re < 1200$. Breakdown is observed to occur when S reaches a well defined threshold $Sc \approx 1.3 - 1.4$ which is independent of Re and nozzle diameter used. This critical value is found to be in good agreement with a simple criterion derived in the same spirit as the first stage of Escudier & Keller's (1983) theory whereby breakdown is considered as a non-dissipative axisymmetric transition between two distinct states. Four distinct forms of vortex breakdown are identified : the well documented bubble state, a new cone configuration in which the vortex takes the form of an open conical sheet and, two associated spiral bubble and spiral cone states, which are only observed at large Reynolds numbers. The two flow configurations, bubble or cone are observed to coexist above the threshold Sc at the same values of the Reynolds number Re and swirl parameter S. In an intermediate range of Reynolds numbers, the breakdown threshold displays hysteresis lying in the ability of the breakdown state to remain stable for $S < Sc$ once it has taken place. Below the onset of breakdown, i.e. when $0 < S < Sc$, the swirling jet is highly asymmetric and takes the shape of a steady helix. By contrast above breakdown onset, cross-section visualizations indicate that the cone and the bubble are axisymmetric.

• Billant, P., Chomaz, J.M. & Huerre, P. (1997) Experimental study of vortex breakdown in swirling jets. Submitted to J. Fluid Mech.

• Delbende, I., Chomaz, J.M. & Huerre, P. (1997) Absolute/convective instabilities in the Batchelor vortex : a numerical study of the linear impulse response. Submitted to J. Fluid. Mech.

• Loiseleux, T., Chomaz, J.M. & Huerre, P. (1997) The effect of swirl in jets and wakes : absolute and convective instabilities of the Rankine vortex with axial flow. Submitted to Phys. Fluids.

• Olendraru, C., Sellier, A., Rossi, M. & Huerre, P. (1996) Absolute/convective instability of the Batchelor vortex. C. R. Acad. Sci. Paris, **323**, 153-159.

SPECTRAL CHARACTERISTICS OF TURBULENT CONICAL VORTEX BREAKDOWN IN NON-CAVITATING SWIRLING FLOWS AT HIGH REYNOLDS NUMBERS

T. Sarpkaya and F. Novak

Department of Mechanical Engineering
Naval Postgraduate School
Monterey, CA 93943

Vortices may experience breakdown depending on the nature and nurture of their creation and evolution. The literature is abound with studies of vortex breakdown (e.g., Sarpkaya 1971, Leibovich 1978; Wedemeyer 1982; Délery 1994; Althaus, Brücker, and Weimer 1995) partly because of its intrinsic interest and partly because of its practical applications in the destruction of wing-tip vortices to manage aircraft traffic, in the improvement of the handling characteristics of fighter-type aircraft, and in the area of combustion to stabilize the flame. These applications involve turbulent flows at high Reynolds numbers in or about complex geometries. Even though experiments regarding the occurrence of breakdown in swirling flows in complex combustion chambers have been reported (Chen et al., 1990), the majority of the experimental and numerical studies dealt with laminar breakdowns. Until recently, it was not appreciated that the global structure of the breakdown in turbulent swirling flows is significantly different from that in laminar swirling flows. Recently, Sarpkaya (1995) discovered a fourth type (turbulent conical breakdown) in non-cavitating swirling turbulent flows at relatively high Reynolds numbers and small swirl numbers in a slightly-diverging tube apparatus, previously used by Sarpkaya (1971, 1974). The turbulent conical breakdown resembles a conical wedge or a sharp-nosed missile whose apex is at the free stagnation point where the turbulent vortex core meets the wedge. It differs significantly from the three previously-known types observed at much lower Reynolds numbers (double-helix, spiral, and nearly-axisymmetric). It also differs in many ways from the cone-like or hyperboloid-like laminar breakdowns observed by numerous researchers (e.g., Sarpkaya 1971; Faler and Leibovich 1978; Billant, Chomaz, and Huerre 1994) at very low Reynolds numbers and sufficiently high swirl numbers.

The preliminary results (Sarpkaya, 1995) reported only a kaleidoscopic picture of the evolution of the new breakdown topology and limited velocity and rms measurements in the range of Reynolds numbers from about 50,000 to 225,000. The present paper describes detailed velocity, turbulence and

spectral measurements at numerous sections and comparisons with more recent theoretical models regarding the inception of the breakdown.

The velocity and turbulence measurements were made at 25μm increments with a 3-D (Dantec) LDV system in both the back-scatter and forward-scatter modes at numerous cross sections upstream and downstream of the free-stagnation point for three Reynolds numbers: Re = UD/ν = 125,000, 190,000 and Re = 250,000. These corresponded to Reynolds numbers (based on the vortex core diameter) of about 12,000, 19,000, and 25,000. The measurements at each section were repeated to assess their repeatability so as to accumulate archival quality data for the assessment of phenomenological models, computer codes, and turbulence models. A regular as well as a high-speed video system (30 fps and 2500 fps, respectively) were used to record the new flow features.

The data were subjected to extensive spectral analysis. The power spectra of the fluctuations (obtained in the coincidence mode at very high data rates) were evaluated for each component at all sections upstream as well as downstream of the breakdown. The velocity distributions, turbulent shear stresses, and spectral data were used to understand the physics of the turbulent conical breakdown and to assess some of the recently-proposed phenomenological models. The results refute the conjectures that the circumstances of breakdown are insensitive to the Reynolds number and the local turbulence properties. These two factors have a strong influence not only on the development of the swirling flow prior to its breakdown but also on its topology after the onset of breakdown.

Althaus, W., Bruckert, Ch., and Weimer, M., (1995) "Breakdown of slender vortices," Chapter 9 in *Fluid Vortices* (Ed. S. Green), Kluwer Press.

Billant, P., Chomaz, J.-M., and Huerre, P., (1994) "L'éclatement tourbillonnaire dans tous ses états," Lettre de l'Association Universitaire de Mechanique **106**, 3.

Chen, R. H., Driscoll, J. F., Kelly, J., Namazian, M., and Schefer, R. W., (1990) "A Comparison of Bluff-Body and Swirl-Stabilized Flames," *Combust. Sci. and Tech.* **71**, 197.

Delery, J. M., (1994) "Aspects of vortex breakdown," *Prog. Aerospace Sci.* **30**, 1-59

Faler, J. H., and Leibovich, S., (1978) "An experimental map of the internal structure of a vortex breakdown," *J. Fluid Mech.*, **86**, 313.

Leibovich, S., (1978) "The structure of vortex breakdown," *Ann. Rev. Fluid Mech.* **10**, 221.

Sarpkaya, T., (1971) "On stationary and travelling vortex breakdowns," *J. Fluid Mech.* **45**, 545.

Sarpkaya, T., (1974) "Effect of Adverse Pressure Gradient on Vortex Breakdown," *AIAA J.* **12**, 602

Sarpkaya, T., (1995) "Turbulent Vortex Breakdown," *Phys. Fluids*, Vol. 7(10), pp. 2301-2303.

Wedemeyer, E., (1982) "Vortex breakdown," AGARD-VKI Lecture Series 121 High Angle of Attack Aerodynamics.

VORTEX BREAKDOWN AS A CATASTROPHE

Vladimir SHTERN

Department of Mechanical Engineering
University of Houston, Houston TX 77204-4792

A view on vortex breakdown (VB) as a fold catastrophe is developed. Despite the fourty-year studies, there is still no consensus on the VB mechanism and even notion. Analysis of VB theories reveals that they fail to explain some phenomena significant for understanding and applications of VB. In particular, none of theories predict bi-stability and hysteretic transitions (HT) which are typical and problematic features of swirling flows (SFs). For example, HT are dangerous for aircraft (this has been the main practical motivation for VB studies) and cause undesirable sequences in various devices of vortex technology.

The hysteretic VB over delta wings was observed in experiments by Lowson (1964). Muylaert (1980), and Gersten *et al.* (1985, 1988) used blowing to control this VB. Two stable solutions and jump transitions have been found by direct numerical simulations of the Navier-Stokes equations for VB in a diverging pipe (Beran & Culick 1992 and Lopez 1994). Although these physical and numerical experiments clearly demonstrate the effect, a theory has to be developed to explain the mechanism of hysteretic VB.

A proper mathematical tool is the catastrophe theory (e.g. see Arnold 1984). The theory claims that hysteresis typically appears as a *cusp* catastrophe and occurs as *fold* catastrophes. First, Trigub (1985) related VB to the fold catastrophe and found such a fold in inviscid solutions for SFs in a diverging pipe. Then this view has been developed by Saffman (1992) and Buntine and Saffman (1995). In the cited works, the fold corresponds to a unidirectional flow having no stagnation point. Therefore, VB occurs there due to non-existence rather than the appearance of stagnation flow (Saffman 1992). Goldshtik and Hussain (1996) found further examples of folds for inviscid SFs in a straight pipe.

A serious limitation of the inviscid theory is that the dependencies of the hydraulic head and circulation on stream function are given only at an inflow boundary, but they are undetermined inside a circulatory cell. This does not allow calculations of flows having circulatory cells without some conjectures. Conjectures made in prior works are questionable; e.g. the hollow core model (Escudier & Keller 1983) contradicts to asymptotic features (discussed below) of exact NSE solutions as $Re \to \infty$. Also the inviscid theory cannot to explain the appearance of hysteresis through a *cusp catastrophe*. This occurs at a finite Re, i.e. involves viscosity.

The viscous theory of HT related to VB has been developed in details for conically similar solutions of the Navier-Stokes equations. Goldshtik & Shtern (1990) found solution non-uniqueness resulting from cusp and fold catastrophes in the Taylor-Serrin near-wall vortex. Shtern and Hussain obtained analytical solutions describing HT in a model tornado (1993) and a wide generalization of Long's swirling jet (1996). These studies revealed that: (a) a recirculatory domain (RD) can develop due to swirl even in a creepy flow where neither HT nor instability occur, (b) hysteretic VB appears together with the opposite phenomena - jump vortex consolidation; (c) hysteretic VB and development of RD occur at nearly the same values of the swirl number as $Re \to \infty$, (d) swirl decays in RD, but the meridional flows inside and outside RD stay of the same order of magnitude as $Re \to \infty$.

Turbulence strongly influences HT and flow topology. Experiments by Sarpkaya (1995) show that the turbulent conical wake downstream of VB diminishes RD ('bubble') as Re increases and RD disappears for very large Re. Shtern (1996) applied the uniform eddy viscosity, ν_t, to model turbulent VB. Here, the eddy viscosity is considered as a step function of polar angle

θ to agree with observation by Sarpkaya (1995). The relation, $\nu_t = (a^2\Gamma^2+b^2J)^{1/2}$, encompasses those by Schlichting for a swirl-free round jet and by Squire (1965), Govindaraju & Saffman (1971), Albring (1981) for trailing vortices; Γ is circulation and J is the flow force of a swirling jet.

Figure 1 shows the problem schematic and coordinates. This SF is induced by a half-line vortex. 1 of circulation $\Gamma = \nu\Gamma_c$ and the flow force J acting on plane 2. Viscosity is eddy (ν_t) for $\theta < \theta_t$ and molecular (ν) for $\theta > \theta_t$. Figure 2 is a map of flow states on the parameter plane (Γ_c, M), $M = 2\pi J/\Gamma^2$. Curve S separates one- and two-cell flow patterns shown by the inserts, F_1 and F_2 are folds terminating at cusp K. These results are for the laminar flows. According to the model, transition to turbulence occurs at $\Gamma_c = 32$ where curves S_t and F_t (corresponding to separation and fold in the turbulent flows) branch from S and F_1, respectively. These results show that turbulence suppresses flow separation and HT and qualitatively agree with Sarpkaya's observations.

REFERENCES.

Albring, W. 1981 *Elementarvorrgänge fluider Wirbelbewegungen*. Akademie-Verlag, Berlin.
Beran, P.S. & Culick, F.E.C. 1992 *J. Fluid Mech.* **242**, 491.
Buntine, J.D. & Saffman, P.G. 1995 *Proc. R. Soc.Lond. A* **448**, 1.
Govindaraju, S.P. & Saffman, P.G. 1971 *Phys. Fluids* **14**, 2074.
Escudier, M.E. & Keller, J.J. 1983 AGARD CP No. 342 *Aerodyn. of vort. type flows*, pap.25.
Gersten, K., Kiske, S., Pagendarm, H.-G., Schmitz, O. & Schmucker, A. 1985 "Wirbelsrtromungen in der Flugtechnik", RWTH Aachen, 101.
Goldshtik M. & Hussain, F. 1996 *Phys Fluids (accepted).*
Goldshtik, M.A. & Shtern V.N. 1990 *J. Fluid Mech.* **218**, 483-508.
Lopez, J.M. 1994 *Phys. Fluids* **6**, 3683.
Lowson, M.V. 1964 *J. of Roy. Aeronautical Soc.* **68** (641), 343.
Muylaert, I.M. 1980 *VKI Project Report* 1980-21.
Saffman, P.G. 1992 *Vortex dynamics*. Cambridge University Press.
Sarpkaya, T. 1995 *Phys. Fluids* **7**, 2301-2303.
Schlichting, H. 1979 *Boundary-Layer Theory*, McGrow-Hill.
Schmucker, A. & Gersten, K. 1988 *Fluid Dynamics Research*, **3**, 268.
Shtern, V. & Hussain F. 1993 *Phys. Fluid A*, **5**, 2183.
Shtern V. 1996 *Fluid Mechanics and Its Applications*, **37**, 187, Kluwer.
Shtern, V. & Hussain, F. 1996 *J. Fluid Mech.* **309**, 1.
Squire, H.B. 1965 *Aero.Quart.* **16**, 302.
Trigub V.N. 1985 *J. Appl. Math and Mech.* **49**, 166.

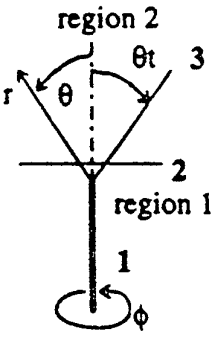

Figure 1

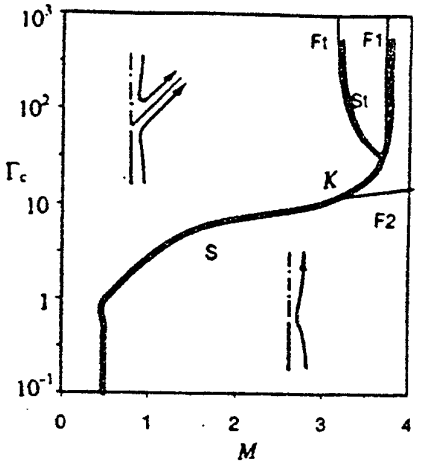

Figure 2

Turbulent Vortex Breakdown: A Numerical Study

Robert E. Spall
Department of Mechanical and Aerospace Engineering
Utah State University
Logan, UT 84322-4130
(801) 797-2878 (phone)
(801) 797-2417 (fax)
spall@fluids.me.usu.edu

Thomas B. Gatski
Aerodynamic and Acoustic Methods Branch
NASA Langley Research Center
Hampton, VA 23681-0001
(757) 864-5552 (phone)
(757) 864-8816 (fax)
t.b.gatski@larc.nasa.gov

The majority of numerical work concerning vortex breakdown has concentrated on low Reynolds number, laminar flows. One of the primary contributions of these studies have been to provide insight into the internal structure of vortex breakdown. However, in most technological applications of interest, the vortex breakdown arises within a turbulent, swirling flow, and the applicability of the laminar results to these flows is questionable. In fact, Sarpkaya (1995) presented experimental results for vortex breakdown in non-cavitating, high Reynolds number swirling flows and considered the resulting breakdown fundamentally distinct from the various forms of laminar breakdown.

These high Reynolds number breakdowns are characterized by the lack of a distinct bubble (immediately following what appears to be the stagnation point, the flow expands in a sharp, nominally axisymmetric cone of turbulent flow) and appear to be the most robust of all breakdown forms. Outside of the combustion community (where the breakdown is referred to as a central toroidal recirculation zone, and where geometries typically include such complicating factors as dilution jets and rapid expansions), the only recent numerical work aimed at studying the internal structure of turbulent vortex breakdown is that of Spall and Gatski (1995). They presented results for the unsteady, three-dimensional turbulent breakdown of an unconfined longitudinal vortex employing the algebraic Reynolds stress model of Gatski and Speziale (1993). Their results showed some qualitative agreement with Sarpkayas experimental data (i.e., robustness, lack of asymmetries) but in the absence of common boundary conditions a closer comparison was deemed unwarranted.

Several distinct approaches to modeling these high Reynolds number swirling flows exist, ranging from solutions to the Reynolds-averaged Navier-Stokes (RANS) equations, to large eddy simulations (LES), to direct numerical simulations (DNS). However, to date, DNS and LES simulations utilizing spectral schemes have been limited primarily to geometrically simple configurations, and for the case of DNS, the restrictions include relatively low Reynolds numbers.

Higher-order finite-difference techniques enjoy more flexibility in terms of geometries and boundary conditions, but with the lack of spectral accuracy, their built-in low-pass filter may tend to confuse the issue of resolved scales versus subgrid-scale motions. One must conclude that in the near future, it is unlikely that LES or DNS approaches will be available as computational tools to be utilized in the investigation and solution of turbulent flow problems intechnologically important applications such as wake-vortex alleviation and flame stabilization.

Hence, we are motivated in the present study to employ the RANS equations to numerically study vortex breakdown in high Reynolds number turbulent swirling flows. The

geometry considered is modeled after the axisymmetric diverging tube test section employed in the experimental work of Sarpkaya (1995). Several features contribute to the complex nature of this flow, including the existence of a weak adverse pressure gradient (diverging tube), body forces arising from the strongly swirling flow, and an internal separation point (at breakdown). Thus, although the geometry is somewhat simplified from that of (for instance) most combustors, it does represent an excellent test case to ascertain the capabilities of the RANS equations. In particular, the suitability of both two-equation and differential Reynolds stress closure models for vortex breakdown flows is being evaluated.

Initial calculations have been performed for a steady, axisymmetric mean flow using the standard K-ε, an RNG-based K-ε, and a full differential Reynolds stress model (DRSM). The calculations were performed using a pressure-based finite volume code on a 298x140 grid with significant stretching toward the duct centerline. At the inlet, approximately 20 grid points were contained within the vortex core. A grid resolution study, performed by halving the number of grid points in each direction, did not significantly alter the results. All calculations were performed at a Reynolds number of 130,000. Inlet boundary conditions were derived from experimental data provided to the investigators by Sarpkaya (Private Communication).

In the experimental work of Sarpkaya, the location of breakdown was bounded by x=3.3 and x=4.6. Each of the two-equation models failed to predict the occurrence of this breakdown. In fact, these models produced quite similar results, with minimum mean (dimensionless) axial velocities along the centerline on the order of 0.5. The DRSM performed much better, with a minimum value occurring along the axis at x=3.3.
Depending upon the specification of the dissipation at the inlet boundary, the DRSM predicted flows ranging from near stagnation to those exhibiting a very small recirculating region. These results are consistent with the experimental results of Sarpkaya in which the large bubble-like region that is the hallmark of the observed laminar, nominally axisymmetric breakdowns are absent. Downstream of the breakdown, the DRSM predicted a very slow recovery of the axial velocity. This behavior is considerably different from that of the two-equation models, which (when sufficient swirl is present to promote breakdown) tend to predict a rapid recovery of the mean axial velocity.

It may also be ascertained from the results to date that high levels of diffusivity alone are not responsible for the poor performance of the two-equation models. For instance, levels of turbulent viscosity for the RNG-based model are much lower than those of the standard model, however the resulting mean flow profiles are quite similar. Rather, it is more likely that the failure of these models should be attributed to their inability to properly account for the Reynolds stress anisotropies.

Motivated by these results, work is ongoing to further investigate the performance of both algebraic and differential stress models in predicting fully three-dimensional breakdown in turbulent swirling flows (within the same diverging tube geometry). Toward that end, computed Reynolds stresses will be compared with experimental data, and the role of stress anisotropies in the breakdown process will be ascertained. The ultimate goal of the work is to develop models that are suitable for engineering analysis of strongly swirling flows.

References

Gatski, T.B. and Speziale, C.G. 1993 „On Explicit Algebraic Stress Models for Complex Turbulent Flows", J.Fluid Mech., Vol 254, pp. 59-78.

Sarpkaya, T. 1995 „Turbulent Vortex Breakdown," Phys. Fluids, Vol. 7, pp. 2301-2303.

Spall, R.E. and Gatski, T.B. 1995 „Numerical Calculations of Three-Dimensional Turbulent Vortex Breakdown", Int. J. Numer. Methods Fluids, Vol 20, pp. 307-318.

Breakdown of spinning tube flows

Ch. Brücker, Aerodynamic Institute, RWTH Aachen

Extended Abstract

Vortex breakdown (VB) is a highly unsteady and three-dimensional event that happen to slender vortices with strong non-linear character [1]. The evolution of vortex breakdown and instabilities as well as the characteristics of VB in turbulent flows are still not well known and understood [2]. Due to the sensitivity of VB against boundary conditions [3] and disturbances in the flow, experiments are difficult which could help clarify these questions. Detailed parameter studies with controlled boundary conditions are required including independent variation of the physical characteristic parameters of the slender vortex flow, i.e. the Reynolds-number defined with the core size and the Rossby number defined with the core vorticity. Most of the lab-examined parameter studies of vortex breakdown have been made by flow visualization in tubes with guide vanes where the tube Reynolds-numbers and swirl angle has been changed systematically. However, in these kinds of slender vortex generators, the characteristic circumferential velocity is coupled to the axial one and the results can not be related to the characteristic physical numbers without the often lacking detailed measurements of the velocity profiles. This renders comparison of VB in different setups difficult.

For our studies of turbulent VB a flow channel with a spinning tube was designed, where the swirl is introduced at the entrance by a honeycomb and maintained over the tube length. This provides a solid body rotation within the tube extending nearly over the complete diameter. Variation of the core Reynolds-number and the swirl expressed through the Rossby-number could be done independently. A diffuser at the end of the tube induces an adverse pressure gradient to promote VB. In conclusion, a turbulent slender vortex is generated with a sharply defined core bounded by the spinning tube. In addition, through that the slender vortex core is axially forced by the spinning tube and the radial pressure gradient in the vortex is linear with the radius it let expect increased structural stability of near-axisymmetric modes of VB. Therefore these investigations could help to clarify the mechanisms and conditions responsible for transition of the breakdown types and their stability/instability behaviour.

Detailed simultaneous measurements of the axial, radial and circumferential velocity profiles for various Re_C up to Re_C = 10.000 (defined with the vortex core diameter) and Ro-numbers up to Ro=0.7 were carried out with DPIV simultaneously using a radial and axial light-sheet and a two-camera setup. By rapid scanning of the radial light-sheet through the flow along the axis we obtained the 3-D flow field over time in the breakdown region [4]. Figure 1 shows a flow visualization picture of near-axisymmetric breakdown in the flow channel at a Reynolds-number of 8000 and Ro =0.35. This structure could be observed very stable in position over time. The length-to-diameter ratio of the recirculation region at these conditions is ca. 4.7 and exceeds the typical value of 1.4-1.7 found in tube flows with guide vanes at lower Reynolds-numbers [1]. The shape of the recirculation region resembles a cone which may be a hint on similarities to the conical type of VB found by Sarpkaya in turbulent pipe flows at Re > 100.000 [5].

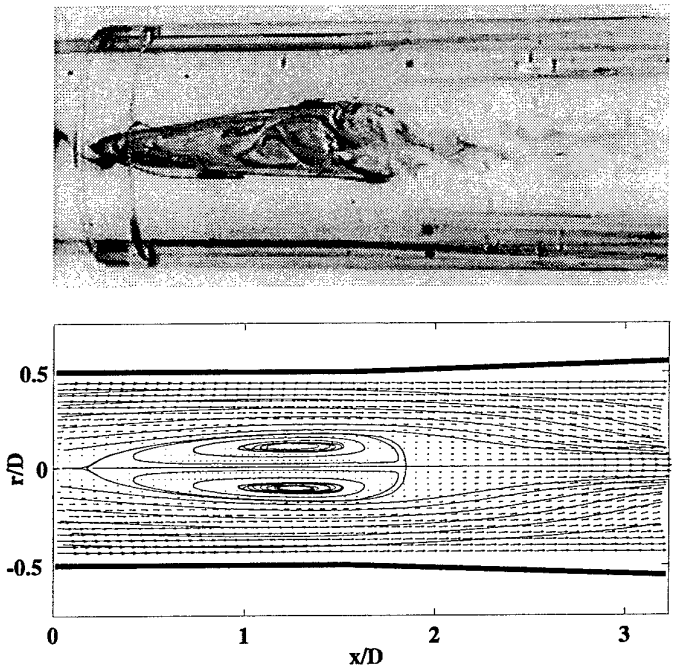

Figure 1: conical breakdown (Re_C=8000, Ro=0,35)

However, his given Reynolds-numbers are based on the tube diameter and no information of the vortex core size is provided so that comparison of Re_C is not possible. Detailed DPIV measurements revealed that at the downstream end of the bubble, the outer flow surrounding the cone turns back, focus on the axis and extends in a jet-like tail of high swirl further downstream. The axial position of the cone base approximately coincides with the beginning of the diffuser while the top of the bubble reaches into the straight pipe. While the axial position and surface of the cone has been observed stable over time, certain fluctuations exist in the downstream part at the cone base in the region where the jet establishes on the axis. It is well seen in the experiments, that the cone base and the jet are sources of spiral instabilities that excite sometimes the more upstream recirculation region. The jet generation at the cone base can be explained by the following: the fluid particles at the outer surface of the cone are transported into regions of higher axial and circumferential velocity and get increased rotational energy by viscous action. As soon they are driven back to the axis downstream of the cone due to imbalance of radial pressure gradient and angular momentum, conservation of continuity and angular momentum leads to increased axial and circumferential velocity close to the axis that built up the swirling jet. Hence, a new thin slender vortex core has been generated nested within the spinning flow. In most cases, this new slender vortex evolves farther downstream in a spiral. This may be explained by the changed profile of radial pressure gradient which is no longer linear proportional to the radius but of higher degree yielding a maximum at the yet present inflection point of the circumferential velocity profile.

References

[1] Althaus, W., Brücker, Ch., Weimer, M. (1995) *Breakdown of slender vortices.* In: Fluid vortices (ed. Green, S.I.), Kluwer Acad. Publ., Netherlands, 1995, Chapt. IX, 373-426

[2] Brücker, Ch. and Althaus, W. (1995) Study of vortex breakdown by particle-tracking-velocimetry (PTV). Part 3: Time-dependent structure and development of breakdown modes. *Experiments in Fluids* **18**, 174-186

[3] Krause, E. (1990) The solution to the problem of Vortex Breakdown. Lecture Notes in Physics **371**, 33-50, Springer Verlag

[4] Brücker, Ch. (1996) Spatial correlation analysis for 3-D SPIV: Simulation and application of dual-color light-sheet scanning. Proc. 8th Int. Symp. Laser Anem., Lisbon, 4.2.1-4.2.7

[5] Sarpkaya, T. (1995) Turbulent vortex breakdown. *Phys. Fluids* **7**(10), 2031-2303

Review of the Aachen Work on Vortex Breakdown

W. Althaus, Aerodynamisches Institut of the RWTH Aachen, Germany

Vortex breakdown is investigated since 1980 at the Institut für Luft- und Raumfahrt (ILR) and the Aerodynamisches Institut (AIA) of the RWTH Aachen in the frame of the Sonderforschungsbereich 25 "Wirbelströmungen in der Flugtechnik". The work of ILR dealt with the experimental investigations of spiral-type breakdown, whereas the research at AIA focused on both, experimental investigations and numerical simulations of bubble- and spiral-type breakdown and the transition between these states.

In the experiments at ILR tip vortices were generated in water flow by a rectangular planform with a Clark-Y profile as cross-section with a rounded wing tip. The axial and tangential velocity distribution were varied by the aspect ratio of the profile, the shape of the rounded wing tip and the angle of attack. The breakdown of the tip vortex was enforced by a variable positive pressure gradient. The influence of this pressure gradient and the vortex strength on spiral-type breakdown were investigated. The path of the vortex core was visualized by milk or gas bubbles and velocity profiles were obtained by LDV-measurements. Calculating the stability of velocity profiles of a nearly undisturbed vortex upstream of breakdown point showed, that hydrodynamic instability is not a sufficient criterion for vortex breakdown. Furthermore, it was noticed, that tip vortices enhance the influence of the positive pressure gradient in such a way that stagnation of the axial flow could happen if the swirl rate is high enough. The vortex undergoes spiral-type breakdown and a stagnation point followed by a limited region of reversed flow, as it is typical for vortex breakdown, was observed. In order to alleviate the vortex wake some special devices as a spoiler on the wing tip or a half-delta wing tip were experimentally investigated. Both result in a remarkable reduction of the tangential velocity thus reducing the rolling moments imposed on a vortex encountering aircraft.

The research at AIA started with the numerical simulation of vortex breakdown using the quasi-cylindrical approximation. It was shown that, in the frame of this approximation, only the approximate location of breakdown could be determined, whereas the region downstream could not be simulated. To describe bubble-type breakdown the complete Navier-Stokes equations for time-dependent, axially symmetric flows were solved. The influence of the inflow and boundary conditions on the solution were examined. During the simulation the vortex ring, which is typical for bubble-type breakdown, migrates upstream with time. If the ring reaches the inflow plane, the solutions do not converge any longer. Thus, it was concluded, that the complete Navier-Stokes equations for time-dependent and three-dimensional flows have to be solved. Based on the concept of artificial compressibility and a new iterative procedure for the boundary conditions, which prevents the vortex ring from migrating into the inflow plane, the bubble- and spiral-type breakdown and the transition between both states were successfully simulated. The internal structure of the bubble depends on Reynolds number and changes during its evolution. A vortex ring-like structure is generated due to the redistribution of axial

into circumferential vorticity. This ring-like structure induces a velocity against the main flow direction which may lead to the formation of a stagnation point and a limited region of reversed flow resulting in bubble-type breakdown. The spiral-type breakdown is characterised by an abrupt kink followed by a corkscrew winding of the vortex filament. It was shown that vortex breakdown is always connected with a transition from a super- to a subcritical flow state. However, hydrodynamic instability is not a basic mechanism leading to breakdown, but only a secondary effect. The instability against spiral-type disturbances was shown to be not a sufficient condition for breakdown.

The time-dependent results of the numerical simulation were compared with an experimental flow visualization which is shown in a video. Due to the excellent agreement of this comparison it was concluded that the numerical simulation describes the underlying mechanisms of vortex breakdown physically correct and the analysis was continued with the numerical data. The process of vortex breakdown is strongly influenced by the boundary conditions. Therefore, no generally valid criterion for breakdown can be deduced without taking them into account. The breakdown process is initiated by the development of an axisymmetric vortex ring-like structure, which moves upstream, grows in time and its evolution can be described by a feedback-model. This phase is characterized by a high degree of axial symmetry and a stagnation point on the vortex axis. The mass flow into the bubble is compensated by the growing bubble volume and, later on, the sweeping away of structures with high axial vorticity. In the transition phase the vortex ring-like structure is tilted and gyrates around the vortex axis. The stagnation point moves away from the axis and rotates around it. This tilting induces a growing asymmetry, finally leading to spiral-type breakdown. In the course of time, the stagnation point moves farther away from the axis, disappears for some time, and reappears again. Contrary to bubble-type breakdown the existence of a stagnation point is not necessary for spiral-type breakdown. Accompanying PIV-measurements confirmed all the numerical results and theoretical explanations. By applying a scanning method it was possible to measure the quasi- three-dimensional and time-dependent velocity distribution. The vortex ring-like structure, its tilting and gyrating were verified experimentally. Sarpkaya's assumption, that the ring-like structure is responsible for the exchange of mass between bubble and outer flow, could be proved. For spiral-type breakdown the growing displacement of the stagnation point from the vortex axis and its rotation were shown. The location of the stagnation point is mainly determined by the inductive effect of the first spiral winding.

In addition to the simulation of a free vortex the breakdown of a slender vortex in a slightly diverging circular tube for a Reynolds number of Re = 3200 based on the tube diameter of the inflow section is numerically simulated and the results compared with the experiments of Sarpkaya and Faler and Leibovich. The location of the breakdown point and the diameter of the bubble show a good agreement with the experimental data.

An essential part of this work is published in: Althaus, W.; Brücker, Ch.; Weimer, M.: Breakdown of Slender Vortices. In: Fluid Vortices. Ed. S. I. Green, Kluwer Academic Publishing, Chapter IX, pp. 373-426, 1995

SESSION 6

VORTEX SOUND

This Page Intentionally
Left Blank

Sound Generation by Interactions of Two Vortex Rings

Katsuya Ishii , Shizuko Adachi*, Hiroyuki Maru[1]

Department of Computational Science and Engineering,
Nagoya University, Nagoya 464-01, Japan
*RIKEN, Wako, Saitama 351-01, Japan

A theory of vortex sound formulated in the form of multipole expansions is applied to the oblique collisions of two vortex rings with various angles. Using the theoretical formula for the far-field acoustic pressure excited by a time-dependent localized vorticity distribution, the coefficients of the multipole modes of the wave pressure are estimated by the numerical data of computer simulation. Time evolution of the vorticity field is obtained by solving a viscous incompressible vorticity equation with a vorticity-potential method developed for a three-dimensional vorticity field in a bounded domain.

The previous experimental and numerical studies on the vortex sound from the collision of vortex rings dealt with the typical two situation: (1) the head-on collision of two vortex rings and (2) the oblique collision at a right angle. In the head-on collision, there occur the stretching and the viscous vanishing of the vortex lines. The vortex sound emitted from the head-on collision dominantly consists of quadrupole modes and does not include octapole modes. On the other hand, the vortex rings in the oblique collision at a right angle experience the cut-and-connect of vortex lines as well as the stretching and the viscous vanishing. The quadrupole modes of vortex sound from this collision are also dominant, but the time development of the amplitudes of vortex sound is different from that of the head-on collision. In addition, the octapole mode can be observed clearly. These changes of vortex sound result from the difference of vortex dynamics. However, the analysis of these two typical cases does not make it clear which phenomenon has the important role in the vortex sound emission.

Numerical simulations are carried out for the vortex rings with the same core and ring parameters but the different 23 initial angles $2\theta'$ between the axes of rings in Fig. 1 (0(head-on collision) $\leq 2\theta' \leq 132°$), and the details of the vortex motion during the oblique collision are studied numerically. The vorticity-potential method for solving a viscous incompressible vorticity equation is used. The quadrupole and octapole mode amplitudes are evaluated with a time-dependent vorticity distribution and a vector potential. Computed main-mode amplitudes of the wave pressure excited by the vortex motion are found to be consistent with those of the experimentally observed acoustic wave in the case of the head-on collision and the oblique collision at a right angle. The results show that the cut-and-connect phenomena is scarcely observed in the collision of rings with a small angle $2\theta'(< 20°)$. In these small angles cases, the amplitudes of octapole modes of the far-field acoustic pressure is much smaller than those in the oblique collision at a right angle. In these angles, the time behavior of quadrupole modes is also similar to that of the head-on collision. The difference between the maximum value of quadrupole mode in the head-on collision and that in the oblique collision becomes linearly large as the angle

[1]present address YAMAHA

between rings is larger. The phenomena of strong local stretching and cut-and-connect of vortex lines are observed. When the angle is nearly 90°, this difference and the absolute value of quadrupole mode has maximum. As the angle become larger than 90°, the maximum value of quadrupole sound mode becomes smaller. The rapid cut-and-connect phenomena of vortex lines occurs after the vortex rings with these angles collide. This is one example of the fact that the time development of amplitude modes of far-field acoustic pressure is strongly related to the dynamics of vortex phenomena(the stretching, vanishing and the cut-and-connect of the vortex lines etc). We discuss the relationship between the phenomena in vortex dynamics and the vortex sound, and the possibility of the observation of the vortex phenomena by using the far-field acoustic data.

References

[1] T.Kambe, T.Minota, M.Takaoka, Phys. Rev. **E48**, 1866(1993).

[2] K. Ishii, K. Kuwahara, C.H. Liu, Computers Fluids,22 589(1993).

[3] S. Adachi, K. Ishii, K.Kambe, ZAMM(to be published).

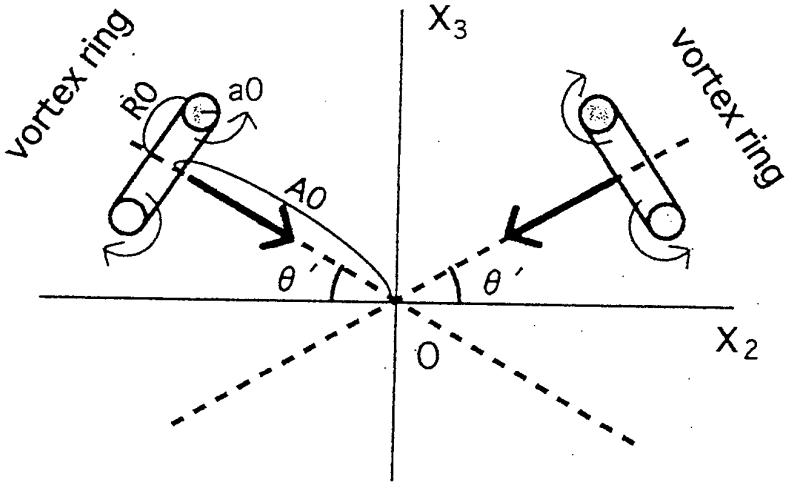

fig.1. Setup of the collision of two vortex rings and coordinate system.

Acoustic waves generated by collisions of two vortex rings

Osamu INOUE and Yuji HATTORI
IFS, Tohoku University, Sendai 980-77, Japan

Three-dimensional, unsteady, compressible flow fields produced by collisions of two vortex rings are simulated numerically, and the basic natures of the sound generated by the collisions are clarified. The Navier-Stokes equations are solved by a finite difference method. For spatial derivatives, a sixth-order accurate compact Padé scheme proposed by Lele (1992) is adopted. The fourth-order Runge-Kutta scheme is used for time-integration. The non-reflecting boundary conditions (Poinsot and Lele 1992) are imposed. Non-uniform mesh system is applied in this study to save the computation time, because a large computational domain is required in order to capture the sounds in far fields. Two different types of of a vortex ring are considered, depending on the initial vorticity distribution: Hill's spherical vortex and Gaussian type.

As an example of the computational results, the contour lines of the vorticity and the sound pressure are presented in Fig.1 and Fig.2, respectively, for the case of a head-on collision of Gaussian type vortex rings. The translational Mach number (M) of a vortex ring is 0.15, and the Reynolds number (Re) based on the circulation of a vortex ring is 1800. The core radius of a vortex ring is $0.17R$, where R is the radius of the vortex ring. The initial distance between the two vortex rings is $16R$. The computational domain is $-180R \leq z, r \leq 180R$. As seen from Fig.1, the two vortex rings come closer to each other along the z-axis, and then stretch in the r-direction after collision at around $t = 66$. The sound pressure in Fig.2(a) shows that after collision an acoustic wave is generated having a quadrupolar component; that is, the sound pressure varies circumferentially from positive to negative to positive to negative. Then the second acoustic wave follows, also having a quadrupolar componet but with opposite alternating signs of circumferential pressure variation to the first wave (Fig.2(b)). The peak sound pressures of the first acoustic sound measured along the z-axis ($\theta = 0°$) and y-axis ($\theta = 90°$) are presented in Fig.3 for three different cases of a vortex ring. In the figure, a_0 is the ratio of the core radius to the ring radius, and the pressures at $\theta = 90°$ doubled. Figure 3 shows that in the far field the sound pressure decays in inverse proportion to the distance r and the pressure at $\theta = 0°$ is twice as large as that at $\theta = 90°$. These results confirm the theoretical prediction on the far-field sound.

References

Lele SK (1992) Compact finite difference schemes with spectral- like resolution. *J.Comp.Phys.* 103:16-42.

Poinsot T, Lele SK (1992) Boundary conditions for direct simulation of compressible viscous flows. *J.Comp.Phys.* 101:104-129.

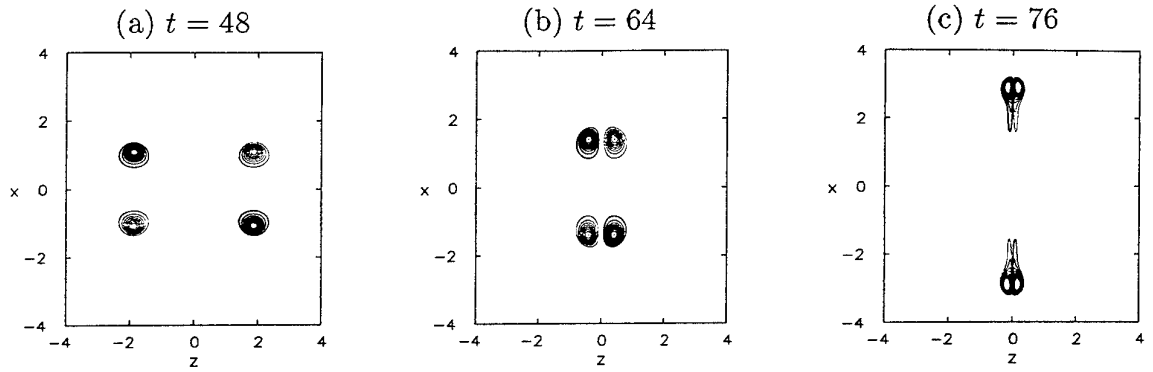

Fig.1. Head-on collision of two-vortex rings. Vorticity. M=0.15, Re=1800.

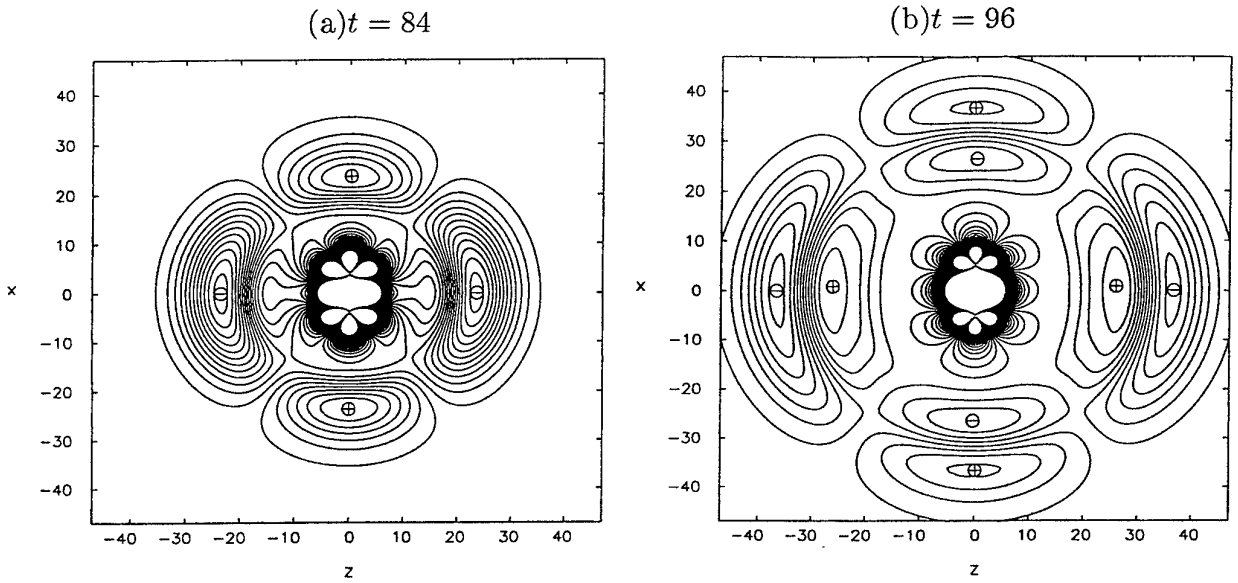

Fig.2. Isobars for the same case as in Fig.1.

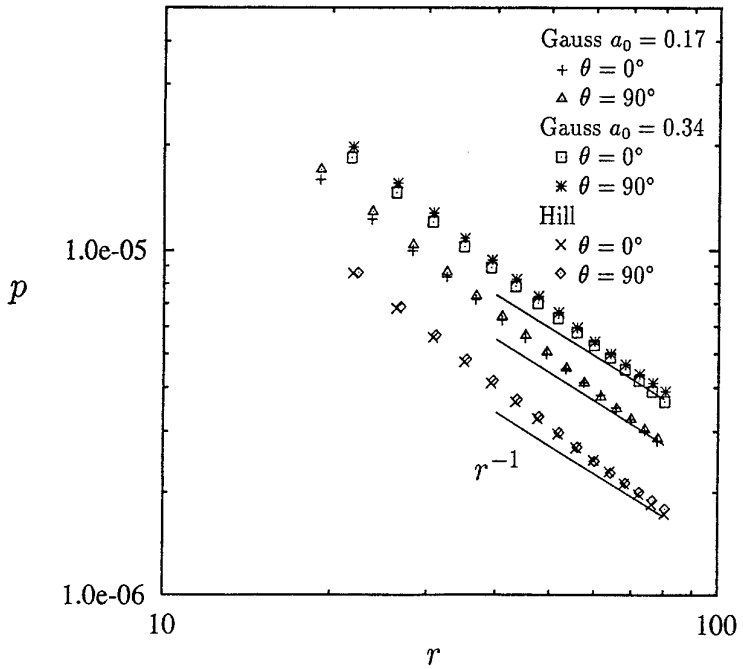

Fig.3. Dependence of the sound pressure on the distance r.
The first sound.

Noise Emission due to Slender Vortex – Solid Body Interactions

Omar M. Knio
Department of Mechanical Engineering
The Johns Hopkins University
Baltimore, MD 21218, USA

Lu Ting
Courant Institute of Mathematical Sciences
New York University
New York, NY 10012, USA

Extended Abstract

Interactions between slender vortices with moving and/or stationary solid bodies play a major role in a large number of applications. Examples include pumps, turbines, propellers, helicopter blades, etc... In this paper, we consider the simplified example of slender vortex filament interacting with a stationary rigid sphere. The simplification enables us to isolate several interesting phenomena that are relevant both to vortex dynamics and to sound emission.

The evolution of the flow field due to the motion of the slender vortex in the presence of the sphere is analyzed using a slender vortex simulation scheme which we have recently constructed [1,2]. The flow is of high Reynolds number R_e and the viscous effect will be present only for the evolution of the vortical core structure. The scheme is based on the discretization of the filament centerline into desingularized vortex elements and transport of these elements according to the local centerline velocity. The latter is the sum of the self-induced velocity and the additional velocity due to the presence of the sphere. The self-induced filament velocity is evaluated using a desingularized line Biot-Savart integral which accounts for the evolution of filament core structure [1,2]. The additional velocity field due to the presence of the rigid sphere is evaluated using an explicit "image" formula [3], which relates it to the flow field in free space induced by a vorticity field.. The radiated sound is analyzed using an explicit formula which exploits the known far-field behavior of the self-induced and image velocities. The far field sound due to the filament in free space is dominanated by quadrupoles with strengths related to the second moments of vorticity and there is no dipoles because the first moments are time-invariant. See for example [4]. In [3], we show that the additional contributions due to the presence of the sphere are dipoles and quadrupoles, whose strengths are defined respectively by the weighted first and second moments of vorticity. The weighting functions depend on the configuration of the filament centerline and are time-dependent. The monopole sound accounting for the compressibility effect is not included in [3]. The additional monopole due the presence of the sphere is obtained by the method given in [4]. The numerical examples shown here do not include the

monopole sound because the strength of the monopole depends only on the evolution of the core structure and is of higher order, $O(1/R_e)$, relative to the strengths of the quadrupoles. The numerical model is applied to compute the far-field sound generated by the passage of a slender vortex filament over a rigid sphere. Simulations of axi-symmetric vortex rings are first performed and are used to study the effects of filament core size and diffusion. The sphere is centered at the origin with radius R. At $t = 0$, the ring lies in the plane $z = -L$ with radius a_0 and center $A(0, 0, -L)$ and core size $\delta_0 \ll a_0$. The acoustic field shows the variation of the strengths of the axial quadrupole and dipole as the ring passing over the sphere. Without the sphere, there is no dipole while the strength of the axial quadrupole varies slowly due to viscous diffusion of the core structure. To demonstrate asymmetric interaction problems, we first compare the dynamics of a slender filament which has an initial elliptical centerline with or without the sphere. The initial ellipse lies in the plane $z = -L$ with center $A(0, 0, -L)$. The interaction effects are seen clearly in their far field acoustic signatures. Next, we study the asymmetric results of perturbed rings. We begin with the axi-symmetric problem. For a small initial radius $R \gg a_0 \gg \delta_0$, the slender filament theory remains applicable and the ring will passing over the sphere with the ring radius stretched by a factor $O(R/a_0)$. If the initial vortex ring is perturbed or displaced in its initial plane with the center being $A(0, h_0, -L)$, the dynamics of the filament and the flow field will be slightly perturbed flow the axi-symmetric case, when the displacement is small, $h_0 \ll a_0$. There is a critical displacement h_0^*, above which we see a distinct change of the dynamics of the filament and the far field sound. The flow field becomes asymmetric, the filament center line becomes non-planar with $O(1)$ stretching while *gliding* over the sphere. It is clear that when the initial scaled displacement $h_0/(R + a_0)$ is sufficiently large, i. e., the filament is far above the sphere, the filament will move forward with small perturbation due to the presence of the sphere. Thus for a given L/R, there is an upper bounded on $h_0/(R + a_0)$ above which the filament will *glide* over the sphere.

References

[1] R. Klein & O.M. Knio, "Asymptotic vorticity structure and numerical simulation of slender vortex filaments," *J. Fluid Mech.* **284**, 275 (1995).

[2] R. Klein, O.M. Knio & L. Ting, "Representation of Core Dynamics in Slender Vortex Filament Simulations," *Phys. Fluids* **8**, 2415 (1996).

[3] O.M. Knio & L. Ting, "Vortical Flow Outside a Sphere and Sound Generation," to appear in *SIAM J. Appl. Math.*, **57** August 1997.

[4] L. Ting & R. Klein, *Viscous Vortical Flows*, Lecture Notes in Physics **374**, Springer-Verlag, 1991.

Multiple scattering of ultrasonic waves by slender vortices

Maurizio Baffico and Fernando Lund
Departamento de Física, Facultad de Ciencias Físicas y Matemáticas,
Universidad de Chile. Casilla 487-3, Santiago, Chile

The propagation of ultrasound through a flow that is made up of many slender, randomly distributed vortices, is studied in a multiple scattering approximation. Effective medium equations are derived. They yield an effective speed of sound, as well as an attenuation length. As an example, these quantities are explicitely calculated when the vortices are vortex rings.

Formulation of the problem

There is increasing evidence, numerical as well as experimental, that slender vortices are an important feature of turbulent flows [1]. The question naturally arises, what is their precise role. One obstacle that stands in the way of progress towards answering this question is the paucity of accurate quantitative experimental data. In the past, ultrasound has been proposed as a possible diagnostic tool to probe nonintrusively turbulent flows [2] In this paper we wish to make an assesment of thhis possibility, by way of considering a flow in which slender vortices are the *only* structures present. This flow will surely affect the way an acoustic wave propagates through it, and it is our aim to find out precisely what this effect is.

Method

There are two basic ingredients in our methodology: One, the vortical flow is assumed to be of low Mach number M, and to remain undisturbed by the ultrasonic wave. Two, a multiple scattering approach. We discuss them in turn.

Consider first the scattering of an acoustic wave by a single vortex. This problem is well posed if the vortical flow is of low Mach number, if the velocities associated with the acoustic wave are small compared to the velocities associated with the vortical flow, and if the ultrasound frequency is high compared to any frequency of interest associated with the vortical flow. Under these circumstances, the equation that describes the propagation of an acoustic wave of pressure p_s, density ρ_s and velocity $\vec{v}_s$ is, to order M^2,

$$\nabla^2 p_s(\vec{x}) - \frac{1}{c_0^2}\partial_{tt} p_s = -2\rho_0 \partial^2_{ij}(u_i v_{s_j}) + \partial^2_{ij}(\rho_s u_i u_j) - \frac{\delta c^2}{c_0^2}\partial_{tt} p_s \,, \quad (1)$$

where $\vec{u}$ is the velocity associated with the vortex, c_0 is the speed of sound in the abscence of any flow and δc^2 is the variation in the speed of sound induced by the vortical flow.

In order to study ultrasound propagation through a flow that is made up of many vortex filaments we use a multiple scattering approach [3]. In this method the wave is supposed to propagate coherently through an effective medium that changes the speed of propagation and attenuates its amplitude. Both effects are accounted for by way of a complex index of refraction. The power of this approach lies on the fact that it is possible to establish formulae for the index of refraction and attenuation length in terms of averages of the scattering amplitude for a single vortex, the average being over all possible vortex states.

The scattering cross section for an acoustic wave by a vortex is computed in a Born approximation. The first approximation vanishes, so a second order approximation becomes necessary. The resulting integrals are numerically evaluated with vorticity having a Gaussian distribution inside the vortex ring.

Effective medium equations are established, so that plane wave solutions $e^{i\vec{p}\cdot\vec{x}}$, where $\vec{p} = \hat{k}_0(p_r + ip_i)$ with real p_r y p_i, yield an effective speed of sound, $c^* = \nu/p_r$, where ν is the acoustic frequency. The index of refraction $\mathcal{N}$ is defined by:

$$\mathcal{N} = \frac{c^*}{c_\infty} = \left(1 - \frac{1}{2}\frac{n\mathrm{Re}\left\{\left\langle T_{0_k}(\vec{k},\vec{k})\right\rangle_{int}\right\}}{k^2}\right),$$

Similarly, the attenuation length Λ is given by:

$$\frac{1}{\Lambda} = p_i = \frac{n\left\langle\sigma_T(k)\right\rangle_{int}}{2},$$

where $T_{0_k}(\vec{k},\vec{k})$ is proportional to the foward scattering amplitude by a single vortex filament and n is the density of vortex filaments, which is assumed small. The brackets indicate an average over all possible filament orientations.

Results

A flow that can be modeled as a system of weakly interacting slender vortices renormalizes the speed of sound propagation and attenuates its amplitude. Figure 1 shows results for the change in sound velocity, $1 - \mathcal{N}$, in units of $n^* M^2$, where $n^* = nR^2\epsilon$ is dimensionless density, as a function of wavelength for various vortex core thickness. We see that the thinner the core, the greater the effect. This can be understood since thinner filaments of the same circulation will have a stronger vorticity concentration. Also, there is a maximum when the wavelength is of the same order of the ring radius. This is also an expected effect. Finally, the index of refraction decreases as a function of wavelength, but note that it does not vanish.

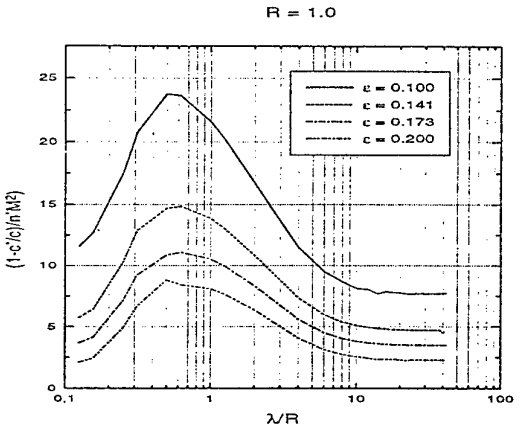

Figure 1: Index of refraction for an acoustic wave propagating through a flow that is modeled as a dilute ensemble of vortex rings.

Although results have been presented for circular vortex rings, the method we have used is flexible enough to accomodate filaments of any shape, suggesting that measurements of ultrasound attenuation and (acoustic) index of refraction could provide data amenable to quantitative comparison with theory for turbulent flows.

Acknowledgements

This work has been supported by FONDECYT Grants 1960892 and 2950011, the Andes Foundation and a Cátedra Presidencial en Ciencias.

Referencias

[1] O. Cadot,S. Douady & Y. Couder, *Characterization of low pressure filaments in a three–dimensional turbulent flow*, Phys. Fluids **7**, 630–646 (1995) and references therein.

[2] F. Lund & C. Rojas, *Ultrasound as probe of turbulence*, Physica D **37**, 508-514 (1989).

[3] L.L. Foldy, *The multiple scattering of waves*, Phys. Rev. **67**, 107–119 (1945).

Vortex Dynamics in Nonuniform Compressible Flow

K. Ehrenfried and G.E.A. Meier

DLR-Institut für Strömungsmechanik
Göttingen, Germany

Abstract:
The convection of vortices and turbulence in flows is often connected with the generation of sound. Well understood and experimentally investigated are the mechanisms of vortex-vortex and vortex-body interactions. In recent investigations it became obvious, that also single vortices in accelerated flows can produce sound of considerable strength.

A first underlying question is, how a vortex reacts when it is convected through the throat of a two-dimensional Laval nozzle with a transonic flow regime. At the end of the supersonic region a vortex-shock interaction takes place, in which strong acoustical disturbances are generated. The vortex-shock interaction was studied intensively elsewhere and is not considered in the present paper. Here the acceleration of the vortex in the convergent part of the nozzle and its passage through the sonic line is the central point of interest. Both, transonic and pure subsonic cases were studied. When the vortex undergoes an acceleration it is stretched in streamwise direction. But the rotation of the vortex prevents a total distortion of its shape and causes the preservation of a more or less circular structure. Of special interest is the transonic case, where the mass flux at the sonic line reaches its maximum. The vortex reduces the total mass flux during its passage and generates disturbances, which propagate in all directions.

The convection of vortices in convergent nozzles and Laval nozzles is investigated experimentally and numerically. All studies are done for plane cases. The experiments are performed in a transonic wind tunnel, where Mach-Zehnder interferometry is used to visualize the density field in the test section. Various nozzles can be installed, and an array of pressure transducers is available to measure the pressure distribution along a line through the nozzles. Further upstream of the nozzle a cylinder with rectangular cross section and sharp edges is mounted between the side walls of the wind tunnel. This cylinder generates a vortex street, which is convected downstream through the nozzle. Thus, a series of vortices passes the throat of the nozzle, where their dynamic response is investigated. In figure 1 interferometric photographs of the throat region are shown. The flow direction is from left to right. The time delay between the images is $\Delta t = 0.1ms$. In this experiment the width of the throat was $100mm$. The nozzle was operated under transonic flow conditions with a shock wave further downstream far outside of the viewspace. In the three images the passage of a counter-clockwise rotating vortex is shown. Noticeable are the disturbances which appear as sharp indentations of the interferometric fringes.

In addition, the numerical computations allow the study of the passage of a single, isolated vortex instead of a series of vortices. In the latter case interactions between the vortices are possible and might influence the process. The Euler equations are solved numerically using a high order finite-volume method. The numerical method is optimized, to reduce the numerical viscosity and minimize the unwanted, artificial dissipation of vortices, and to guarantee still a stable and sharp capturing of moving shock waves. The simulations start with a steady undisturbed nozzle flow, where a vortex is inserted upstream of the throat in a region with constant cross section. This is done in a way that no disturbances occur due to the insertion. At the beginning the vortex is simply convected downstream without changes, until its acceleration starts in the convergent part of the nozzle. Different mo-

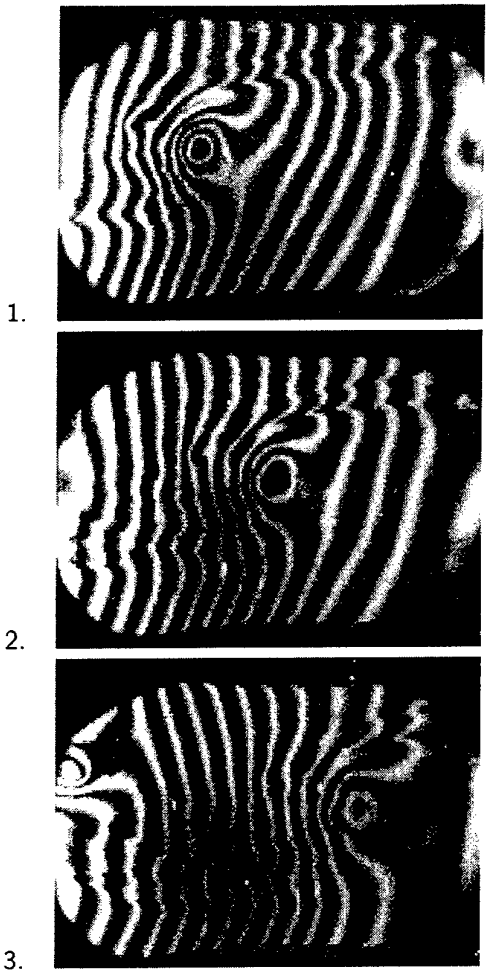

Figure 1: Interferometric photographs of vortex convection in a transonic Laval nozzle ($\Delta t = 0.1ms$)

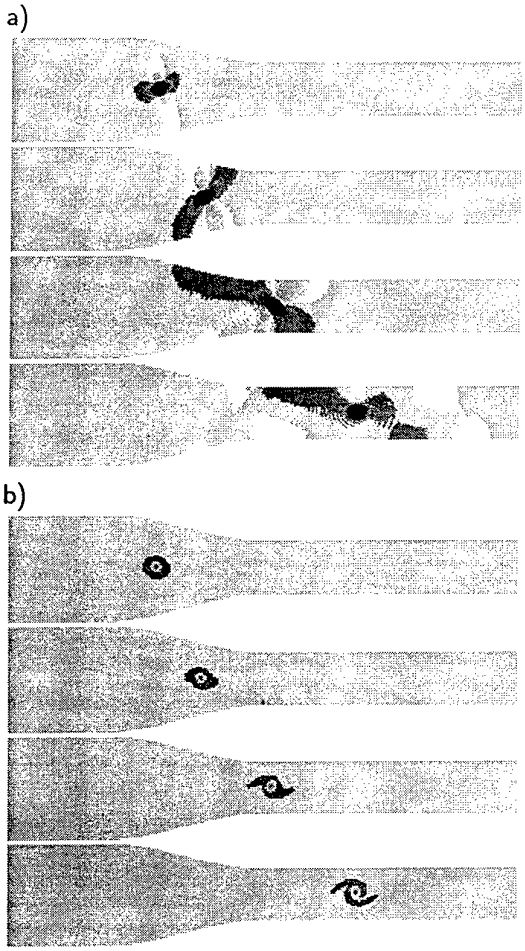

Figure 2: Numerically computed vortex convection in a duct with convergent section – solution at four equidistant times; a) pressure fluctuation ($p' = p - p_{steady}$); b) vorticity

dels are used for the vortex. Additionally the insertion of a hot spot, which has the same density distribution as the vortex but no rotation, is investigated for comparison.

To examine the generation of sound the pressure fluctuations are computed by subtracting the steady value from the actual pressure. A typical example for a clockwise rotating vortex is shown in figure 2a. The results show that a quadrupol like pressure field is generated, when a vortex enters a region with accelerated flow. The strength of the sound depends on the vortex strength and structure, but the generated pressure waves are small compared to the pressure variation in the nozzle flow or inside the vortex core. The vorticity distribution in the vortex becomes distorted and looses its axially symmetric form. Later the vorticity field shows a spiral pattern (see figure 2b). In the transonic case stronger pressure waves are observed, when a vortex passes through the throat of a Laval nozzle.

SESSION 7

AIRCRAFT AND HELICOPTER VORTICES

This Page Intentionally
Left Blank

EFFECTS OF COUPLED AND UNCOUPLED BENDING TORSION MODES ON TWIN-TAIL BUFFET RESPONSE[†]

Osama A. Kandil[*], C. H. Liu[**] and Essam F. Sheta[***]

ABSTRACT

Modern combat aircraft are designed to fly and maneuver at high angles of attack and at high loading conditions. This is achieved, for example in the F/A-18 fighter, through the combination of a leading-edge extension (LEX) with a delta wing and the use of highly swept-back vertical tails. The LEX maintains lift at high angles of attack by generating a pair of vortices that trail aft over the top of the aircraft. The vortex entrains air over the vertical tails to maintain stability of the aircraft. This combination of LEX, delta wing and vertical tails leads to the aircraft excellent agility. However, at some flight conditions, the vortices emanating from the highly-swept LEX of the delta wing breakdown before reaching the vertical tails which get bathed in a wake of unsteady highly-turbulent, swirling flow. The vortex-breakdown flow produces unsteady, unbalanced loads on the vertical tails which in turn produce severe buffet of the tails and has led to their premature fatigue failure. An extensive experimental investigation has been conducted to study vortex-twin tail interaction on a 76° sharp-edged delta wing with vertical twin-tail configuration by Washburn, Jenkins and Ferman[1].

In this paper, the interactions of unsteady vortex-breakdown flow of a 76° sharp-edged delta wing with the vertical twin-tail configuration of Washburn et. al. is computationally produced and investigated. The formulation of the problem consists of three sets of governing equations along with certain initial and boundary conditions. The first set is the unsteady, compressible, Reynolds-averaged Navier-Stokes (NS) equations. The second set consists of the aeroelastic equations for coupled or uncoupled bending and torsional responses of the twin tail. The third set consists of equations for deforming the grid due to the deflections of the twin tail in bending and torsion. These sets are sequentially solved accurately in time at each time step.

The turbulent model in the NS equations is the Baldwin and Lomax algebraic model which is modified by Schiff and Degani for separated flows. The NS equations are solved using the implicit, flux-difference splitting (Roe Scheme) finite-volume scheme. A multi-block grid consisting of four blocks is used for the solution of the fluid-flow problem. The fluid-flow

† This work is supported by NASA Langley Research Center under Grant No. NAG-1–994.

* Professor and Eminent Scholar, Aerospace Engineering Dept., Old Dominion Univ., Norfolk, VA, USA.

** Senior Scientist, Aerodynamic Methods and Acoustics Branch, NASA Langley, Hampton, VA, USA.

*** Ph.D. Research Assistant, Aerospace Engineering Dept., Old Dominion Univ., Norfolk, VA, USA.

equations are used to obtain the flow-field vector and the normal-force and twisting-moment coefficients on the twin tail. The aeroelastic equations treat each of the twin tail as a cantilevered beam with variable mass and cross-sectional area along the elastic axis. The solution of the two elastic equations is obtained by using modal analysis (six mode shapes for each of the bending and torsional responses) and the Galerkin method to obtain 12 ordinary-differential equations for the generalized coordinates. Using the normal-force and twisting-moment coefficients obtained from the solution of the fluid flow problem, these equations are solved using a four-stage Runge-Kutta scheme, and the bending and torsional deflections are obtained. Once the bending and torsional deflections are obtained, interpolation equations are used to obtain the new grid coordinates. This method is coded in the FTNS3D program.

The computational applications include a subsonic flow case of a delta wing-twin tail configuration which is pitched at two angles of attack; 25° and 30°. The twin tails are considered for three spanwise separation distances; an inboard, a mid-span and an outboard locations. Each of these three cases are solved for coupled and uncoupled bending-torsional mode response. The computational results are in good agreement with the experimental data of Washburn, et. al. A sample of the comparison is given in Table (1). The effects of coupling or uncoupling bending and torsional responses will be presented.

Parameter	Position	FTNS3D	WASHBURN
Mean Root Bending Moment With Flexible Tails	Inboard	$5.62X10^{-5}$	$7.43X10^{-5}$
	Midspan	$4.22X10^{-5}$	$6.05X10^{-5}$
	Outboard	$3.62X10^{-5}$	$5.70X10^{-5}$
Lift Coefficient With Rigid Tails	Inboard	1.0423	1.17
	Midspan	1.0515	1.12
	Outboard	1.0674	1.17

Table (1) Validation of FTNS3D computational results with Washburn, et. al. experimental results.

References

1. Washburn, A. E., Jenkins, L. N. and Ferman, M. A., "Experimental Investigation of Vortex-Fin Interaction," AIAA 93–0050, AIAA 31st ASM, Reno, NV, January 1993.

INTERACTION OF WING VORTICES AND PLUMES IN SUPERSONIC FLIGHT

P.M. Sforza
Department of Mechanical, Aerospace, and Manufacturing Engineering
Polytechnic University, Brooklyn, NY 11201

Wing tip vortices became a topic of intense interest and scrutiny in the mid-1960s when it was recognized that they posed a hazard to following aircraft during terminal operations. Airport safety considerations prompted substantial research efforts led by the FAA and NASA through the mid-1970s. However, vortex behavior in supersonic flight received no similar sustained impetus and therefore is presently characterized by a sparse database. Renewed interest in supersonic cruise vehicles, both commercial and military, has awakened a corresponding concern for fundamental insights regarding vortex wakes. Several important problems illuminate the need for such information: interaction of tip vortices with shock waves and flow fields of downstream surfaces; entrainment of engine plumes into wing vortices (or fuel jets into scramjet injector vortices); and vortex confinement of entrained material for long times after aircraft passage. In practical applications these can influence stability and control characteristics, alter the wake signature of the vehicle, and increase atmospheric residence times of possible pollutants, respectively. The object of this paper is to interpret and apply the results of the few past and recent experiments to the second problem, vortex entrainment.

SST jet plumes stream through a wing wake flow field dominated by one or more trailing vortices. Overcamp and Fay (1973) studied dispersion of SST exhaust products taking into account only global characteristics of trailing vortices and the stratospheric atmosphere. They considered the near wake to involve no appreciable interaction and the intermediate wake to be dominated by engulfment of the exhaust plume into the trailing vortex system. Miake-Lye, Martinez-Sanchez, Brown, and Kolb (1991) developed a simplified *ad hoc* model to account for the capture of exhaust effluents by the trailing vortex. They also emphasized differences between supersonic and transonic aircraft wake systems which lead to quite different dispersion characteristics. Quackenbush, Teske, and Bilanin (1993) incorporated a Reynolds-averaged turbulent flow module within a large-scale wake code to attempt to account for the vortex entrainment of SST plumes. These studies are limited by lack of an experimental database for validating the assumptions utilized, particularly with respect to initializing the plume mixing and reaction problem.

Recent experimental studies of flow behind an SST cranked arrow half-wing by Wang, Sforza, and Pascali (1996) show a complex wake system with three different trailing vortices. There is a leading edge vortex from the inboard delta panel of the planform, a junction vortex from the crank in the leading edge, and a true tip vortex from the supersonic leading edge outboard panel. Transverse vapor screen photographs, Fig.1, show three vortex structures, one of which rotates counter to the two others, entraining scattering particles into a bright wrapping around the cores. Centripetal acceleration within the rotating cores, on the other hand, appears to suppress mixing and to expel scattering particles, causing those regions to appear black. These vortices are completely rolled up in a short distance, on the order of one span, which is typical for low aspect ratio SST planforms. Furthermore, thin wings have a small viscous wake and tip vortices have

been shown by Wang and Sforza (1996) to be uniformly convected at approximately the free stream Mach number.

An idealization of the observed flow field would then place one or more jets in the cross-flow of nearby parallel vortices, all being located on one side of a centerline of symmetry. Development of the interaction between the jet and the vortex is the subject of the present investigation. For low aspect ratio wings small disturbance theory is valid in the inviscid wake, as shown in early studies of trailing vortex roll-up by Spreiter and Sachs (1951). A vortex lattice technique based on those developed for jets in a cross-flow, e.g. Margason (1993), is being applied to the present problem. The results expected include the distance to full engulfment of the jet by the vortex flow, the relationship of the swallowing distance to practical problems of SST and scramjet injector wakes, and the feasibility of validating the interaction behavior by laboratory experiments .

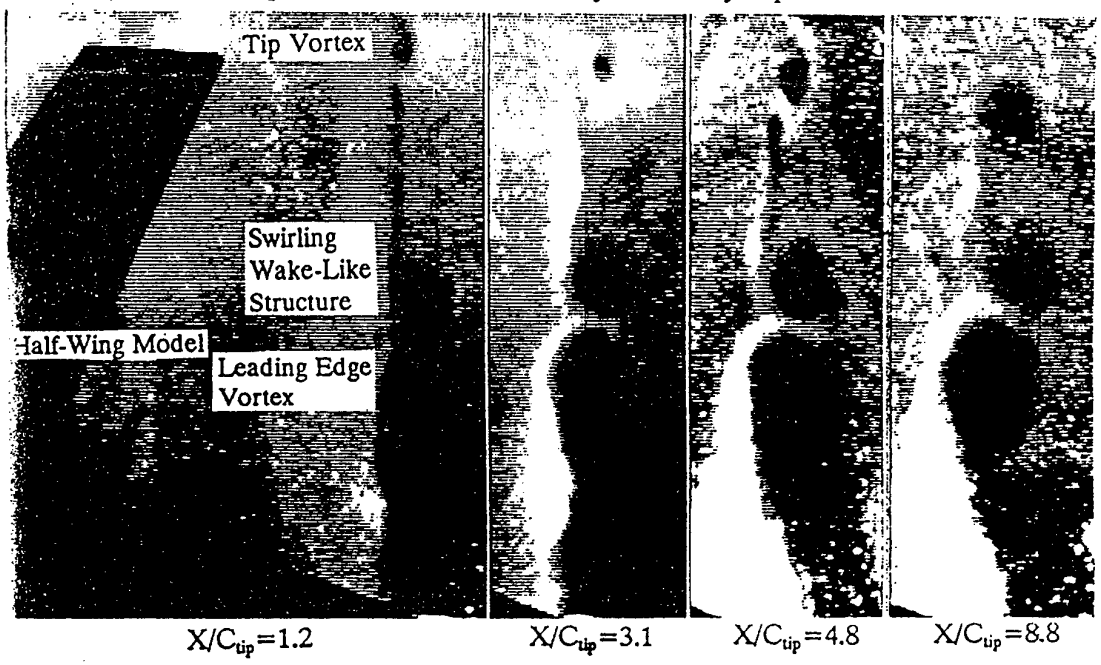

Miake-Lye, R., Martinez-Sanchez, M., Brown, R., and Kolb, C. (1991). Plume and Wake Dynamics, Mixing and Chemistry Behind an HSCT Aircraft, AIAA Paper 91-3158, AIAA Aircraft Design Systems and Operations Meeting.

Overcamp, T.J. and Fay, J.A. (1973). *Dispersion and Subsidence of the Exhaust of a Supersonic Transport in the Stratosphere*, Jl. of Aircraft, *10*, 12, pp. 720-728.

Quackenbush, T.R., Teske, M.E., and Bilanin, A.J. (1993). Computation of Wake/Exhaust Mixing Downstream of Advanced Transport Aircraft, AIAA Paper 93-2944, AIAA 24th Fluid Dynamics Conference.

Wang, F.Y., Sforza, P.M., and Pascali, R. (1996). *Vortex-Wake Characteristics of a Supersonic Transport Wing Planform at Mach 2.5*, AIAA Jl, *34*, 8, pp.1750-52.

Wang, F.Y. and Sforza, P.M. (1996). *Near-Field Experiments on Tip Vortices at Mach 3.1*, AIAA Jl, accepted for publication.

Spreiter, J.R. and Sacks, A.H. (1951). *The Rolling Up of the Trailing Vortex Sheet and Its Effect on the Downwash Behind Wings*, Jl. Aero. Sciences, *18*, 1, pp.21-32.

Margason, R.J. (1993). *Fifty Years of Jet in Cross Flow Research*, in AGARD Conference Proceedings 534.

Dynamics of the Trailing Vortices near the Ground

N.V. Kornev[1] and V.K. Treshkov †
Marine Technical University, 190008 St. Petersburg, Russia
and
G. Reichert ††
Technical University, 38023 Braunschweig, Germany

The vortex behavior near the ground is very **important scientific problem** for many reasons. At present time, many efforts are devoted to enable safe improvements in the capacity of the air transportation system by bringing about a reduction in the in-trailspacing of airplanes. The efforts to solve the problem have been directed at investigating of the vortex behavior near the ground and finding ways to reduce the intensity of the vortices. Another important occurrence of vortex/ground interactions is for ekranoplans (wing-in-ground effect crafts). These flying ships move in the operation area of many other marine vehicles and produce the powerful trailing vortices. The study of the vortex behavior near the ground is very important for choosing the operating regimes and safe routes of the ekranoplans. The detailed study of vortex-wall interaction is also needed to understand the basic mechanisms of the laminar-turbulent transition.

The first part of the paper is devoted to the **trailing vortices** dynamics near the ground **in near field.** The problem has been extensively investigated because of its historical importance in ekranoplan application. A brief summary of these works is presented. The main types of the vortex system and their influence on the aerodynamics, dynamics and stability are discussed for typical wing configurations near the ground. Special attention is attached to the development of the theoretical models. A set of mathematical models of different levels of sophistication are presented including semiempirical models and the advanced free-wake lifting-surface method. The models have been systematically applied to examine their accuracy to quantify the vortex-wing interaction near the ground.

The second part of the paper focuses on the **trailing vortices** behavior **in far field.** The experiments show that the trailing vortex generates viscous boundary-layer flow along the ground that separates and forms the secondary vortex system. The secondary vortices causes the primary trailing vortex to follow the complicated trajectory with multiple rebounding. The phenomenon has been extensively researched theoretically and experimentally. Most of theoretical investigations were carried out using two-dimensional formulation. The experimental observations were made under

[1]Ass. Prof., Department of Hydromechanics
† Professor, Head of Department of Hydromechanics
†† Professor, Head of Institute of Flight Mechanics

some ideal conditions without account of the perturbations. The external perturbations such as the unsteady loading of the vortex generating aircraft and atmospheric turbulence initiate the so-called Crow instability. An important aspect of the present paper is the theoretical study of the three-dimensional Crow instability near the ground. Both inviscid and viscous flow have been considered. The developed analytical model in inviscid flow predicts three types of the vortex instability near the ground depending on the dimensionless height of flight $H = height/span$. In the upper region on the dimensionless height $H \geq 0.575$ the growing perturbations are the planar waves, which are confined to fixed planes inclined at different angles to the horizontal. The instability grows until the vortices come into contact and break up into crude rings. The lifetime of the vortex wake increases with decrease of the height H. At the small height $H \leq 0.438$ the mutual influence of the right and left trailing vortices is weak. The nature of the vortex instability depends mainly on the interaction between the vortex and the ground. The deformed vortex approaches the ground and induces a secondary vortex system. The viscosity plays a key role in the formation of flow at the small height of flight. Due to the self-induction and mutual effects the primary and secondary vortices form the complicated vortex tangle in which the individual vortex tubes are collided, reconnected and annihilated by mutual diffusion of oppositely signed vorticity. As follows from the linear stability analysis the intermediate zone on H ($0.438 \leq H \leq 0.575$) is the zone of the helical instability. Most probably that this instability does not exist isolately. The lowest regions of the helical vortex will approach the ground and undergo the Crow-like instability in the lower region on $H \leq 0.438$. The possible scenario of the vortex trailing instability and decay in ground effect has been proposed as a result of the theoretical analysis.

A new version of the computational vortex method to simulate the viscous wing-vortex-wall interaction is presented in the third part of the paper. The new splitting scheme for a viscous flow with boundaries has been obtained rigorously from the initial-boundary value problem for the Navier-Stokes (NS) equations using Basin's transformation. The mathematical analysis revealed that the decomposition of the viscous flow problem into diffusion, convection and generation of the vorticity on the boundary is only possible if one constructs the approximation of the Navier-Stokes equation of the first order of time interval Δt. To construct the numerical scheme of higher order of Δt we must consider the simultaneous mutual influence of the diffusion, convection and the boundaries. The numerical algorithm based on the splitting scheme was developed with use of vortons representation of the vortex domain and successful tested for problems of the vortex motion.

The authors are grateful for partial support of this work by the Alexander von Humboldt Foundation.

Modifications of the Tip Vortex Structure from a Hovering Rotor using Spoilers

Chee Tung, Research Scientist
Army Aeroflightdynamics Directorate
NASA Ames Research Center, Moffett Field, CA 94035

Justin W. Russell, Graduate Student
Lakshmi N. Sankar, Regents' Professor
School of Aerospace Engineering
Georgia Institute of Technology, Atlanta, GA 30332-0150

SUMMARY

Numerical studies of the tip vortex structure from a hovering rotor with and without spoilers is presented. An unsteady three dimensional Navier-Stokes solver is developed to solve the flowfield. A scheme which is fifth-order accurate in space and second order accurate in time is used to improve the capturing of the tip vortex. Velocity data from the core of the vortex is studied at various planes behind the blade trailing edge for two different tip Mach numbers. This velocity data for the clean rotor is first compared with experimental results obtained for the same rotor test cases. Spoilers of different shape and location are then investigated to see if the tip vortex structure can be favorably altered.

INTRODUCTION

With greater emphasis today being placed on noise reduction both for civil and military rotorcraft, studies of the tip vortices produced by rotors become more and more important. This is because a substantial component of the noise generated by a rotor is due to Blade Vortex Interaction (BVI), which is the effect on one blade due to the tip vortex created by previously passing blades. Preliminary numerical studies by Lee and Smith [1] have shown that vortices with larger core sizes have a less detrimental effect on the lift of a blade during BVI. Hence, if the tip vortex can be somehow altered so that its core size is substantially increased, then both the BVI noise and the vibratory airloads can be reduced.

Early studies by Tangler [2] aimed at reducing "blade slap" have shown that passive devices such as a stub/subwing mounted at the rotor tip can be used to improve slap signature with no noticeable difference in performance of the rotor between the stub/subwing and the square tip. Berry and Mineck [3]

have tested a rotor with a stub/subwing and a winglet, but found a higher torque requirement for one test case in hover and therefore had eliminated these concepts from further testing. More recently, Smith and Sigl [4] have shown that devices such as a stub/subwing can diffuse the tip vortex by as much at 47% with a 9% decrease in drag, and the NASA star tip device can diffuse the tip vortex by 100% with a 67% increase in drag. Green and Duan [5] have also tested a ducted tip for hydrofoils which has shown to make the vortex core size larger. These results offer motivation that a passive device, if properly designed, can be used produce significant increases in vortex core size (thus reducing BVI) with minimal or no loss in rotor performance.

In order to properly study the variety of methods available for tip vortex alteration, an accurate method is needed for tip vortex modeling which can capture the characteristics of the vortex core. The importance of modeling the core correctly can be seen in a theoretical study by Melander and Hussian [6] where they show that the position of vortex filaments (which also affects BVI) depends sensitively on self-induction which is directly related to the internal core dynamics, particularly the core size. More recently, Navier Stokes flow solvers for rotorcraft have proven to yield generally good blade pressure and load distributions. Strawn and Barth [7], Srinivasan and McCroskey [8], Srinivasan et. al [9], Srinivasan and Baeder [10], Srinivasan et al. [11], Duque [12], and Duque and Srinivasan [13] solved hovering rotor flowfields by capturing the rotor wake in an Eulerian fashion, and from first principles. Hariharan and Sankar [14] used higher order methods to solve the flowfield of a rotor in hover from first principles. Ahmad and Duque [15] analyzed the AH-1G two bladed rotor in forward flight mode using structured embedded grids. In addition, a structured/unstructured grid approach was attempted by Duque [16] to solve hovering rotors. However, until now, many studies of the tip vortex of a rotor have been more qualitative than quantitative. Certain global characteristics such as tip vortex trajectory, contraction, and descent have been captured. However, the details of the flow within the core of the vortex have not been resolved. This knowledge is essential to understanding how to alter the tip vortex by active (e.g., blowing) and/or passive (e.g., spoilers, stub/subwings, winglets) means.

The present work addresses both the aspect of tip vortex modeling (i.e., the details of the velocity field within the core) as well as the study of tip vortex alteration by passive devices. The work involving the tip vortex modeling is an extension of the studies by Hariharan where the details of the tip vortex from a fixed wing were modeled [17]. In the case of rotors, the problem is made more complex by the fact that

the vortex structure significantly influences the blade loading and vice versa. The present calculations for a clean rotor are compared with experiments by McAlister et al. [18].

As for the study of the effects of passive devices, it is first important to understand that the goal of the passive device is to diffuse or destabilize the tip vortex. Early theoretical studies by Leibovich and Stewartson [19, 20] have shown that a sufficient condition for vortical flow to be unstable is:

$$V\frac{d\Omega}{dr}\left[\frac{d\Omega}{dr}\frac{d\Gamma}{dr}+\left(\frac{dW}{dr}\right)^2\right]<0$$

where, W is the axial velocity, V is the azimuthal velocity, r is the radial distance from the vortex axis, Ω is the angular velocity V/r, and Γ is the circulation rV. Thus, the passive devices tested will seek to diffuse the vortex (i.e., decrease both $\frac{d\Gamma}{dr}$ and $\frac{dW}{dr}$). These devices include both a spoiler and a stub/subwing. An accurate numerical solution procedure will also be suitable for examining vortex destabilization concepts patterned after the above criterion.

ADDITIONAL WORK TO BE GIVEN IN THE FULL PAPER

The full paper will contain the complete mathematical and numerical formulation. In addition, the paper will contain:

a) Additional comparisons of the clean rotor with experiments at other tip Mach numbers, as well as effects of refining the grid will be given.

b) A CHIMERA grid will be used to resolve the tip vortex for both the clean rotor and the rotor with a spoiler.

c) A parametric study of the spoiler shape and location on the tip vortex structure.

REFERENCES

1. Lee, D.J. and Smith, C.A., "Effect of Core Distortion on Blade-Vortex Interaction", AIAA Journal, Vol. 29, No. 9, September 1991, pp. 1355-1362.
2. Tangler, J.L., "Experimental Investigation of the Subwing Tip and Its Vortex Structure", NASA CR-3058, 1978.
3. Berry, J.D., and Mineck, R.E., "Wind Tunnel Test of An Articulated Helicopter Rotor Model with Several Tip Shapes", NASA-TM-80080, December, 1980.
4. Smith, D.E. and Sigl, D., "Helicopter Rotor Tip Shapes for Reduced Blade Vortex Interaction An Experimental Investigation", AIAA Paper 95-0192.
5. Green, S.I. and Duan, S.Z., "The Ducted Tip--A Hydrofoil Tip Geometry with Superior Cavitation Performance", Journal of Fluids Engineering, Vol. 117, December 1995, pp. 665-672.
6. Melander, M.V. and Hussain, F., "Core dynamics on a vortex column", Fluid Dynamics Research, Vol. 13, No. 1, January 1994, pp. 1-37.
7. Strawn, R.J. and Barth, J.T., "A finite-volume euler solver for computing rotary-wing aerodynamics on unstructured meshes", presented at the 48th Annual forum of the American Helicopter Society, Washington D.C, June 1992.
8. Srinivasan, G. R. and McCroskey, W. J., " Navier-Stokes Calculations of Hovering Rotor Flowfields, " Journal of Aircraft, Vol. 25, No. 10, October 1988, pp. 865-874.
9. Srinivasan, G.R., Baeder, J. D., Obayashi, S. and McCroskey, W. J., "Flowfield of a Lifting Rotor in Hover : A Navier-Stokes Simulation, " AIAA Journal, Vol. 30, No. 10, October 1992.
10. Srinivasan, G.R and Baeder, J.D., "TURNS: A free wake Euler/Navier-Stokes numerical method for helicopter rotors", AIAA Journal, Volume 31, Number 5 May 1993.
11. Srinivasan, G.R, Raghavan, V., Duque, E.P.N and McCroskey, W.J., "Flowfield analysis of modern helicopter rotors in hover by Navier-Stokes method", presented at the AHS International Technical Specialists meeting on Rotorcraft Acoustics and Rotor Fluid dynamics, Oct 1991, Philadelphia, PA.
12. Duque, E. P. N., " A Numerical Analysis of the British Experimental Rotor Program Blade, " 45th Annual AHS Forum, Boston, MA, May 1989.
13. Duque, E. P. N. and Srinivasan, G. R., " Numerical Simulation of a Hovering Rotor using Embedded Grids, " 48th Annual AHS Forum, Washington D.C., June 1992.
14. Hariharan, N., Sankar, L. N., "Higher Order Numerical Simulation of Rotor Flow Field," AHS Forum and Technology Display, Washington, DC., May 1994.
15. Ahmad, J. and Duque, E. P. N., " Helicopter Rotor Blade Computation in Unsteady Flows using Moving Embedded Grids, " AIAA Paper 94-1922, June 1994.
16. Duque, E. P., "A Structured/Unstructured Embedded Grid solver for Helicopter Rotor Flows, " 50th Annual AHS Forum, June 1994.
17. Hariharan, N., "High Order Simulation of Unsteady Compressible Flows Over Interacting Bodies with Overset Grids," Ph.D. Thesis, Georgia Institute of Technology, Atlanta, GA, August 1995.
18. McAlister, K.W., Schuler, C.A., Branum, L., and Wu, J.C., "3-D Wake Measurements Near a Hovering Rotor for Determining Profile and Induced Drag," NASA Technical Paper 3577, August 1995.
19. Leibovich, S. and Stewartson, K., "A sufficient condition for the stability of columnar vortices", Journal of Fluid Mechanics, Vol. 126, July 1982, pp. 335-356.
20. Stewartson, K. and Leibovich, S., "On the stability of a columnar vortex to disturbances with large azimuthal wavenumber: the lower neutral points", Journal of Fluid Mechanics, Vol. 178, August 1986, pp. 549-566.
21. Roe, P.L., "Approximate Riemann Solvers, Parametric Vectors, and Difference Schemes," Journal of Computational Physics, Vol. 39, 1981.
22. Chakravarthy, C.R., "Some Aspects of Essentially Nonoscillatory (ENO) Formulations for the Euler Equations," NASA CR-4285, May 1990.
23. Harten, A. and Chakravarthy, C.R., "Multi-Dimensional ENO Schemes for General Geometries," NASA CR-187637, September 1991.

Measurements of Rotor Tip Vortices Using Laser Doppler Velocimetry

J. Gordon Leishman
Associate Professor
Dept. of Aerospace Engineering,
University of Maryland at College Park,
College Park, MD 20742, United States of America

Abstract of Proposed Paper,
Submitted to the Scientific Committee
IUTAM-Symposium on Dynamics of Slender Vortices, Aachen 1997

Problem Statement: While a good understanding of the essential physics of vortex structures trailed behind fixed-wings has already been obtained, there is a relative dearth of corresponding information on rotors. In particular, we have an inadequate understanding of the wake roll-up process behind the blades, the formation of the tip vortices, and how these vortices diffuse and dissipate as they are convected away from the rotor. Because these effects cannot yet be adequately predicted by means of first principle methods, very careful and detailed measurements are essential. The present work focuses on the use of 3-component laser Doppler velocimetery as a tool for measuring the physics of tip vortex formation, diffusion and dissipation. These new measurements have helped to unravel the intricate flow structure of vortices generated by rotors, will help to validate modern computational models of helicopter wakes, and possibly help understand the important sound producing mechanisms of blade vortex interaction.

Method of Approach: The proposed paper will describe how a series of very comprehensive 3-D velocity field measurements have been made to characterize the physical structure of tip vortices generated by rotors. All the measurements have been performed using state-of-the-art fibre-optic based three-component laser Doppler velocimetry (LDV) system. Additional difficulties in extracting quantities that describe the tip vortex structure, such as velocity profile and core size, will be made in the paper, with attention to such issues as vortex wandering (non-periodicty) and flow seeding (particle dynamics).

Rotors exhibit a complex series intertwining blade tip vortices that lie relatively close to the rotor plane, and have profound effects on the blade loads, vibration levels and noise generation. The proximity of the vortices to the blades means that it is difficult to obtain detailed measurements with conventional probes such as hot wires. For this reason, the application of nonintrusive methods such as LDV to rotor wake studies has received increasing attention. However, LDV instrumentation is very expensive and because of the unsteady (but periodic) nature of the flow field, successful experimental techniques for rotors are only now being developed. In particular, the use of phase-resolved coincident 3-component LDV has only become possible in the last few years.

In the present work, which was conducted at the Center for Rotorcraft Education and Research at the University of Maryland, the detailed flow fields generated by both single and two-bladed rotors have been studied. The single bladed rotor, which provided a baseline for the present measurements, generated a single and almost helical vortex in the rotor flow field, and free from the mutual distortion effects that would be present with multiple blades. The generation of a single vortex also helped to preserve the periodic nature of the flow, which is essential when using LDV.

The rotor used had a blades with a 406 mm radius and 43 mm chord, and used a NACA 2415 airfoil section throughout. The tip Mach number was approximately half of a full-scale helicopter rotor. Both two bladed and one-bladed rotors were tested. A 5W argon-ion laser was the heart of the LDV system. Three laser lines were obtained from a beam splitter unit. Each color was divided into two beams, one of each shifted in frequency by 40 MHz with the use of Bragg cells. The six laser beams were then coupled into 10m length single mode glass fibers, which were sent to the transmitting optics. The transmitting optics had a focal length of up to 2200 mm, although for the present tests 750 mm focal length lenses were used. The transmitting/receiving probes were arranged on a three-axis traverse adjacent to the rotor. The system was arranged in backscatter with non-orthogonal beam crossing angles. Data acquisition was performed using a digital burst processor (TSI IFA-750). A rotating machinery resolver (RMR) was used with a trigger from the rotor to define azimuth bins for the measured data. Velocity data were obtained simultaneously with the azimuth time tag. Based on the assumption of periodic flow (justified from flow visualization), conditional sampling was used to obtain velocity field measurements with respect to the blade azimuth angle. Data acquisition was also windowed to confine the measurements to part of a rotor revolution, thereby increasing the statistical precision of the results. The flow was seeded using atomized olive oil, which gave a mean seed size of 0.8 microns.

Important Results: Probably for the first time, a comprehensive series of measurements have been performed to fully document the physical structure of tip vortices generated by a rotor. The measurements to be reported in the final paper have been performed using coincident three-component LDV. These new measurements have helped establish the detailed structure of the wake roll up behind the blade, the tip vortex formation, and the properties of the tip vortices as they are convected through the flow field. Specific information on the tip vortex itself, such as peripheral velocity profile, core size, axial velocity deficit, turbulence structure and diffusion with wake age were measured with a high spatial and temporal resolution. Attention will also be placed on documenting blade passage effects, which have been noted to change the structure and diffusion characteristics of tip vortices. Such effects have important implications for understanding and predicting blade-vortex interaction phenomena, in general. The paper will conclude with a mathematical treatment and assessment of seed particle dynamics and wandering (non-periodicity) on the measurements.

New results on vortical flows obtained by means of Laser Doppler Anemometry, Particle Image Velocimetry and Rayleigh Scattering

By K.A. Bütefisch and R. Stuff

Abstract.
The flow due to the orthogonal interaction of an advancing helicopter blade with a vortex has been investigated experimentally by applying Laser Doppler Anemometry (LDA) and Particle Image Velocimetry (PIV). The plane under investigation was chosen to be a distance of 0.2 mean chord behind the blade trailing edge, parallel to the blade axis and perpendicular to the plane of rotation. One plane of investigation was chosen for the advancing blade at right angle to the oncoming flow (Ψ=90°), another one for the blade aligned with the flow (Ψ=0°). From the LDA-technique all three components of the time averaged velocity vector were obtained while from the PIV-technique the two inplane components of the instantaneous velocity field were obtained. The Reynolds number based on the mean blade chord was Re=278000. From the LDA-technique the circumferential velocity profile on a straight line across the center of the blade tip vortex as well as the axial velocity profile (See figures 1 and 2) were obtained. In addition, two other vortices.one 90°, the other one 180° old were detected (See figure 3). Also, the decay of the blade tip vortex was obtained from the LDA-technique (See figure 4). The profile of the circumferential velocity, fig.1, suggests a vortex core rotating like a rigid body while the axial velocity profile, fig.2, shows for this core a speed exceeding the oncoming speed by 4%. The oldest vortex shown in fig.3 with a vorticity of Ω=1000 1/s fluctuated in position and intensity considerably more than the other two vortices, and thus, indicating instability or reduced stability. The circumferential velocity profile, such as the one in fig.1 is again reproduced for the instantaneous velocity field as obtained from PIV measurements, see figure 5. The instantaneous velocity profile chosen exhibits a maximum speed, which is 30% higher than the one obtained from LDA, thus indicating the averaging character of the LDA-technique. Also, the rough character of the instantaneous velocity distribution indicates the existence of many small scale vortices, which are smoothed out by the LDA-averaging.
In another experiment the tip vortex of a stationary wing was investigated by means of the PIV-technique. It was observed that depending on the angle of attack the vortex center fluctuated at very low and at very high lift coefficients while for moderate lift coefficients the vortex center remained in almost the same position, see figure 6. The corresponding profile of the instantaneous circumferential velocity, figure 7, exhibits a double kink. One obviously separating an interior vortex core from a cylinder with an annular ring shaped cross-section, which rotates at less angular speed than the interior core. These two cores rotating at different angular speeds may indicate that the interior core contains laminar flow while the outer core contains turbulent flow. The kink between these two cores could not have been detected from applying LDA, since the kink would have been smoothed out by the LDA averaging process. There may be some explanations for the existence of laminar flow in the interior core. One may be the stabilizing effect of a convex boundary layer, which is opposite to the Görtler-Taylor instability at concave walls. Another possible explanation may be linked to the axial velocity component as suggested by Batchelor. This also indicates the necessity of developing the threedimensional PIV-technique.
Another type of flow was investigated by means of the threedimensional LDA-technique and Rayleigh-Scattering. With these non-intrusive methods the vortex on the upper side of a 65° swept back delta wing at 10° angle of attack was investigated, see figure 8. From the LDA-technique the velocity vector for each considered point was obtained. Now, knowing the stagnation conditions the local enthalpy can be calculated from the conservation law of energy. In another experiment without seeding of particles the density distribution across the vortex was found by means of Rayleigh-Scattering. The intensity of Rayleigh-Scattering

depends upon the density of the fluid and is proportional to the inverse wavelength to the power 4. For this reason an ultraviolett laser was used. Thus , the distributions of the density and the enthalpy across the vortex were obtained. With this information the thermodynamic state is fixed and all other thermodynamic properties, such as pressure, entropy, availability etc can be extracted.

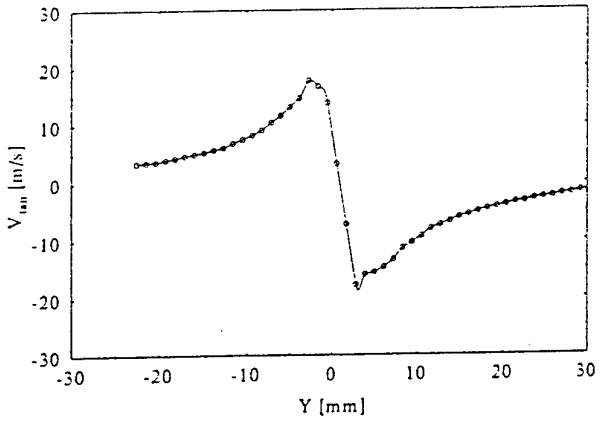

Figure 1: *Tangential velocities along a line through the vortex center obtained by 3D-LDV.*

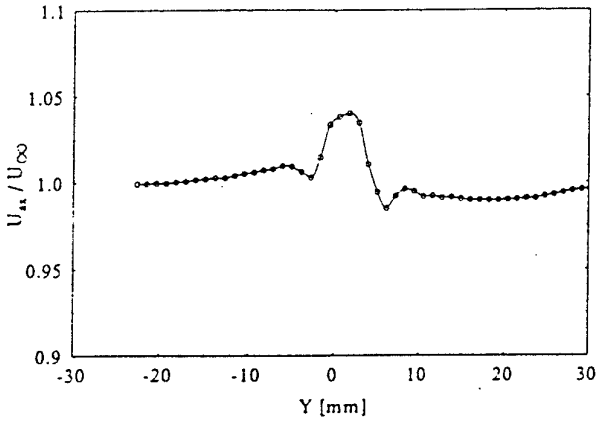

Figure 2: *Axial velocities along a line through the vortex center obtained by 3D-LDV.*

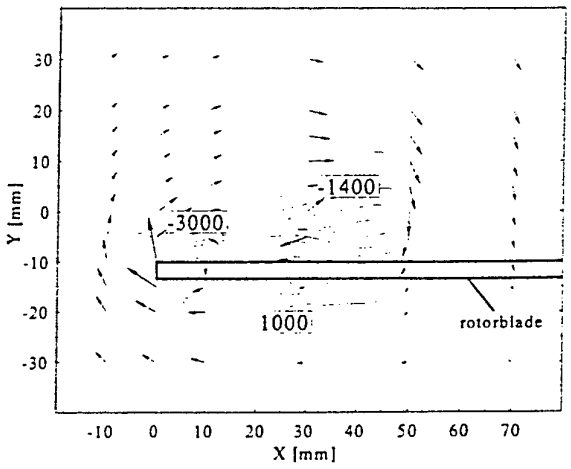

Figure 3: *Velocity vector plot (2D) in a plane 0.2 chord length behind the blade tip as measured by LDV. The vorticity contours were obtained from the velocity data using finite differencing.*

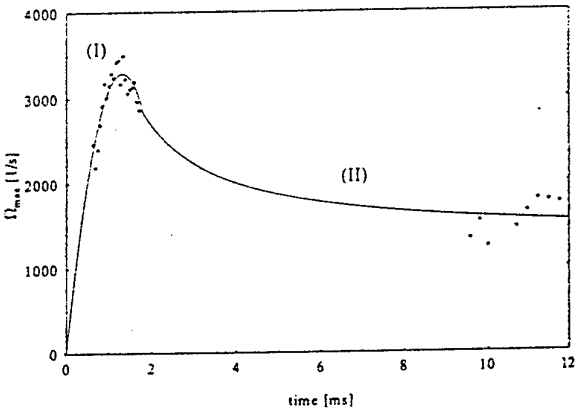

Figure 4 : *Temporal development of maximum vorticity of the blade tip vortex as measured by LDV.*

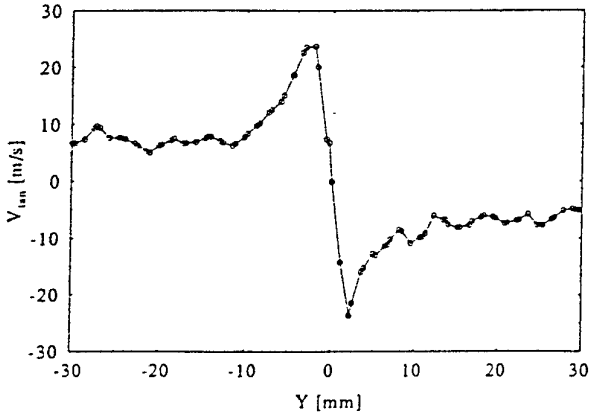

Figure 5 : *Tangential velocitiy along a line through the vortex center as obtained by a single PIV recording.*

ADDRESSES OF PARTICIPANTS

This Page Intentionally
Left Blank

Dr.-Ing. W. Althaus
Aerodynamisches Institut
RWTH Aachen
Wüllnerstr. zw. 5 u. 7
52062 Aachen
Germany
Tel.: +49 (241) 805417
Fax: +49 (241) 8888.257
wolfgang@aia.rwth-aachen.de

Dr. K. Bajer
Institute of Geophysics
University of Warsaw
al. Pasteura 7
02-093 Warszawa
Poland
Tel.: +48 (22) 235281
Fax: +48 (22) 6219712
kbajer@euw.edu.pl

Mr. Chr. Blohm
ZARM
University of Bremen
Am Fallturm
28359 Bremen
Germany
Tel.: +49 (421) 218.4844
Fax: +49 (421) 218.2521
blohm@zarm.uni-bremen.de

Dr. Ch. Brücker
Aerodynamisches Institut
RWTH Aachen
Wüllnerstr. zw. 5 u. 7
52062 Aachen
Germany
Tel.: +49 (241) 805430
Fax: +49 (241) 8888.257
brücker@aia.rwth-aachen.de

Dr. P. Comte
L.E.G.I. - I.M.G.
Domaine Universitaire
B.P. 53
38041 Grenoble Cedex 9
France
Tel.: +33 (4) 768.25121
Fax: +33 (4) 768.25271
pierre.comte@hmg.inpg.fr

Dr. U. Ch. Dallmann
DLR-Institut für Strömungsmechanik
Bunsenstraße 10
37073 Göttingen
Germany
Tel.: +49 (551) 709.2442
Fax: +49 (551) 709.2404
uwe.dallmann@dlr.de

Dr. Daniel Margerit
Laboratoire d'Énergétique et de
Mécanique Appliquée (LEMTA)
URA CNRS 875
2, Av. de la Foret de Haye, BP 160
54054 Vandoeuvre Les Nancy
France
Tel.: +33 (383) 59.5730
Fax: +33 (383) 59.5551
daniel.margerit@ensem.u-nancy.fr

Dr. K. Ehrenfried
DLR-Institut für Strömungsmechanik
Bunsenstraße 10
37073 Göttingen
Germany
Tel.: +49 (551) 709.2813
klaus.ehrenfried@dlr.de

Prof. Y. Fukumoto
Graduate School of Mathematics
Kyushu University 33
Fukuoka 812-81
Japan
Tel.: +81 (92) 642.2762
Fax: +81 (92) 642.2776
yashuhide@math.kyushu-u.ac.jp

Prof. A. Fukuyu
Tokyo Denki University
Ishizaka, Hatoyama, Hiki
Saitama-ken 350-03
Japan
Tel.: +81 (492) 96.2911
Fax: +81 (492) 96.7072
fukuyu@r.dendai.ac.jp

Prof. K. Gersten
Institut für Thermo- und Fluiddynamik
Ruhr-Universität Bochum
Hofleite 15
44795 Bochum
Germany
Tel.: +49 (234) 433388

Prof. P. Huerre
Laboratoire d'Hydrodynamique
École Polytechnique-CNRS
91128 Palaiseau Cedex
France
Tel.: +33 (1) 6933.4990
Fax: +33 (1) 6933.3030
huerre@ladhyx.polytechnique.fr

Prof. F. Hussain
Dept. of Mechanical Engineering
University of Houston
Houston, TX 77204-4792
USA
Tel.: +1 (713) 743.4545
Fax: +1 (713) 743.4503
fhussain@uh.edu

Prof. O. Inoue
Institute of Fluid Science
Tohoku University
2-1-1 Katahira, Aoba-ku
Sendai 980-77
Japan
Tel.+ Fax: +81 (22) 217.5256
inoue@ifs.tohoku-ac.jp

Prof. K. Ishii
Dept. of Computational Science
and Engineering
Nagaya University
Nagoya, Aichi 464-01
Japan
Tel.+ Fax: +81 (52) 789.4660
ishii@nuap.nagoya-u.ac.jp

Prof. O. A. Kandil
Aerospace Engineering Dept.
Old Dominion University
Norfolk, VA 23529-0247
USA
Tel.: +1 (757) 683.4913
Fax: +1 (757) 683.3200
kandil@aero.odu.edu

Dr. S. Kida
National Institute for Fusion Science
Oroshi-cho 322-6
Toki City
Toki-shi 509-52
Japan
Tel.: +81 (572) 58.2248
Fax: +81 (572) 58.262
kida@toki.theory.nifs.ac.jp

Prof. Dr.-Ing. R. Klein
FB 14 - Sicherheitstechnik
Bergische Universität
Gauß-str. 20
42097 Wuppertal
Germany
Tel.: +49 (202) 439.2070
Fax: +49 (202) 439.2047
rupert@uni-wuppertal.de

Prof. O. M. Knio
Dept. of Mechanical Engineering
The John Hopkins University
Baltimore, MD 21218
USA
Tel.: +1 (410) 516.7736
Fax: +1 (410) 516.7254

Dr. N. Kornev
Dept. of Hydromechanics
Marine Technical University
Lotsmanskaya Str. 3
St. Petersburg 190008
Russia
Tel. + Fax: +7 (812) 1572500
kornev@mtu-mic.spb.su

Prof. E. Krause, Ph. D.
Aerodynamisches Institut
RWTH Aachen
Wüllnerstr. zw. 5 u. 7
52072 Aachen
Germany
Tel.: +49 (241) 805410
Fax: +49 (241) 8888257
ek@aia.rwth-aachen.de

Dr. A. N. Kudryavtsev
Inst. of Theoretical & Applied Mechanics
Russian Academy of Sciences
Institutskaya st., 4/1
Novosibirsk 630090
Russia
Tel.: +7 (383) 235.3169
Fax: +7 (383) 235.2268
alex@itam.nsc.ru

Prof. K. Kuwahara
Institute of Space and Astro-
nautical Science
1-22-3, Haramachi
Meguro-ku, Tokyo 152
Japan
Tel.: +81 (3) 3714-6322
Fax: +81 (3) 3714-7430
kuwahara@icfd.co.jp

Prof. St. Le Dizès
Institut de Recherche sur les
Phénomènes Hors Équilibre
12, Ave. Général Leclerc
13003 Marseille
France
Tel.: +33 (491) 505439
Fax: +33 (491) 081637
ledizes@marius.univ-mrs.fr/-ledizes

Prof. J. G. Leishman
Dept. of Aerospace Engineering
University of Maryland at College Park
College Park
Maryland 20742
USA
Tel.: +1 (301) 4051126
Fax: +1 (301) 3149001
leishman@eng.umd.edu

Dr. Thomas Leweke
IRPHÉ, CNRS
Universités Aix-Marseille I et II
12, Avenue Général Leclerc
13003 Marseille
France
Tel.: +33 (491) 505439
Fax: +33 (491) 081637
leweke@marius.univ-mrs.fr

Dr. C. H. Liu
Theoretical Flow Physics Branch
NASA Langley Research Center
Mail Stop 128
Hampton, VA 23665-5225
USA
Tel.: +1 (757) 220-8808
Fax: +1 (757) 220-3611

Prof. F. Lund
Universidad de Chile
Fac. de Ciencas Fisicas Y Mathematicas
Dep. de Fisica
Avda. Blanco Encalada 2008
Casilla 487-3, Santiago
Chile
Tel.: +56 (2) 6784339
Fax: +56 (2) 6967359
flund@camilo.dfi.uchile.cl

Prof. J. E. Martin
Christopher Newport University
50 Shoe Lane
Newport News, VA 23606-299
USA
Tel.: +1 (757) 594.7945
Fax: +1 (757) 594.7919
jamie@pcs.cnu.edu

Prof. E. Meiburg
Dept. of Aerospace & Engineering
University of Southern California
Los Angeles, CA 90089-1191
USA
Tel.: +1 (213) 740.4303
Fax: +1 (213) 740.7774
eckart@spock.usc.edu

Prof. Dr. G. E. A. Meier
DLR-Institut für Strömungsmechanik
Bunsenstraße 10
37073 Göttingen
Germany
Tel.: +49 (551) 709.2177
Fax: +49 (551) 709.2889
g.e.a.meier@dlr.de

Dr.-Ing. M. Meinke
Aerodynamisches Institut
RWTH Aachen
Wüllnerstr. zw. 5 u. 7
52062 Aachen
Germany
Tel.: +49 (241) 804821
Fax: +49 (241) 8888257
meinke@aia.rwth-aachen.de

Prof. H. K. Moffatt
Isaac Newton Institute for
Mathematical Sciences
Clarkson Road
Cambridge CB3 9EW
United Kingdom
Tel.: +44 (1223)-335980
hkm2@newton.cam.ac.uk

Prof. M. Nitsche
100 Mathematics Building
Ohio State University
231 West 18th Avenue
Columbus, OH 43210-1174
USA
Tel.: +1 (614) 292-5710
Fax: +1 (614) 292-7173
nitsche@math.ohio-state.edu

Prof. V. L. Okulov
Institute of Thermophysics
Siberian Branch of RAS
Lavrentyev Ave., 1
630090 Novosibirsk
Russia
Tel.: +7 (3832) 357128
Fax: +7 (3832) 357880
alex@otani.thermo.nsk.su

Prof. Lakshmi N. Sankar
School of Aerospace Engineering
Georgia Techn. University
Mail Stop 0150
Atlanta, GA 30332-0150
USA
Tel.: +1 (404) 894.3014
Fax: +1 (404) 894.2760
lakshmi.sankar@aerospace.gatech.edu

Prof. T. Sarpkaya
Mechanical Engineering
Naval Postgraduate School
700 Dyer Road, Rm: 339
Monterey, CA 93943-5100
USA
Tel.: +1 (408) 656.3425
Fax: +1 (408) 656.2238
sarp@nps.navy.mil

Mr. Wade Schoppa
Dept. of Mechanical Engineering
University of Houston
Houston, TX 77204-4792
USA
Tel.: +1 (713) 743.4551
Fax: +1 (713) 743.4503
mece18l@jetson.uh.edu

Prof. B. Yu. Scobelev
Institute of Theoretical and
Applied Mechanics
Russian Academy of Sciences
Novosibirsk 630090
Russia
Tel.: +7 (3832) 352346
Fax: +7 (3832) 352268
adm@itam.nsk.su

Prof. P. M. Sforza
Mech. & Aerospace Engineering Dept.
Polytechnic University of Brooklyn
Route 110
Farmingdale, New York 11735
USA
Tel.: +1 (516) 755.4205
Fax: +1 (516) 755.4526
sforza@rama.poly.edu

Prof. V.N. Shtern
Dept. of Mechanical Engineering
University of Houston
Houston, TX 77204-4792
USA
Tel.: +1 (713) 743.4547
Fax: +1 (713) 743.4503
mece21w@jetson.uh.edu

Prof. R. Spall
Dept. of Mechanical and
Aerospace Engineering
Utah State University
Logan, UT 84322-4130
USA
Tel.: +1 (801) 797.2878
Fax: +1 (801) 797.2417
spall@fluids.me.usu.edu

Prof. Dr. Lu Ting
Courant Institute of Mathematical Sciences
New York University
251, Mercer Street
New York, N.Y. 10012
USA
Tel.: +1 (212) 998.3139
Fax: +1 (212) 995.4121
ting@ting.cims-nyu.edu

Dr. S. Shtork
Institute of Thermophysics
Siberian Branch of RAS
Lavrentyev Ave., 1
Novosibirsk 630090
Russia
Tel.: +7 (3832) 357128
Fax: +7 (3832) 357880
alex@otani.thermo.nsk.su

Dr. R. Stuff
DLR-Institut für Strömungsmechanik
Bunsenstraße 10
37073 Göttingen
Germany
Tel.: +49 (551) 709.2865
Fax: +49 (551) 709.2830